

Quantum transients

A. del Campo

*Institute for Mathematical Sciences, Imperial College London, SW7 2PG, UK
QOLS, The Blackett Laboratory, Imperial College London, Prince Consort Rd., SW7 2BW, UK*

G. García-Calderón

*Instituto de Física, Universidad Nacional Autónoma de México, Apartado Postal 20 364, 01000
México, D.F., México*

J. G. Muga

Departamento de Química-Física, UPV-EHU, Apdo. 644, 48080 Bilbao, Spain

Abstract

Quantum transients are temporary features of matter waves before they reach a stationary regime. Transients may arise after the preparation of an unstable initial state or due to a sudden interaction or a change in the boundary conditions. Examples are diffraction in time, buildup processes, decay, trapping, forerunners or pulse formation, as well as other phenomena recently discovered, such as the simultaneous arrival of a wave peak at arbitrarily distant observers. The interest in these transients is nowadays enhanced by new technological possibilities to control, manipulate and measure matter waves.

Key words: quantum transients, diffraction in time, Moshinsky function

PACS: 03.75.-b, 03.65.Yz

Contents

1	Introduction	2
2	Diffraction in time	5
2.1	The Moshinsky shutter	5
2.2	Time-dependent shutter	8
2.3	Dissipation	10
2.4	The wave equations	10
3	Transients in free expansion	10
3.1	Phase space representation	13

Email addresses: a.del-campo@imperial.ac.uk (A. del Campo), gaston@fisica.unam.mx (G. García-Calderón), jg.muga@ehu.es (J. G. Muga).

3.2	Propagation of wavepackets with sharp boundaries.	15
4	Beam chopping and formation of pulses	15
4.1	Quantum transients in beam chopping	15
4.2	Formation of single pulses	17
4.3	Arbitrary modulation of a matter-wave source	18
4.4	Diffraction-in-time revival after slow switching	19
4.5	Multiple pulses	20
5	Dynamics of ultracold gases in tight-waveguides	23
5.1	Dynamics in the Tonks-Girardeau regime	23
5.2	Finite interactions: dynamics of Lieb-Liniger gases	26
5.3	Finite interactions: mean-field approach	28
5.4	Turning interactions on and off in a Bose-Einstein Condensate	29
5.5	State reconstruction	29
6	Transient effects with external potentials	30
6.1	Extended quasi-monochromatic initial states	31
6.2	Wavepacket initial states	35
6.3	Relativistic effects in quantum transients	39
7	Time scale of forerunners in quantum tunneling	40
7.1	Transients for a square barrier	40
7.2	Muga-Büttiker analysis of evanescent waves	44
7.3	Forerunners which do tunnel	46
7.4	Barrier opacity and time scale for tunneling as a transient effect	48
7.5	Time scales for relativistic equations	49
8	Transient phenomena caused by a sudden perturbation	50
8.1	Potential steps, resonant tunneling	50
9	Other transient phenomena	52
9.1	Ultrafast propagation and simultaneous arrival of information in absorbing media	52
9.2	Breakdown of classical conservation of energy in quantum collisions	53
9.3	Effect of classically forbidden momenta	54
9.4	Time of arrival and Zeno effect	55
10	Experiments	56
11	Final comments	57
	Acknowledgements	58
A	Propagators in quantum transients	58
B	The Moshinsky function	60
B.1	Integral and differential equations	61
C	The w -function	62
D	Inhomogeneous quantum sources	63
E	Resonant states	64
E.1	Time-independent resonance expansions	66
E.2	Resonance expansion of the retarded time-dependent Green function	69
	References	70

1. Introduction

Transients are temporary phenomena before a system attains a steady-state responding to a sudden change, such as an interaction switch, an excitation, new boundary conditions, or the preparation of an unstable initial state. They are ubiquitous in physics, and frequently described by characteristic times: response times, build-up times, decay times, or times of emission and arrival. In quantum mechanics, matter-wave transients are peculiar and generally distinct from corresponding classical particle phenomena. Typical transients are damped oscillations, forerunners, response to excitations, and trapping or decay processes.

In this work we shall review the theory, results, and experiments of quantum transients of single to few-body systems. We shall leave aside many-body and complex systems, such as electrons in a semiconductor responding to a strong short optical pulse, since they are treated already in several monographs (see e.g. [1,2]) and require specific techniques. We shall nevertheless discuss many-body systems in which effective one-particle pictures are still a useful approximation, e.g. a Bose-Einstein condensate within the mean field Gross-Pitaevskii equation, Tonks-Girardeau gases, or multi-electron systems treated at a Hartree level. Many of the concepts and techniques discussed here are valid for studying exponential-decay processes and deviations from it, but we shall not include decay, or touch it only in passing, since the amount of work on that field and its applications deserve separate monographs and many aspects have already been reviewed [3]. The field covered, in spite of the above exclusions, is still vast, and we have paid special attention to work done by the authors, while making an effort to offer a global perspective.

Quantum transients have frequently been studied *per se*, because of their interesting dynamics. They are often analytically solvable and this has also motivated their use to clarify fundamental questions such as tunneling dynamics, or the Zeno effect. In recent times, with the advent of technological advances such as laser cooling techniques, mesoscopic devices, ultrashort laser pulses and nanotechnology, experiments and applications which were unthinkable one or two decades ago can be implemented or are within reach. This is the case of operations to prepare and control the dynamics of quantum systems for fundamental studies, interferometry and metrology, or for quantum information processing. An understanding of transients is therefore essential: sometimes just to avoid them, as in an atom-laser beam; but also to take advantage of them, for example to transmit information simultaneously to receivers at unknown distances; to optimize gate operations or transport properties in semiconductors, or as diagnostic tools for determining momentum distributions, interactions, and other properties of the system.

A common thread in the mathematical description of many quantum transients is the Moshinsky function, which is related to the Faddeyeva w function, to Fresnel integrals and to the error function. Much of this review is devoted to study phenomena where the Moshinsky function plays a fundamental role. It was introduced with the method of time-dependent boundary conditions used in the dynamical description of heavy-ion collisions [4]. It was later associated with the “quantum shutter” problem, one of the archetypal quantum transient phenomena, which lead to the concept of “diffraction in time” (DIT) [5]. A flurry of experimental and theoretical work has been carried out ever since. The hallmark of DIT consists in temporal and spatial oscillations of Schrödinger matter waves released in one or several pulses from a preparation region in which the wave is initially confined. The original setting consisted in a sudden opening of a shutter to release a semi-infinite beam, and provided a quantum, temporal analogue of spatial Fresnel-diffraction by a sharp edge [5]. Later on, more complicated shutter windows [6], initial confinements [7,8,9,10], time-slit combinations [11,12] and periodic gratings [13,14,15] have been considered [16]. The effects of an external linear potential, e.g. due to gravity, on the DIT phenomenon have also been taken into account [17]. The basic results on Moshinsky’s shutter are reviewed in Section 2.

The quantum shutter problem has important applications indeed, for example the modeling of turning on and off a beam of atoms, as done e.g. in integrated atom-optical circuits or a planar atom waveguide [18], and has been used to translate the principles of spatial diffractive light optics [19,20] to the time domain for matter waves [21]. It is at the

core of different schemes for loading ultracold atoms or Bose-Einstein condensates into traps [22] and, besides, it provides a time-energy uncertainty relation [23,24,25] which has been verified experimentally for atomic waves in a Young interferometer with temporal slits [26,27,28]. The Moshinsky shutter has been discussed in phase space [29,30], for relativistic equations [5,31,32,33,34,35,36,37], with dissipation [38,36], in relation to Feynman paths [39], or for time dependent barriers [6,16,40,41,42].

Transients for the expansion dynamics from box-like traps have also been examined both at single [8,43,9] and many-particle level [44,45,46,47,48], as well as from spherical traps similar to actual experimental magneto-optical traps [10]. The experimental buildup and depth control of box-like (square well) traps for ultracold atoms with an all-optical implementation [49], or in microelectronic chips [50] has excited a great deal of attention for these geometries. The transient effects when the trap is turned off provide information on the initial state and allow for its reconstruction [51]. Once the ballistic dynamics dominates the expansion, the regime of interactions or the momentum distribution can be inferred in a Bose-Einstein condensate [52,53] and effectively one-dimensional gases as well [54,55]. The involved time scales play therefore a key role and are reviewed, at a single-particle level, in Section 3, and with particle interactions in Section 5.

Section 4 deals with pulse formation, a key process in ultracold neutron interferometry, and a timely subject due to the possibilities to control the aperture function of shutters in atom optics, the ionization by ultrashort laser pulses, or the development of atom lasers. Some of the first mechanisms proposed explicitly for building atom lasers implied periodically switching off and on the cavity mirrors, that is, the confining potential of the lasing mode. As an outcome, a pulsed atom laser is obtained. Much effort has been devoted to designing a continuous atom laser, whose principle has been demonstrated using Raman transitions [56,57]. With this output coupling mechanism, an atom initially trapped undergoes a transition to a non-trapped state, receiving a momentum kick due to the photon emission. These transitions can be mapped to the pulse formation, so that the “continuous” nature of the laser arises as a consequence of the overlap of such pulses. The fields of coherent control, femto and attosecond laser pulses and ultracold matter are also merging rapidly creating new opportunities for inducing, studying, and applying quantum interference of matter pulses and the corresponding transients. There is, in summary, a strong motivation for a thorough understanding of matter-wave pulse creation, even at an elementary single-particle level.

The shutter model, with adequate interaction potentials added, see Section 6, has been used to study and characterize transient dynamics of tunneling matter waves [58,171,59,60,61,62,63,32], reviewed in Section 7; Section 8 is devoted to the transient response to abrupt changes of the interaction potential in semiconductor structures and quantum dots [64,65,66]. The study of such transients has been further proposed for potential barrier classification [67].

In Section 9 some transient phenomena different from DIT which have been recently discovered or studied are reviewed. They are intriguing effects such as: ultrafast propagation of a peak which arrives simultaneously at arbitrarily distant observers in an absorbing medium; breakdown of classical conservation of energy in quantum collisions and momentum-space interferences; transients associated with classically forbidden momenta, e.g. negative incident momenta that affect the transmitted part of a wavepacket impinging on a barrier from the left; and the Zeno effect in a time-of-arrival measurement model.

The experimental work is reviewed in Section 10. The first field where transient effects and a corresponding time-energy uncertainty relation were investigated was ultracold neutron interferometry [68,69,70,71,21,72]. Experimental observations of transients have been carried out with ultracold atomic waves where diffraction, phase modulation and interference were studied using temporal slits [26,27,28]. More recently, a double temporal slit experiment with electrons has been performed [73]. The applications of atom interferometry in time domain have also been explored with Bose-Einstein condensates at both theoretical [74] and experimental level [75]. A very recent and relevant result is the realization of an electromagnetic analogy allowing to study DIT phenomena by means of the vertical propagation of the lasing modes emitted from the laterally confined cavities [76]. Note also that transients do not necessarily involve spatial translation and release from traps or shutters. They may be observed in the evolution of internal state populations of an atom due to time-dependent laser excitations [77].

The review ends up with some conclusions and technical appendices. Most sections could be read independently although there are strong links between Sections 3 and 5, or between Sections 6 and 7. Multiple use of some symbols has been unavoidable and the notation is only guaranteed to be consistent within a given section.

2. Diffraction in time

2.1. The Moshinsky shutter

In 1952, Moshinsky tackled the quantum dynamics of a suddenly released beam of independent particles of mass m . The corresponding classical problem, that of a beam with a well defined incident velocity p/m , and initially confined to the negative semi-axis ($x < 0$), admits a trivial solution: the density profile is uniform for $x < pt/m$ and vanishes elsewhere. In non-relativistic quantum mechanics, we shall first consider a quasi-monochromatic atomic beam of nominal momentum $\hbar k$ (or velocity $v_k = \hbar k/m$) impinging on a totally absorbing shutter located at the origin $x = 0$,

$$\psi(x, t = 0) = e^{ikx} \Theta(-x), \quad (1)$$

where $\Theta(x)$ is the Heaviside step function defined as $\Theta(x) = 1$ for $x > 0$ and 0 elsewhere. Note that, in spite of the prominent role of k , the state is not really monochromatic because of the spatial truncation. Such state is clearly not normalized, but it can be considered as an elementary component of a wave packet truncated (fully absorbed) at the origin. Since for $t > 0$ the shutter has been removed, the dynamics is free and the time evolution can be obtained using the superposition principle,

$$\psi(x, t) = \int_{-\infty}^{\infty} dx' K_0(x, t|x', t' = 0) \psi(x', t' = 0), \quad (2)$$

with the free propagator

$$K_0(x, t|x', t') = \left[\frac{m}{2\pi i \hbar (t - t')} \right]^{\frac{1}{2}} e^{i \frac{m(x-x')^2}{2\hbar(t-t')}}, \quad (3)$$

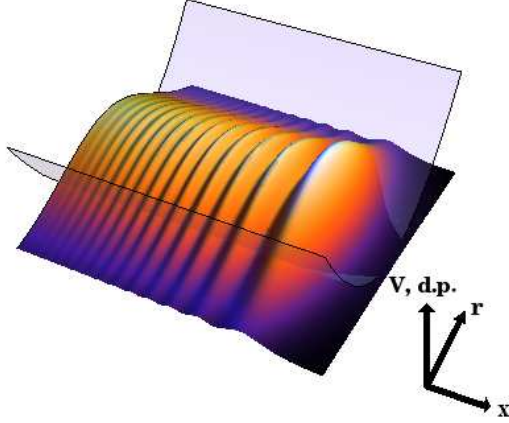


Fig. 1. Snapshot of the density profile of a suddenly released beam, confined transversely to a harmonic trap along a waveguide, and exhibiting diffraction in time in the longitudinal direction, see Eq. (6).

see Appendix A for a brief account of propagators and their role in quantum transients. Following customary practice, we shall liberally speak of $|\psi(x, t)|^2$ as a “density” even if it is dimensionless.

In a seminal paper [5], Moshinsky proved that

$$\psi(x, t) = M(x, k, t). \quad (4)$$

This is a simple compact result, which constitutes the main reference case for more complex setups. M is the so-called Moshinsky function [4,5,24],

$$M(x, k, t) := \frac{e^{i\frac{mx^2}{2\hbar t}}}{2} w(-u), \quad u = \frac{1+i}{2} \sqrt{\frac{\hbar t}{m}} \left(k - \frac{mx}{\hbar t} \right). \quad (5)$$

Many of its properties relevant to the study of quantum transients are listed in Appendix B. Here we just note that it can be related to the Faddeyeva function $w(z) := e^{-z^2} \operatorname{erfc}(-iz)$ [78,79], see Appendix C. Such solution entails the diffraction in time phenomenon, a set of oscillations in the beam profile (see Fig. 1) in dramatic contrast with a classical monochromatic and homogeneous beam density $\Theta(pt/m - x)$.

The “diffraction in time” (DIT) term was introduced because the quantum density profile, $|M(x, k, t)|^2$, admits a simple geometric interpretation in terms of the Cornu spiral or clothoid, which is the curve that results from a parametric representation of the Fresnel integrals C and S , see Fig. 2 and Eq. (C.6). As shown also by Moshinsky [5], it follows that

$$|M(x, k, t)|^2 = \frac{1}{2} \left\{ \left[\frac{1}{2} + C(\theta) \right]^2 + \left[\frac{1}{2} + S(\theta) \right]^2 \right\}, \quad (6)$$

with

$$\theta = \sqrt{\frac{\hbar t}{m\pi}} \left(k - \frac{mx}{\hbar t} \right). \quad (7)$$

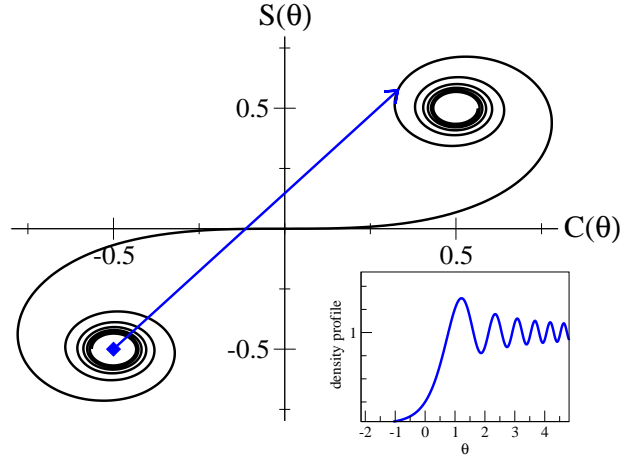


Fig. 2. Cornu spiral. The density profile characteristic of the diffraction in time, Eq. (6), is given by half the distance from the point $(-1/2, -1/2)$ to any point of the spiral.

This is precisely the form of the intensity profile of a light beam diffracted by a semi-infinite plane [19], which prompted the choice of the DIT term. The probability density is half the distance from the point $(-1/2, -1/2)$ to any other point of the Cornu spiral. In such representation the origin corresponds to the classical particle with momentum p released at time $t = 0$ from the shutter position. Thanks to it, the width of the main fringe, δx , can be estimated from the intersection between the classical and quantum probability densities [5,12], leading to a dependence of the form

$$\delta x \propto (\pi \hbar t / m)^{1/2}. \quad (8)$$

Moreover, any point of constant probability deviates from the classical spacetime path. In particular, the principal maxima and minima obey

$$\begin{aligned} x_{max}(t) &= pt/m - \sqrt{\frac{\pi \hbar t}{m}} \theta_{max}, \\ x_{min}(t) &= pt/m - \sqrt{\frac{\pi \hbar t}{m}} \theta_{min}, \end{aligned} \quad (9)$$

where $\theta_{max} = 1.217$, $\theta_{min} = 1.872$ are specific values for the totally absorbing shutter. Therefore, the quantum signal is slowed down for $t \lesssim (m\pi\hbar\theta_{min/max}^2/p^2)^{1/4}$ with respect to the classical case, $x_{cl}(t) = pt/m$.

A more general type of initial state was considered in [24,12],

$$\psi(x, t = 0) = e^{ikx} + R e^{-ikx}, \quad (10)$$

with $R = \exp(i\alpha\pi)$ corresponding to a shutter with reflectivity $|R|^2 = 1$. Under free evolution, $\psi(x, t) = M(x, k, t) + R M(x, -k, t)$. For such a beam, the visibility of the fringes increases monotonically from $\alpha = 0$ (cosine initial condition, see 7.2 below) to $\alpha = 1$ for which the shutter is equivalent to a totally-reflecting hard-wall potential, see Fig. 3 and Appendix D.

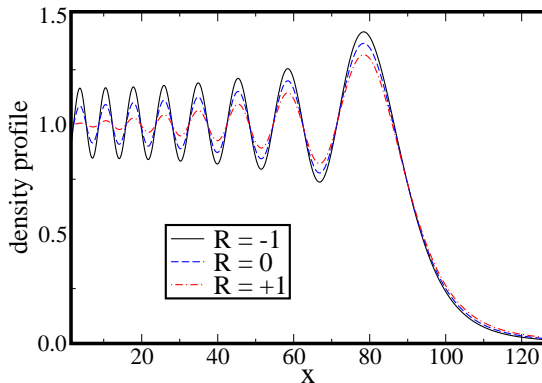


Fig. 3. Enhancement effect of the reflectivity of the shutter on the visibility of the diffraction-in-time fringes of a suddenly released quasi-monochromatic matter-wave beam (in $\hbar = m = 1$ units).

The possibility of closing the shutter after a time τ to form a pulse was studied by Moshinsky himself [23,24]. This is the essential step of a chopper in an ultracold neutron interferometer used for velocity selection. For small values of τ a time-energy uncertainty relation comes into play, broadening the energy distribution of the resulting pulse. For the initial condition (10), with $R = +1$, the explicit calculation of the energy spread ΔE in the resulting wavepacket leads to

$$\Delta E \tau \simeq \hbar. \quad (11)$$

Using the full width at half-maximum (FWHM) of the energy distribution, it was found that [12]

$$\text{FWHM}(E) \tau \gtrsim 2\hbar. \quad (12)$$

The time-energy uncertainty relation lacks the simple status of that holding for position and momentum observables, having many different non-equivalent versions reviewed in [25]. The one for chopped beams as discussed here [23,24] was experimentally observed and will be further discussed in Section 10.

2.2. Time-dependent shutter

The paradigmatic result by Moshinsky rests on the sudden approximation for the removal of the shutter. The effect of a more realistic time dependence has also been looked into. In [6,16], the shutter potential $V(x, t) = \gamma\delta(x)/t$ was assumed, which reduces to an infinite wall at $t = 0$ and vanishes asymptotically for $t \rightarrow \infty$. Using the Laplace transform method, the associated propagator can be related to the free one [6], from which the time-dependent wavefunction can be calculated by numerical integration. Scheitler and Kleber analyzed the flux at the origin $x = 0$ and found that the effect of the slow removal of the shutter is to suppress the DIT fringes in the current. It turns out that the Massey parameter $\beta = \gamma k/\hbar$ identifies qualitatively two different regimes: for $\beta \lesssim 1$, one recovers the sudden approximation; but for $\beta \gtrsim 5$ the particle will experience a quasi-static barrier, no DIT-like transients in the current are observed, and the flux is indeed well-described by the equilibrium current

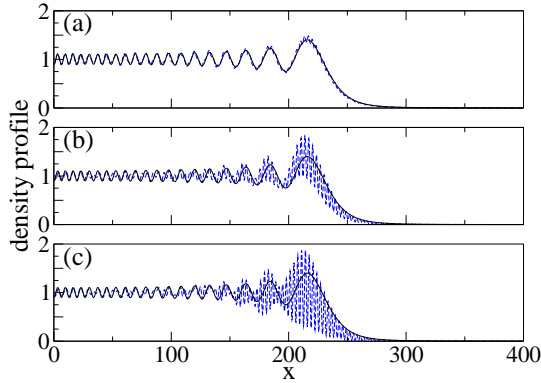


Fig. 4. Snapshots of the density profile of a chopped beam ($\hbar = m = 1$) with $\gamma = 0.5$ (a), 5 (b), and 20 (c) taken in all cases at $t = 250$ with $k = 1$. The solid line corresponds to the sudden totally reflecting shutter ($\gamma = 0$), while the

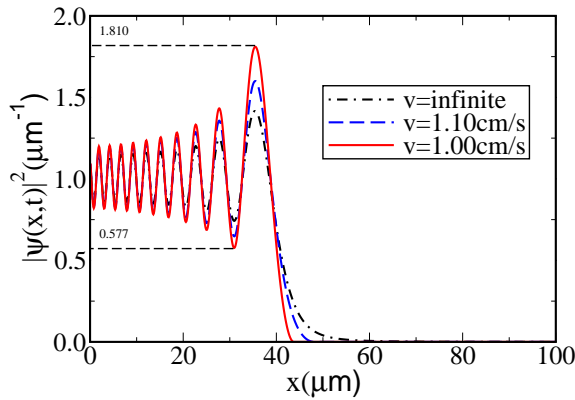


Fig. 5. Characteristic modulation of the density profile of a matter-wave beam of ^{87}Rb atoms induced by a totally reflecting mirror which is displaced at constant velocity $v > v_k$ ($v_k = 1.0$ cm/s). The amplitude of the oscillations is maximized as v approaches the velocity of the beam v_k , when the density exceeds by more than 80% the classical case. In the limit $v \rightarrow \infty$ the dynamics reduces to the diffraction in time setup with the lowest fringe visibility.

$$J(x=0, t) = \frac{\hbar k}{m} T \left(E = \frac{\hbar^2 k^2}{2m} \right) \quad \text{with} \quad T(E) = \frac{E}{E - \frac{m\gamma^2}{2\hbar^2 t^2}}, \quad (13)$$

which is the transmission probability for a δ -barrier of strength γ/t . Nonetheless it is noteworthy that the dynamics of the density profile can be dramatically distorted with respect to the reference case (see Eq. (4)) as shown in Fig. 4, due to the partial reflection from the shutter at short times.

DIT is actually a delicate quantum phenomenon, easily suppressed or averaged out. An exception is the effect of an alternative removal of the shutter consisting of its displacement along the direction of the propagation of the beam. For a mirror moving with velocity v [42], the constructive interference with the reflected components leads to an enhancement of DIT. In particular, the sharpness of the fringes in the density profile and their visibility are maximized whenever $v \rightarrow pt/m$, as illustrated in Fig. 5.

2.3. Dissipation

It is clear that DIT requires quantum coherence. From this point of view it should come as no surprise that the presence of dissipation leads to its suppression. This was shown by Schuch and Moshinsky [38] using the phenomenological Caldirola-Kanai model [80,81], which describes dissipation without explicitly considering the degrees of freedom of the environment, though it is roughly tantamount to the Caldeira-Leggett model in the Ohmic regime [82]. Within this approach, the fringes in the DIT analytical solution are washed out as the time of evolution goes by.

2.4. The wave equations

One may wonder if DIT could be observed in other systems, such as in the electromagnetic field [5]. Let us consider the ordinary wave equation

$$\frac{\partial^2 E(x,t)}{\partial x^2} = \frac{1}{c^2} \frac{\partial^2 E(x,t)}{\partial t^2}, \quad (14)$$

where the speed of light c . Moshinsky showed that no DIT phenomenon arises, the solution being

$$E(x,t) = \Theta(t - x/c) \left[e^{i(kx - \omega t)} - \frac{1}{2} \right], \quad (15)$$

with $\omega = ck$, which oscillates uniformly for $t < x/c$ and vanishes elsewhere, in contrast to the DIT solution. Therefore, the DIT is absent in the free propagation of light. DIT may however be seen in constrained geometries, such as waveguides. Moreover, a relativistic approach to the diffraction in time using the Klein-Gordon equation [5] shows that the probability density is restricted to the accessible region $x < ct$, at variance with the non-relativistic solution $\psi(x,t) = M(x,k,t)$ which is non-zero everywhere already for $t = 0^+$, see also 7.5. A similar discussion of DIT in the Dirac equation can be found in [83]. Finally, a mapping from space to time serves also to observe DIT from the vertical emission of a lasing mode in a laterally confined cavity [76]. More on this in Section 10.

3. Transients in free expansion

The free dynamics of a suddenly released matter-wave is frequently used to probe the properties of the initial state and its relaxation quantum dynamics [51]. The first studies generalizing the Moshinsky shutter setup in the context of neutron interferometry focused on rectangular wavepackets of the form $e^{ikx} \chi_{[0,L]}$, where the characteristic function in the interval $[a,b]$ is $\chi_{[a,b]} = \Theta(b-x) - \Theta(a-x)$ [7,8]. We shall discuss the more realistic case of particle-in-a-box eigenstates,

$$\phi_n(x,t=0) = \sqrt{\frac{2}{L}} \sin(n\pi x/L) \chi_{[0,L]}(x), \quad (16)$$

with $n \in \mathbb{N}$. Box-like traps have been implemented in the laboratory both in an all-optical way [49] and with microchip technology [50]. The expansion after suddenly switching off

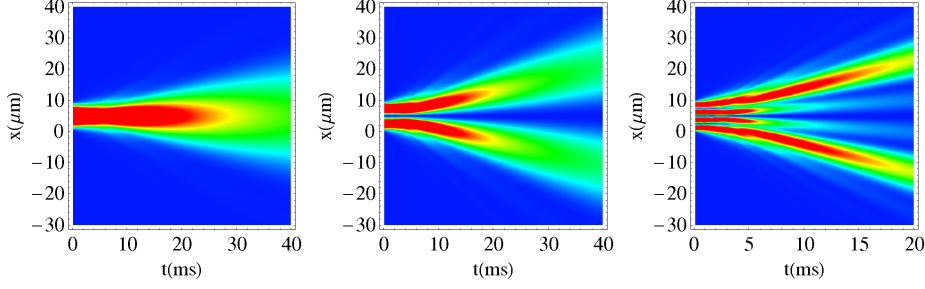


Fig. 6. (Color online) Free expansion of the $n = 1, 2, 4$ eigenstates for a ^{87}Rb atom released from a hard-wall trap of $10\mu\text{m}$, see Eq. (17).

the confining potential has been analyzed at short [9] and arbitrary times [12]. Using the superposition principle and introducing $k_n = n\pi/L$, the time evolved wavefunction is

$$\begin{aligned} \phi_n(x, t) &= \int_{-\infty}^{\infty} dx' K_0(x, t|x', t' = 0) \psi(x', t' = 0) \\ &= \frac{1}{2i} \sqrt{\frac{2}{L}} \sum_{\nu=\pm 1} \nu [e^{i\nu k_n L} M(x - L, \nu k_n, t) - M(x, \nu k_n, t)]. \end{aligned} \quad (17)$$

Registration of the probability density at a given point as a function of time, allows to distinguish the following two regimes. Whenever the de Broglie wavelength is of the order of the box trap, which is to say $n \sim 1$, the particle expands following a bell-shaped profile with few transients as sidelobes. This is the *Fraunhofer* limit of diffraction by a narrow slit in time. The DIT shows up for excited states $n \gg 1$, which corresponds to the so-called *Fresnel* regime, in which the effect of the two edges of the trap can be identified [9]. The space-time density profile is actually richer in structure as shown in Fig. 6.

In what follows we shall compare the dynamics with the expansion from a harmonic trap. Let us first recall the spectrum of the harmonic oscillator (HO) trap, $Sp(H_{HO}) = \{E_l^{HO} = \hbar\omega(l + 1/2) | l = 0, 1, 2, \dots\}$, and that of the hard-wall (HW) trap, $Sp(H_{HW}) = \{E_n^{HW} = (\hbar\pi n/L)^2/(2m) | n = 1, 2, 3, \dots\}$. The condition for the n -th eigenstate of the HW trap to have the same energy than the $(n - 1)$ -th eigenstate of the HO leads to

$$\omega = \frac{\hbar n^2 \pi^2}{(2n - 1)mL^2}. \quad (18)$$

The eigenstates of the harmonic oscillator trap are well-known to be given by

$$\phi_n(x, t = 0) = \left(\frac{m^2 \omega^2}{\pi \hbar^2}\right)^{1/4} e^{-\frac{m\omega x^2}{2\hbar}} H_n\left(\sqrt{\frac{m\omega}{\hbar}} x\right), \quad (19)$$

where $H_n(x)$ are the Hermite polynomials [79]. Although the time-evolution of such eigenstates can be calculated for a broad variety of functional dependencies $\omega(t)$ [84], in the following we shall restrict ourselves to $\omega(t) = \omega\Theta(-t)$ which is tantamount to the time-evolution under the free propagator $K_0(x, t|x', 0)$ in (3) for $t > 0$. The evolution is

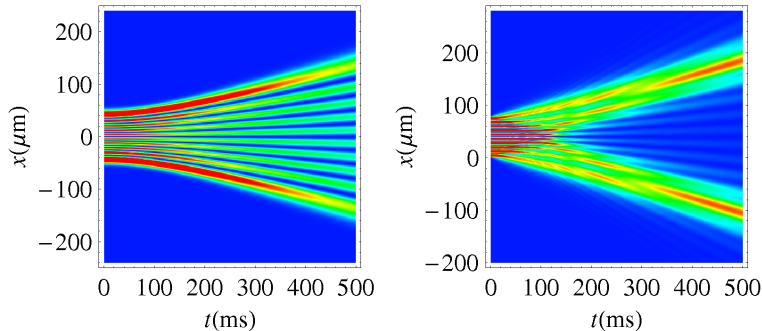


Fig. 7. Density plots of the probability density for the dynamical evolution of a ^{87}Rb atom in the tenth eigenstate released from a harmonic (left) and box (right) traps. $L = 80 \mu\text{m}$ and ω is chosen so that the energies of the eigenstate in both traps coincide.

given in terms of a scaling law of coordinates up to an additional phase which will play no role in our discussion. Indeed, it reads [84]

$$\phi_n(x, t) = \frac{1}{\sqrt{b}} \phi_n\left(\frac{x}{b}, t=0\right) e^{i\frac{m\dot{b}^2}{2\hbar} \frac{t}{b} - i\tau\omega(n+1/2)}, \quad (20)$$

where $\tau := \int_0^t dt' / b^2(t')$ and b must be a solution of $\ddot{b} + \omega(t)b = 0$ with $b(0) = 1$ and $\dot{b}(0) = 0$. An instantaneous turn-off of the harmonic potential at $t = 0$ leads to $b(t) = \sqrt{1 + \omega^2 t^2}$. Figure 7 shows the expansion of a single particle wavefunction suddenly released from a HO and a HW trap. If the particles are in the ground state of the trap the evolution is alike. However, for any excited state a remarkable difference appears. For the former case, the scaling law gives rise to a uniform spreading without affecting the initial quantum structure. As can be seen in the x - t density plot, the full width at half maximum (FWHM) becomes linear for any $t \gg \omega^{-1}$. By contrast, whenever the initial trap is box-like, the density profile exhibits a bifurcation into two main branches after the semiclassical time

$$t_n = \frac{mL}{2p_n} = \frac{mL^2}{2n\pi\hbar} \quad (21)$$

of expansion [12]. This is the result of the mapping of the underlying momentum distribution to the density profile expected asymptotically. Indeed, the probability density in k -space for a box eigenstate is $|\tilde{\phi}_n(k)|^2 = \frac{2\pi n^2}{L^3} [1 - (-1)^n \cos(kL)] / (k^2 - k_n^2)^2$, and has two main peaks at $k = \pm k_n$ except for the ground state: $|\tilde{\phi}_1(k)|^2$, is a bell-shaped distribution centered at $k = 0$.

The more general dynamics in an expanding box has been described in [43,85]. The transient dynamics of particles released from a cylindrical trap has also been discussed in [86] and from spherical traps in [23,10,87]. We recall that the 3D s-wave case is tantamount to the 1D problem in half space, with a hard-wall at $x = 0$. One can exploit the method of images [16] to write down the propagator,

$$K_s^{3D}(r, t|r', 0) = K_0(r, t|r', 0) - K_0(-r, t|r', 0), \quad (22)$$

and the wavefunction in the radial coordinate as

$$\psi_s^{3D}(r, t) = \psi_0(r, t) - \psi_0(-r, t), \quad r > 0, \quad (23)$$

where $\psi_0(r, t) = \int_{-\infty}^{\infty} dr' K_0(r, t|r', t' = 0)\psi_0(r', t' = 0)$, $\psi_0(r', t' = 0)$ being the radial wavefunction of the initial state. The effect of interactions during the expansion will be considered in Section 5.

3.1. Phase space representation

3.1.1. The Wigner function

The Wigner function [88],

$$W(x, p) := \frac{1}{\pi\hbar} \int_{-\infty}^{\infty} dy \psi(x+y)^* \psi(x-y) e^{2ipy/\hbar}, \quad (24)$$

is the best known quasi joint probability distribution for position and momentum. Nowadays, it is possible to study it experimentally as has been demonstrated in a series of works [89,90,91,92,93,94]. We recall that the marginals of the Wigner function are precisely the momentum and coordinate probability densities, this is, $\int dx W(x, p) = |\tilde{\psi}(p)|^2$ and $\int dp W(x, p) = |\psi(x)|^2$.

In the context of the Moshinsky shutter, its time evolution was derived for the free case problem [29] and in the presence of a linear potential [95]. The Wigner function for a cut-off plane wave initial condition is ¹

$$W(x, p; p_0, t = 0) = \frac{1}{\pi} \frac{\sin[-2x(p_0 - p)/\hbar]}{p_0 - p} \Theta(-x), \quad (25)$$

which clearly assumes negative values. If the potential is linear or quadratic, the time evolved Wigner function follows classical trajectories,

$$W(x, p; t) = \iint dx_i dp_i \delta[x - x_{cl}(x_i, p_i, t)] \delta[p - p_{cl}(x_i, p_i, t)] W(x_i, p_i; t = 0). \quad (26)$$

For (25) the result is limited to the classically accessible region of phase space. Moreover, we may take the limit $\hbar \rightarrow 0$ to find the classical distribution [29,96,97,95], in which no hint about the quantum oscillations -hallmark feature of DIT- remains.

Similarly, one can describe the time evolution of the eigenstates of a hard-wall trap. At the beginning of the experiment the Wigner function is given by [98]

$$W_{\phi_n}(x, p) = \mathcal{P}_n(x, p) \chi_{[0, L/2]}(x) + \mathcal{P}_n(L - x, p) \chi_{[L/2, L]}(x), \quad (27)$$

where

$$\mathcal{P}_n(x, p) = \frac{2}{\pi\hbar L} \left\{ \sum_{\nu=\pm 1} \frac{\sin[2(p/\hbar + \nu n\pi/L)x]}{4(p/\hbar + \nu n\pi/L)} - \cos\left(\frac{2n\pi x}{L}\right) \frac{\sin(2px/\hbar)}{2p/\hbar} \right\}.$$

Figure 8 shows the stretching of the Wigner function along the x -axis as time goes by. The momentum distribution, being bimodal for all $n > 1$, is responsible for the splitting

¹ Since $\psi(x, t = 0) = e^{ip_0 x/\hbar} \Theta(-x)$ is dimensionless, $W(x, p)$ here has dimensions $[p]^{-1}$.

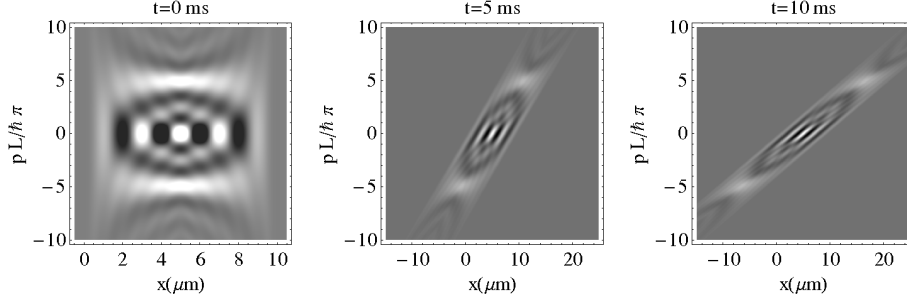


Fig. 8. Time evolution of the Wigner function for the fifth eigenstate of the box trap ($L = 10\mu\text{m}$, for a ^{87}Rb atom). As time goes by, the the quasi-probability distribution is stretched along the x -axis. The gray scale varies from black to white as the function value increases, corresponding the background gray to zero value. Note in particular the presence of negative values (in black), telltale sign of the non-classicality of the state.

in real space for $t > t_n$ already noticeable at $t = 5$ ms. For a general Hamiltonian the propagation of a Wigner function obeys the quantum Liouville equation [88,99]

$$\partial_t W(x, p; t) + \frac{p}{m} \partial_x W(x, p; t) - \sum_{l=0}^{\infty} \frac{(-1)^l (\hbar/2)^{2l}}{(2l+1)!} \partial_x^{2l+1} V(x) \partial_p^{2l+1} W(x, p; t) = 0. \quad (28)$$

In such a way, the phase space description of transient effects can be extended to tunneling problems as well [30,100].

The Wigner function has been also proposed to study the quantum transient response to changes in an externally applied voltage in semiconductor structures [101], see also Section 8, dynamics of polaron formation in compound semiconductors [102], or for transients in scattering processes [103] and classical-quantum comparisons [104].

3.1.2. Symplectic tomography

A related representation in phase space is symplectic tomography [105]. The wave function $\psi(x)$ or the density matrix $\rho(x, x')$ can be mapped onto the standard positive distribution $\mathcal{W}(X, \mu, \nu)$ of the random variable X depending on two real extra parameters, μ and ν . The symplectic tomogram can be related to the Wigner function $W(x, p)$ [88],

$$\mathcal{W}(X, \mu, \nu) = \int W(x, p) \delta(X - \mu x - \nu p) \frac{dx dp}{2\pi\hbar} \quad (29)$$

as its Radon transform. The parameters μ and ν can be expressed in the form $s \cos \theta$, $\nu = s^{-1} \sin \theta$, so that $s > 0$ is a real squeezing parameter and θ is a rotation angle. Then the variable X is identical to the position measured in the new reference frame in the phase-space which has new scaled axes sz and $s^{-1}p$ and rotated by an angle θ . The Moshinsky solution in the tomographic representation reads [29]

$$\mathcal{W}(X, \mu, \nu) = \frac{1}{2|\mu|} \left\{ \left[\frac{1}{2} + C(\xi) \right]^2 + \left[\frac{1}{2} + S(\xi) \right]^2 \right\}, \quad (30)$$

where

$$\xi = \frac{k(\mu\tau + \nu) - X}{\sqrt{2\mu(\mu\tau + \nu)}} \quad (31)$$

with $\tau = \hbar t/m$. In the reference frame with $(\mu, \nu) = (1, 0)$, the quantum tomogram reduces to the density profile in Eq. (6).

3.2. Propagation of wavepackets with sharp boundaries.

The sharp boundaries of the initial wavefunction considered so far, which also arise naturally in the Zeno dynamics under periodic spatial projections [106], might cast some doubt on the realizability of DIT. The study of the generic time propagation of initially confined wave-packets has shed new light on the effects of the boundaries on quantum transients at short times [107,108,109]. In the spirit of the Moshinsky shutter, let us consider a state $\psi(x, t = 0)$ with support in the negative semiaxis ($x < 0$), and denote its Fourier transform by

$$g(k) = \frac{1}{(2\pi)^{1/2}} \int \psi(x, t = 0) e^{-ikx} dx. \quad (32)$$

For any $t > 0$ it follows that

$$\psi(x, t) = \frac{1}{(2\pi)^{1/2}} \int g(k) M(x, k, t) dk. \quad (33)$$

An expansion of the Moshinsky function with respect to k , allows to perform the integral in (33), and to express the solution in terms of derivatives of the initial state $\psi(x, t = 0)$ at the boundary $x = 0$,

$$\psi(x, t) = \frac{1}{(2\pi)^{1/2}} M\left(x, -i\frac{\partial}{\partial y}, t\right) \psi(y, t = 0) \Big|_{y=0}. \quad (34)$$

Expanding in a power series of $(\hbar t/2m)^{1/2}x = \eta$, one finds for $\hbar t/2mx^2 \ll 1$,

$$\begin{aligned} \sqrt{2\pi}\psi(x, t) &= \sqrt{\frac{i}{\pi}} e^{\frac{imx^2}{2\hbar t}} \{ \eta - 2i\eta^3(1 + x\partial_y) \\ &\quad - 4\eta^5[3(1 + x\partial_y) + x^2\partial_y^2 + \dots] \} \psi(y, t = 0) \Big|_{y=0}. \end{aligned} \quad (35)$$

So, for short times, the value of the wavefunction depends exclusively on $\psi(x, t = 0)$ and has a $t^{1/2}$ dependence, whereas should $\psi(x, t = 0)$ vanish, higher order terms are to be considered. The effect of the exact wave packet boundary may however be washed out at longer times as demonstrated by the revival effect, see 4.4.

4. Beam chopping and formation of pulses

4.1. Quantum transients in beam chopping

Diffraction in time is generally associated with the release of a matter wave initially confined in a given region of space. Nonetheless, the opposite problem is of great physical interest in interferometry, namely, the chopping of a beam by a shutter, or mirror.

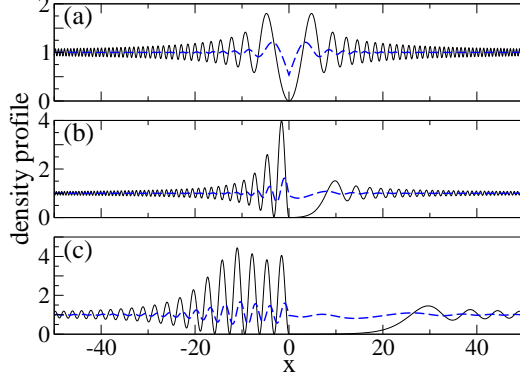


Fig. 9. Snapshots of the density profile of a chopped beam ($\hbar = m = 1$) with a) $k = 0$ at $t = 5$, b) $k = 1$ at $t = 5$, and c) $k = 1$ at $t = 20$. The solid line corresponds to the totally reflecting shutter ($\nu \rightarrow \infty$) in Eq. (36), while the dashed line is for a finite δ -potential with $\nu = 0.25$, see Eq. (38).

Consider a monochromatic beam described by a travelling plane-wave $\psi(x, t = 0) = e^{ikx}$ and the action of a totally reflecting mirror suddenly turned on at $x = 0$ and $t = 0$. For all $t > 0$ the beam is effectively split into two different parts. Noticing that the corresponding propagator is that of a hard-wall at the origin, $K_{wall}(x, t|x', 0) = K_0(x, t|x', 0) - K_0(-x, t|x', 0)$, the evolution of the beam is

$$\psi(x, t) = \begin{cases} M(x, k, t) - M(-x, k, t), & x < 0 \\ M(-x, -k, t) - M(x, -k, t), & x \geq 0, \end{cases} \quad (36)$$

where we have neglected the width of the mirror for simplicity. From the asymptotic properties of the Moshinsky function (see Appendix B) it is clear that the matter wave $\psi(x) = 2i \sin(kx) e^{-i \frac{\hbar k^2 t}{2m}}$ is eventually formed at the left of the mirror. The effect of finite reflectivity of the shutter can be taken into account considering a delta mirror $V(x) = \eta \delta(x)$ which represents a weak and narrow potential. The explicit dynamics is slightly more involved, for the propagator is [110]

$$K_\delta(x, t|x', 0) = K_0(x, t|x', 0) + \varkappa M(|x| + |x'|, -i\varkappa, \hbar t/m), \quad (37)$$

with $K_0(x, t|x', 0)$ as in (3) and $\varkappa = m\eta/\hbar^2$. Using the integrals in Appendix B, it turns out that

$$\psi(x, t) = e^{ikx - i\hbar k^2 t/2m} - \sum_{\nu=\pm 1} \frac{\varkappa}{\varkappa - i\nu k} [M(|x|, \nu k, t) - M(|x|, -i\varkappa, t)], \quad (38)$$

which asymptotically, at long times, tends to

$$\psi(x, t) \sim e^{-i\hbar k^2 t/2m} \left[\frac{k}{k + i\varkappa} e^{ikx} - \frac{\varkappa}{k - i\varkappa} e^{-ikx} \right]. \quad (39)$$

This is nothing but the stationary scattering state of the mirror with the energy of the initial beam (notice that $\frac{k}{k + i\varkappa}$ and $-\frac{\varkappa}{k - i\varkappa}$ are the corresponding transmission and

reflection probability amplitudes, respectively). The dynamical buildup of this standing matter-wave after the action of the shutter is illustrated in Fig. 9.

Further work on beam chopping and pulse formation has almost invariably been carried out using the “quantum source approach”, to which we now turn our attention.

4.2. Formation of single pulses

The quantum mechanical effects of beam chopping have been studied in time-dependent neutron optics [111,112]. The energy distribution of the initial beam is expected to be modified in this process in agreement with a time-energy uncertainty relation [23,24]. In this section we examine the formation of a single-pulse of duration τ from a quasi-monochromatic quantum source $\psi(x=0, t) \sim e^{-i\omega_0 t}$ modulated according to a given aperture function $\chi^{(1)}(t)$.² Here, the superscript denotes the creation of a single pulse [23,24,111,112,113,11,12,15], and the free dispersion relation holds, $\omega_0 = \hbar k_0^2/2m$. Many works have been carried out within this approximation in neutron interferometry [111,112,114], considering also a triangular [111,113] or more general apodized aperture functions [12], atom-wave diffraction [11], tunneling dynamics [58,115,116,117,33,34,32], and absorbing media [36]. After the experimental realization of a guided atom laser [118], the same formalism has been employed to describe the dynamics in such system [15].

For the sake of concreteness, let us focus on the family of aperture functions

$$\chi_n^{(1)}(t) = \sin^n(\Omega t)\Theta(t)\Theta(\tau - t), \quad (40)$$

with $\Omega = \pi/\tau$ [12,15]. The solution for an arbitrary aperture function is described in Section 4.3. We first note that the energy distribution varies for increasing n and T . The energy distribution of the associated wavefunction is proportional to $\omega^{1/2}|\widehat{\psi}_n^{(1)}(x=0, \omega)|^2$ [119,15], where $\widehat{\psi}_n^{(1)}(x=0, \omega) = (2\pi)^{-1/2} \int dt \exp[i(\omega - \omega_0)t]\chi_n^{(1)}$. For increasing n , the aperture function becomes smoother broadening the energy distribution. Similarly, the smaller the time for pulse formation τ , the broader is its associated energy distribution. Indeed, whenever $\hbar\omega_0\tau < 1$, the distribution is shifted to higher energy components.

As an example, let us consider the case $\chi_0^{(1)}(t) = \Theta(t)\Theta(\tau - t)$ corresponding to a rectangular single-slit in time which is switched on and off at infinite velocity. The time evolution of the pulse is given by

$$\begin{aligned} \psi_0^{(1)}(x, k_0, t; \tau) = & [M(x, k_0, t) + M(x, -k_0, t)] \\ & - \Theta(t - \tau)e^{-i\omega_0\tau} [M(x, k_0, t - \tau) + M(x, -k_0, t - \tau)]. \end{aligned} \quad (41)$$

If $t < \tau$, before the pulse has been fully formed, the problem reduces to that of a suddenly turned-on source, $\psi_0^{(1)}(x, k_0, t < \tau) = M(x, k_0, t) + M(x, -k_0, t)$, discussed in 2.1. An explicit calculation of the energy distribution of the resulting pulse, taking the overlap of the wavefunction with the free particle eigenstates which vanish at the closed shutter [23,24], shows that

² Baute, Egusquiza and Muga [119] have made explicit the relation between a source boundary condition where $\psi(x=0, t)$ is specified for $t > 0$ and the standard initial value problem in which $\psi(x, t=0)$ is specified. The simple “Kirchhoff boundary condition” $\psi(x=0, t) = \Theta(t)e^{i\omega_0 t}$ is discussed further in 7.2, see also [120].

$$\mathcal{P}(E; E_0, \tau) = \mathcal{N} \sqrt{E} \frac{\sin^2[(E - E_0)\tau/2\hbar]}{(E - E_0)^2},$$

\mathcal{N} being a normalization constant. Such distribution is peaked at the energy of the initial beam $E_0 = \hbar\omega_0$ if $E_0\tau \gtrsim \hbar$ and shifted to higher energies otherwise [15]. Indeed, for some measure of the width ΔE it leads to the time-energy uncertainty relation $\Delta E\tau \simeq \hbar$ [23,24,25,12].

It is illuminating to consider a slightly more complicated aperture function, such as the sine-square (Hanning) function,

$$\chi_2^{(1)}(t) = \sin^2(\Omega t) \Theta(t) \Theta(\tau - t) = \frac{1}{2} \left[1 - \frac{1}{2} \cos(2\Omega t) \right] \Theta(t) \Theta(\tau - t). \quad (42)$$

Defining $k_\beta = \sqrt{2m(\omega_0 \pm 2\Omega)/\hbar}$ with $\beta = \pm 1$, the resulting pulse is described by the time-dependent wavefunction

$$\psi_2^{(1)}(x, k_0, t; \tau) = \frac{1}{2} \left[\psi_0^{(1)}(x, k_0, t; \tau) - \frac{1}{2} \sum_{\beta=\pm 1} \psi_0^{(1)}(x, k_\beta, t; \tau) \right], \quad (43)$$

where the effect of the apodization is to subtract to the pulse with the source momentum two other matter-wave trains associated with k_β , all of them formed with rectangular aperture functions. The effect of creating the pulse by a smooth modulation as opposed to the sudden rectangular aperture function, is to suppress the diffraction sidelobes in the density profile, at the expense of broadening the corresponding energy distribution. These two features are the key elements of apodization in classical optics and Fourier analysis, and hence the effect was dubbed *apodization in time* [12,15].

4.3. Arbitrary modulation of a matter-wave source

Though the dynamics of matter-wave sources associated with different aperture functions has been worked out in detail [24,111,112,113,11,12], it is desirable to tackle the general case. In order to do so, we consider an arbitrary aperture function $\chi(t)$ which is zero outside the interval $[0, \tau]$ [15]. An analytical result can be obtained in such case by means of Fourier series. Noting that

$$\chi(t) = \sum_{r=-\infty}^{\infty} c_r e^{i\frac{2\pi r t}{\tau}} \Theta(t) \Theta(\tau - t) \quad \text{with} \quad c_r = \frac{1}{\tau} \int_0^\tau \chi(t) e^{-i\frac{2\pi r t}{\tau}} dt, \quad (44)$$

the wavefunction at the origin can be written as the coherent superposition of its Fourier components modulated with a rectangular aperture function

$$\psi_\chi(x=0, k_0, t) = \sum_{r=-\infty}^{\infty} c_r e^{-i\omega_r t} \Theta(t) \Theta(\tau - t), \quad (45)$$

with $\omega_r = \omega_0 + 2\pi r/\tau$. Clearly, the subsequent dynamics for $x, t > 0$ reads

$$\psi_\chi(x, k_0, t; \tau) = \sum_{r=-\infty}^{\infty} c_r \psi_0^{(1)}(x, k_r, t; \tau), \quad (46)$$

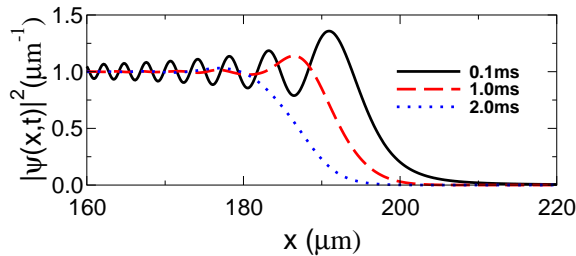


Fig. 10. Apodization in time. Removal of the sudden approximation in the switch of a matter wave source leads to the suppression of oscillations in the beam profile characteristic of the diffraction in time. The ^{87}Rb beam profile is shown at $t = 20\text{ms}$, and $\hbar k_0/m = 1\text{cm/s}$. For increasing τ the amplitude of the oscillations diminishes and the signal is delayed.

where $\psi_0^{(1)}(x, k, t; \tau)$ is defined in Eq. (41), and $\hbar k_r = \sqrt{2m\hbar\omega_r}$, with the branch cut taken along the negative imaginary axis of ω_r . The upshot is that the dynamics of a source with an arbitrary aperture function can be described in terms of the coherent superposition of rectangular pulses associated with each of the Fourier components.

4.4. Diffraction-in-time revival after slow switching

The dynamics of a matter-wave source can be tamed by switching it slowly. For the sake of concreteness, we introduce the continuous switching function

$$\chi^{switch}(t) = \begin{cases} 0 & \text{if } t < 0, \\ \chi(t), & \text{if } 0 \leq t < \tau, \\ 1, & \text{if } t \geq \tau, \end{cases} \quad (47)$$

with a characteristic time scale τ , which we shall refer to as the switching time. The family for which $\chi(t) = \sin^n \Omega_s t$ with $n = 0, 1, 2$ and $\Omega_s = \pi/2\tau$ was considered in [15,121], where it was shown that for fixed τ , the apodization of the beam increases with the smoothness of $\chi(t)$, this is, with n . Note that for $n = 0$, one recovers the sudden aperture $\chi_0(t) = \Theta(t)$ which maximizes the diffraction-in-time fringes. We shall consider a sine-square modulation in what follows ($n = 2$), and concentrate on the dependence on τ .

Increasing the switching time τ leads to an apodization of the oscillatory pattern. As a result the fringes of the beam profile are washed out, see Fig. 10. In this sense, the effect is tantamount to that of a finite band-width source [34], and as already remarked, this is the essence of apodization (in time), the suppression of diffraction by means of broadening the energy distribution [122,19].

However, the apodization lasts only for a finite time after which a *revival* of the diffraction in time occurs, as shown in Fig. 11. The intuitive explanation is that the intensity of the signal from the apodization “cap” associated with the switching process during the interval $[0, \tau]$, decays with time, whereas the intensity of the main signal (coming from the step excitation for $t > \tau$) remains constant. For sufficiently large times, the main signal, carrying its diffraction-in-time phenomenon, overwhelms the effect of the small cap. Indeed, from the linearity of the Schrödinger equation, it follows that the wavefunction is the sum of a “half-pulse” term associated with the switch released during the interval

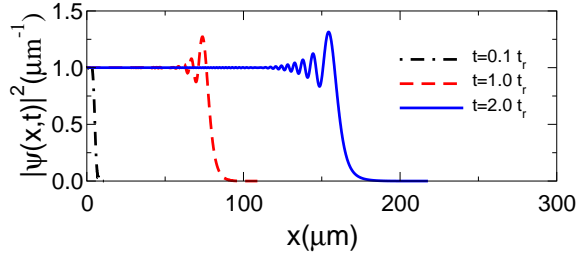


Fig. 11. Revival of the diffraction in time. During the time evolution of an apodized source, there is a revival of the diffraction in time in the time scale $t_r = \omega_0 \tau^2$ ($\tau = 1\text{ms}$, $\hbar k_0/m = 0.5\text{cm/s}$, and $t_r = 16.8\text{ms}$ for a ^{87}Rb source which is switched on following a sine-square function).

$[0, \tau]$ and a semi-infinite beam suddenly turned on at time $t = \tau$. The revival time can be estimated to be [15,121]

$$t_r \approx \omega_0 \tau^2, \quad (48)$$

and plays a similar role to the Rayleigh distance of classical diffraction theory, but in the time domain [123]. The smoothing effect of the apodizing cap cannot hold for times much longer than t_r . This is shown in Fig. 11, where the initially apodized beam profile eventually develops spatial fringes, which reach the maximum value associated with the sudden switching at $t \approx 2t_r$.

4.5. Multiple pulses

4.5.1. Application to atom lasers

Knowledge of the dynamics associated with a single-pulse $\psi^{(1)}(x, t)$ can be used to tackle matter wave sources periodically modulated in time. Frank and Nosov first described the periodic action of a quantum chopper in ultracold neutron interferometry leading to multiple rectangular aperture functions [13,14]. More recently, del Campo, Muga and Moshinsky [15] found the general dynamics of an atom source under an arbitrary aperture function as described in 4.3, and applied it to the description of an atom laser in the non-interaction limit. The experimental prescription for an atom laser depends on the “out-coupling” mechanism. Here we shall focus on the scheme described in [124,125]. The pulses are extracted from a condensate trapped in a magneto-optical trap (MOT), and a well-defined momentum is imparted on each of them at the instant of their creation through a stimulated Raman process. The result is that each of the pulses $\psi^{(1)}$ does not have a memory phase, the wavefunction describing the coherent atom laser being then

$$\phi^{(N)}(x, k_0, t) = \sum_{j=0}^{N-1} \psi^{(1)}(x, k_0, t - jT; \tau) \Theta(t - jT). \quad (49)$$

Such modulation describes the formation of N consecutive $\chi^{(1)}$ -pulses, each of them of duration τ and with an “emission rate” (number of pulses per unit time) $1/T$. The Heaviside function $\Theta(t - jT)$ implies that the j -th pulse starts to emerge only after jT . We can impose a relation between the out-coupling period T and the kinetic energy

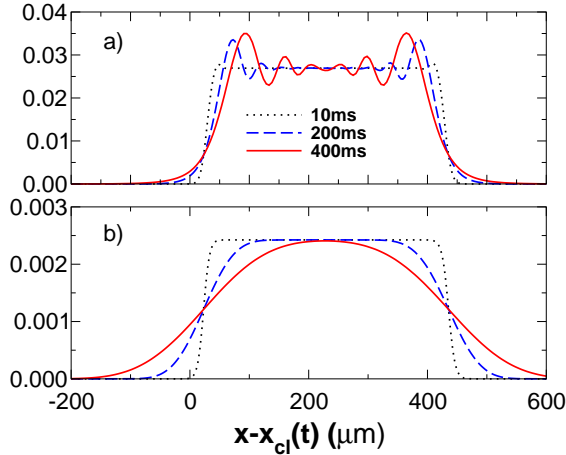


Fig. 12. Dynamics of the density profile of an atom laser a) coherently constructive, b) incoherent case. Note that $x_{cl} = \hbar k_0 t / m$ is the classical trajectory. In all cases the norm is relative to the incoherent case, as explained in the text. (^{23}Na source, modulated by a sine-square function with $\tau = 0.833\text{ms}$, $T = 0.05\text{ms}$, moving at 3.73cm/s , for which the revival time is 174.4ms .)

imparted to each pulse $\hbar\omega_0$, such that $\omega_0 T = l\pi$: if l is chosen an even (odd) integer the interference in the beam profile $|\phi^{(N)}|^2$ is constructive (destructive).

The diffraction in time is a coherent quantum dynamical effect, so we may expect it to be affected by noise in the environment. If the phases between different pulses are allowed to fluctuate, the interference pattern is blurred [126]. Moreover, if there is no phase coherence between different pulses, the resulting density profile becomes the incoherent sum of the single-pulse densities, $\rho(x, t) = \sum_j |\psi^{(1)}(x, k_0, t - jT; \tau)|^2 \Theta(t - jT)$, which we shall use as a reference case.

One advantage of employing stimulated Raman pulses is that any desired fraction of atoms can be extracted from the condensate. Let us define s as the number of atoms out-coupled in a single pulse, $\psi^{(1)}$. The total norm for the N -pulse incoherent atom laser is simply $\mathcal{N}_{inc} = sN$. A remarkable fact for coherent sources is that the total number of atoms \mathcal{N}_c out-coupled from the Bose-Einstein condensate reservoir depends on the nature of the interference [127]. Therefore, in Fig. 12 we shall consider the signal relative to the incoherent case, namely, $|\phi^N(x, t)|^2 / \mathcal{N}_{inc}$.

Note the difference in the time evolution between coherently constructive and incoherent beams in Fig. 12. At short times both present a desirable saturation in the probability density of the beam. However, in the former case a revival of the diffraction in time phenomena takes place in a time scale $\omega_0 \tau^2$, similar to the smooth switching considered in 4.4, whereas the latter develops a bell-shape profile. This revival time can actually be related to the frequency of the BEC reservoir trap ω_{trap} , which determines the width of the out-coupled pulses [121]. Assume that the atoms are out-coupled from the n -th longitudinal mode of the reservoir trap, whose spatial width is $\xi_n = [(n + 1/2)\hbar / m\omega_{trap}]^{1/2}$. Using $\omega_0 = \hbar k_0^2 / 2m$, and the semiclassical relation $\tau_n = m\xi_n / \hbar k_0$, the revival time becomes

$$t_r^{(n)} = \left(n + \frac{1}{2}\right) \frac{1}{2\omega_{trap}}. \quad (50)$$

For a non-interacting BEC, one can take $n = 0$. Therefore, when the trap of the BEC reservoir is very tight, DIT will arise ever since the creation of the atom laser beam, while if the trap is wide, so will be the out-coupled pulses and apodization will suppress the oscillations on the density profile for times smaller than the revival time. Conversely, if the initial front of the beam profile is known to be smoothed out in a given length scale ξ , it can be shown that density modulations arise in the time scale $m\xi^2/\hbar^2$.

4.5.2. Coherent control

As an outlook, the techniques of “coherent control” [128,129,130], could merge with the atom laser to design matter-wave pulses for specific aims. A remarkable example is the deterministic generation of arbitrary de Broglie wave-fronts in atom lithography [131]. Coherent control has been applied in recent years to a wide range of systems in atomic, molecular, solid-state physics, semiconductor devices, biology or quantum information. The basic idea is to make use of quantum interference to manipulate the dynamics with the aid of a control field, typically formed by laser light. Examples of objectives so far are selective bond breaking, choosing a reaction pathway, or performing a quantum information operation. The experimental output may be used in the optimization procedure with closed-loop learning control techniques. Instead of a control field made of light, we envision the formation of control matter-fields by combining matter-wave pulses with tunable intensity, energy, timing and phase. An elementary example is the formation of a continuous atom laser by constructive interference, as discussed above, and other applications may follow in which the elementary pulses and their transients will be helpful building blocks for analyzing the resulting matter field.

4.5.3. Ultra-short laser pulses

Ultrashort laser pulses in femtosecond or attosecond time domains are a basic tool in coherent control research and applications. These nowadays manipulable pulses are able to induce many transient phenomena for nuclear or electronic motion. Using pump and probe or streaking methods, the transient dynamics following a system excitation may be recorded and/or steered. A detailed account is out of the scope of this review and impossible to summarize here, but we shall mention briefly some recent examples to show that there exists a link with work on elementary quantum transients which has not been fully exploited and is worth pursuing.

Strong field ionization of atoms via tunnelling can be nowadays followed with attosecond resolution so that some aspects of electron tunnelling (see others in Section 7) can be observed [132,133]. Impressive “streaking techniques” are used for this purpose, in which emission times and momenta of electrons are mapped, thanks to the action of the short pulses on the ejected electron, into final ion and electronic momenta which are readily observable with time-of-flight detectors. The emission may also be controlled so as to produce double or multiple time slits with few-cycle pulses and the corresponding interference-in-time phenomena [134]. Simple models for apodized pulses or time-dependent shutters (see e.g. Section 2.2) could be contrasted with these experimental procedures and may help to interpret the observed results and design new experiments.

5. Dynamics of ultracold gases in tight-waveguides

The models described so far do not explicitly consider quantum statistics and rigorously only apply to single-particles. Therefore, even though the use of semi-infinite beams and quantum sources is suitable to describe neutron optics and ideal atom waves, a more rigorous approach is desirable. As already pointed out by Stevens, a consistent interpretation for several -non-interacting- particles requires the appropriate quantum symmetrization [135]. Moreover, there is nowadays a flurry of theoretical and experimental work dealing with ultracold atomic gases in the non-linear and strongly interacting regimes.

Ultracold atoms in waveguides, tight enough so that the transverse degrees of freedom are frozen out [136,137], are accurately described by the Lieb-Liniger (LL) model,

$$\hat{\mathcal{H}}_{LL} = -\frac{\hbar^2}{2m} \sum_{i=1}^N \frac{\partial^2}{\partial x_i^2} + g_{1D} \sum_{1 \leq i < j \leq N} \delta(x_i - x_j), \quad (51)$$

exactly solvable by coordinate Bethe ansatz [138]. This model describes N bosons in one-dimension interacting with each other through a short-range δ -function. The use of such pseudo-potential is justified provided that the scattering is restricted to s -wave type in the zero-energy limit of relevance to ultracold temperatures, when the details of the true interparticle potential become unimportant [139].

The cloud can then be characterized by the interaction parameter $\gamma = mg_{1D}L/\hbar^2N$, where g_{1D} is the one-dimensional coupling strength, L the size of the system, m and N the mass and number of atoms respectively; γ can be varied [136] allowing to realize the mean-field regime ($\gamma \ll 1$) or the Tonks-Girardeau regime ($\gamma \gg 1$) [140].

5.1. Dynamics in the Tonks-Girardeau regime

We shall next consider the dynamics of strongly interacting bosons confined in a tight-waveguide, the so-called Tonks-Girardeau (TG) gas. In the TG regime, bosons mimic an effective Pauli exclusion principle as a result of the repulsive interactions rather than the quantum statistics itself. The Fermi-Bose (FB) duality [141,142,143,144] provides the many-body wavefunction of N strongly interacting bosons from that of a free Fermi gas with all spins frozen in the same direction. The Fermi wavefunction, antisymmetric under permutation of particles, is built as a Slater determinant, with one particle in each eigenstate ϕ_n of the trap,

$$\psi_F(x_1, \dots, x_N) = \frac{1}{\sqrt{N!}} \det_{n,k=1}^N \phi_n(x_k). \quad (52)$$

Whenever the position of two particles coincide, the wavefunction ψ_F vanishes as a consequence of the Pauli exclusion principle. This contact condition is the desirable one in the TG gas due to the effectively infinite repulsive interactions. Symmetrization can then be carried out “by hand”, applying the so-called “antisymmetric unit function”

$$A = \prod_{1 \leq j < k \leq N} \text{sgn}(x_k - x_j), \quad (53)$$

so that

$$\psi_B(x_1, \dots, x_N) = \mathcal{A}(x_1, \dots, x_N)\psi_F(x_1, \dots, x_N). \quad (54)$$

This is the Bose-Fermi map introduced by Girardeau in 1960 [141]. A remarkable advantage of this mapping is that it holds for time dependent processes (governed by one-body external potentials), since the \mathcal{A} operator does not include time explicitly [144,142]. The glaring upshot is that as far as local correlation functions are concerned, to deal with the many-body TG gas it suffices to work out the single particle problem, since

$$|\psi_B(x_1, \dots, x_N; t)|^2 = |\psi_F(x_1, \dots, x_N; t)|^2. \quad (55)$$

In particular, from the involutivity of the \mathcal{A} operator ($\mathcal{A}^2 = 1$) and the fact that $\langle \phi_n | U^\dagger U | \phi_m \rangle = \delta_{nm}$, where U is the time-evolution operator, it follows that the time-dependent density profile can be calculated as [144]

$$\rho(x, t) = N \int |\psi_B(x, x_2, \dots, x_N; t)|^2 dx_2 \cdots dx_N = \sum_{n=1}^N |\phi_n(x, t)|^2. \quad (56)$$

Once the single-particle time evolution is known, we are ready to study the spreading of the TG gas through its density profile, Eq. (56).

For the HO trap, several studies have been carried out describing the scaling law governing the expansion of the TG gas [54,145] as well as the dynamical fermionization of the system exhibited in the momentum distribution [146,147]. Here, we shall focus on the transition to the ballistic regime in the expansion from both HO and HW traps. Moreover, we shall be interested in low number of particles N , where the mean-field approach is not accurate, missing the spatial anti-bunching in the density profile [148,144]. If we are to compare the expansion from both traps, it seems natural to consider that, for the same number of particles, the total energy of the TG gas is to be the same. Then, the following relation must hold between the harmonic frequency and the length of the box,

$$\omega = \frac{\hbar\pi^2(N+1)(2N+1)}{6mL^2N}. \quad (57)$$

For the HO trap, the similarity transformation

$$\rho(x, t) = \frac{1}{\sqrt{1 + \omega^2 t^2}} \rho\left(\frac{x}{\sqrt{1 + \omega^2 t^2}}, 0\right) \quad (58)$$

has been shown to hold, where the ballistic regime sets for $t \gg \omega^{-1}$ [54]. However, as we have already discussed, no such simple expression can be obtained for the hard-wall trap, exhibiting the dynamics a lack of self-similarity (which should be clear once the transient features entailed in Eq. (17) are recognized), see Fig. 13. The $\pm p_N = \pm \hbar N \pi / L$ components govern in this case the width of the expanding cloud for $t \gtrsim t_N = mL^2 / 2N\pi\hbar$.

Figure 14 shows the variation in time of the full width at half maximum (FWHM) for a TG gas expanding from both types of traps. The transition to the ballistic regime is sharp for the HW trap at t_N , whereas for the HO happens gradually, and only sets for $t \gg \omega^{-1}$. This fact, together with transient versus self-similar dynamics, points out the relevance of the confining geometry.

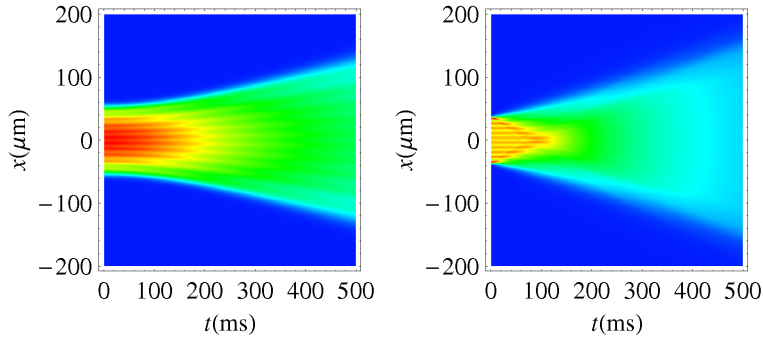


Fig. 13. Density plots of the probability density ρ for a TG gas composed of $N = 10$ atoms of ^{87}Rb released from a harmonic (left) and box-like (right) trap. $L = 80 \mu\text{m}$, and the frequency ω is chosen according to Eq. (57).

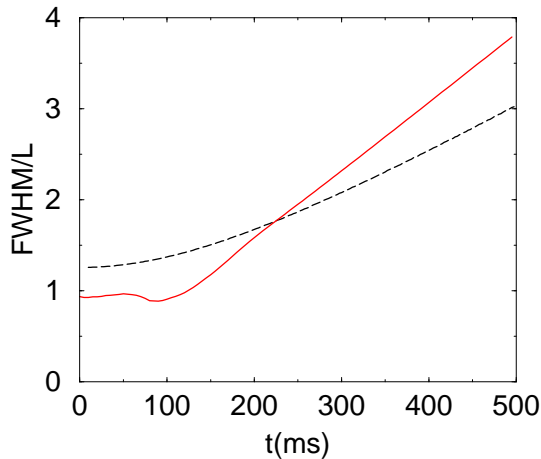


Fig. 14. Time dependence of the FWHM of a cloud of $N = 10$ ^{87}Rb atoms in the Tonks-Girardeau regime, released from a box-like ($L = 80 \mu\text{m}$, solid line) and harmonic (dashed line) traps. Note that the transition to the ballistic regime is sudden when the gas is released from a box-like trap, but smooth if initially confined in a harmonic trap (parameters as in Fig. 13).

The density profile we have described so far in the TG regime, is actually the same that for spin-polarized non-interacting fermions. We note that for the latter the momentum distribution

$$n(k) = \frac{1}{2\pi} \int dx dy e^{ik(x-y)} \rho(x, y) \quad (59)$$

remains invariant under time evolution provided that the momentum operator commutes with the purely kinetic Hamiltonian. Since the reduced single-particle density matrix (RSPDM) of spin-polarized fermions is

$$\rho(x, y) = N \int dx_2 \dots dx_N \psi_F(x, x_2, \dots, x_N)^* \psi_F(y, x_2, \dots, x_N),$$

$$= \sum_{n=1}^N \phi_n^*(x) \phi_n(y), \quad (60)$$

the momentum distribution is the sum

$$n_F(k) = \sum_{n=1}^N |\tilde{\phi}_n(k)|^2, \quad (61)$$

$\tilde{\phi}_n$ denoting the Fourier transform of ϕ_n .³ However, the momentum distribution of an expanding Tonks-Girardeau gas exhibits a transient dynamics. An efficient way to compute the RSPDM has been recently derived by Pezer and Buljan [149] explicitly using the Bose-Fermi map and the Laplace expansion of the determinant, see also [150]. Thanks to the orthonormality of the single-particle eigenstates, the RSPDM is given by

$$\rho_{TG}(x, y) = \sum_{l, n=1}^N \phi_l^*(x) A_{ln}(x, y) \phi_n(y), \quad (62)$$

where

$$\mathbf{A}(x, y) = (\mathbf{P}^{-1})^T \det \mathbf{P}, \quad (63)$$

and the elements of the matrix \mathbf{P} are

$$P_{ln} = \delta_{ln} - 2 \int_x^y dz \phi_l^*(z) \phi_n(z) \quad (64)$$

for $x < y$ with no loss of generality. A generalization of this result for hard-core anyons can be found in [151].

From (59) and (62), the time-evolving $n(k, t)$ can then be found. For $t = 0$ it presents a prominent peak at $k = 0$, whereas as the cloud expands and the particles cease to interact, the interaction energy is gradually transformed into kinetic energy, and the asymptotic momentum distribution is the quasi-momentum distribution, namely, the flat one typical of the dual Fermi system. This is the so-called dynamical fermionization [146,147], illustrated in Fig. 15 for a TG gas expanding from a box-like trap.

In conclusion, strongly repulsive interactions tend to suppress quantum transients in the density profile, while enriching the dynamical picture in the momentum space. Conversely, attractive interactions have been shown to lead to an enhancement of density modulations in both expanding clouds and propagating beams [152].

5.2. Finite interactions: dynamics of Lieb-Liniger gases

Whenever the interactions are finite, the exact dynamics of ultracold gases becomes a highly non-trivial subject. The first steps to cope with it made use of a hydrodynamical approach [137,54,145] and numerical simulations, but only recently have the required

³ Note the errata of the published version (Physics Reports 476, 1-50, 2009), where in Eq. (60) ψ_n^* should read ϕ_n^* , and in Eqs. (62) and (64) ψ_l^* should read ϕ_l^* , as corrected here.

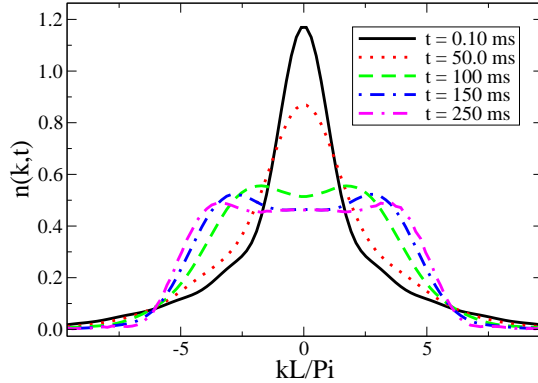


Fig. 15. Dynamical fermionization of $N = 5$ ^{87}Rb atoms in the Tonks-Girardeau regime, released from a box ($L = 80 \mu\text{m}$). The asymptotic momentum distribution is that of a spin-polarized ideal Fermi gas.

analytical techniques been developed [153,154,155]. Within the Lieb-Liniger model the wavefunction of the gas $\psi_B(x_1, \dots, x_N, t)$ describes N identical δ -interacting bosons in one-dimension governed by the Hamiltonian (51) [138]. It is customary to express the corresponding time-dependent and many-body Schrödinger equation (TDMBSE) with ‘‘Lieb-Liniger’’ units ($2m = 1, \hbar = 1$) in the form

$$i \frac{\partial \psi_B}{\partial t} = \sum_{i=1}^N \left[-\frac{\partial^2}{\partial x_i^2} + V(x_i, t) \right] \psi_B + \sum_{1 \leq i < j \leq N} 2c \delta(x_i - x_j) \psi_B. \quad (65)$$

We assume that the gas is initially confined in an external potential $V(x)$, which is suddenly turned off at $t = 0$, so that the cloud starts expanding. Therefore for $t > 0$ the domain of each coordinate is the whole real line $x_j \in \mathbb{R}$.

The wavefunction ψ_B is totally symmetric under permutations of particles, and hence it suffices to focus on the fundamental sector $R_1 : x_1 < x_2 < \dots < x_N$, where the TDMBSE reduces to

$$i \frac{\partial \psi_B}{\partial t} = - \sum_{i=1}^N \frac{\partial^2 \psi_B}{\partial x_i^2}. \quad (66)$$

The Lieb-Liniger contact conditions are responsible for creating a cusp in the wave function when two particles touch. This can be expressed as a boundary condition at the borders of R_1 [138],

$$\left[1 - \frac{1}{c} \left(\frac{\partial}{\partial x_{j+1}} - \frac{\partial}{\partial x_j} \right) \right]_{x_{j+1}=x_j} \psi_B = 0. \quad (67)$$

These boundary conditions can easily be rewritten for any permutation sector. In the TG limit ($c \rightarrow \infty$), the cusp condition implies an effective exclusion principle whereby the wavefunction identically vanishes when two particles are in contact [141]. Exact solutions of the time-dependent Schrödinger equation (65) can be obtained by using a Fermi-Bose mapping operator [156,154,155] acting on fermionic wave functions. Assume $\psi_F(x_1, \dots, x_N, t)$ is an antisymmetric (fermionic) wave function, which obeys the

Schrödinger equation for a non-interacting Fermi gas, $i\frac{\partial\psi_F}{\partial t} = -\sum_{i=1}^N \frac{\partial^2\psi_F}{\partial x_i^2}$. Then, the wavefunction of the Lieb-Liniger gas can be written as

$$\psi_B = \mathcal{N}_c \hat{O}_c \psi_F, \quad (68)$$

using the generalized Fermi-Bose mapping operator

$$\hat{O}_c = \prod_{1 \leq i < j \leq N} \left[\text{sgn}(x_j - x_i) + \frac{1}{c} \left(\frac{\partial}{\partial x_j} - \frac{\partial}{\partial x_i} \right) \right], \quad (69)$$

up to the normalization constant \mathcal{N}_c [156]. This surprising result states that the time evolution of a Lieb-Liniger gas at a given time t can be computed from that of non-interacting fermions at the same time, and only then take into account the interactions through the generalized Fermi-Bose map. The applicability of this map is not limited to the expansion dynamics of an excited Bose gas initially confined in an external potential $V(x)$, for it actually describes the ground state whenever $[\hat{O}_c, V(x)] \approx 0$. Nonetheless, as the gas expands in 1D, the linear density decreases while the effective coupling constant becomes larger, prompting the system to enter the strongly interacting regime. Indeed, the asymptotic form of the wavefunction can be probed to possess the Tonks-Girardeau structure [155]. However, the properties of this asymptotic state can considerably differ from the properties of the Tonks-Girardeau gas in the ground state of an external potential [155]. We note that such dynamics is restricted to free expansion, while the inclusion of specific boundary conditions (periodic, Dirichlet, Neumann) and its extension to other quantum statistics (interacting fermionic or anyonic systems) and multi-component, multi-channel problems remain as interesting open problems.

5.3. Finite interactions: mean-field approach

By now, it should be clear that suddenly released matter-waves initially confined in a compact support exhibit quantum transients. Nonetheless, the effect of strongly repulsive interactions tends to smooth out the density profile in the resulting dynamics, as in the Tonks-Girardeau gas. In this section we discuss the effect of the interactions on quantum transients within the mean-field approach.

Weakly interacting ultracold gases in 1D are then described by the Gross-Pitaevskii equation, as a result of approximating the wavefunction of the Bose-Einstein condensate by the Hartree-Fock ansatz $\Psi(x_1, \dots, x_N) = \prod_{i=1}^N \phi(x_i)$. For an effectively 1D Bose-Einstein condensate, in the presence of some external potential $V(x)$ (i.e. the trap) the condensate wavefunction $\Phi(x) = \sqrt{N}\phi(x)$ obeys the 1D time-dependent Gross-Pitaevskii equation

$$i\hbar \frac{\partial \Phi(x, t)}{\partial t} = -\frac{\hbar^2}{2m} \frac{\partial^2 \Phi(x)}{\partial x^2} + \left[V(x) + g_{1D} |\Phi(x)|^2 \right] \Phi(x), \quad (70)$$

where m is the atomic mass, and $g_{1D} = -2\hbar^2/m a_{1D}$ the effective 1D coupling parameter, a_{1D} being a known function of the three-dimensional scattering length [136]. In the mean-field regime, for low enough temperatures, the phase fluctuations can be suppressed [157]. Making use of time-dependent shutters a way to enhance the diffraction in time was shown in [42]. An alternative way is to make the interactions in the system attractive, (say, by

means of a Feshbach resonance [51]) as discussed in [152]. Quantum transients arising in suddenly released matter-waves can then be enhanced in systems governed by attractive interactions and suppressed in the repulsive case.

Indeed, it is worthy to consider the case in which the mean-field interaction dominates over the kinetic energy (but at boundaries). In such a case, the so-called Thomas-Fermi approximation assumes that the kinetic energy can be neglected in the Hamiltonian so that the time-independent Gross-Pitaevskii equation reads $\mu\Phi_{TF}(x) = [V(x) + g_{1D}|\Phi_{TF}(x)|^2]\Phi_{TF}(x)$, where μ is the chemical potential. The Thomas-Fermi wavefunction is then given by $\Phi_{TF}(x) = [(\mu - V(x))/g_{1D}]^{1/2}$ whenever $\mu > V(x)$ and zero elsewhere. The dynamics of the Thomas-Fermi density profile $n_{TF}(x) = |\Phi_{TF}(x, t)|^2$ after switching off the trap obeys well-known scaling laws with no transient behavior whatsoever [158,159]. For instance, for the case of a harmonic trap $V(x, t) = m\omega(t)^2x^2/2$,

$$n_{TF}(x, t) = \frac{1}{b(t)} n \left[\frac{x}{b(t)}, t = 0 \right], \quad (71)$$

where the scaling coefficient satisfies the differential equation $\ddot{b} = \omega^2/b^2$ subjected to the initial conditions $b(0) = 1$, and $\dot{b}(0) = 0$. Clearly, the dynamics entailed in Eq. (71) lacks any DIT-related transient.

5.4. Turning interactions on and off in a Bose-Einstein Condensate

The world of cold atoms provides many interesting transients due to the possibility to turn on and off interatomic and/or external interactions. Ruschhaupt *et al.* [160] have examined the short-time behavior of a Bose-Einstein condensate when the interatomic interaction is negligible for the preparation in the harmonic trap, and strongly increased when the potential trapping is removed. A quantum interference effect in momentum space is then found in the Thomas-Fermi regime: the momentum distribution expands due to the release of mean field energy and the number of peaks increases with time one by one because of the interference of two positions in coordinate space contributing to the same momentum. The effect is stable in a parameter range and could be observed with current technology. Interestingly enough, similar abrupt changes in time of the coupling constant g_{1D} [161] and density perturbations [162] can also induce self-modulations in the density profile and shock waves. The appearance of shock waves is a phenomenon also present in classical non-linear equations and is out of the scope of this review. We refer the reader to the good existing works on the topic [163,164,165]. More generally, the dynamics after a quantum quench in the Hamiltonian in a many-body system exhibits non-trivial quantum transients, i.e. see [166] and reference therein. Nonetheless, one has to bear in mind that the nature of this type of transient is dramatically different of those related to the DIT, for the non-linear interactions entail a dispersion relation different from the free one.

5.5. State reconstruction

The advances in the dynamical description of ultracold atoms in tight-waveguides have paved the way to the study of transients of Lieb-Liniger gases [153,154,155]. Nevertheless,

the sudden quench of interactions using Feshbach resonances [51] combined with a switch of the confining potential stands for its applications in tomography of trapped ultracold gases [55]. The evolution of the essentially free single-particle density profile, $n_0(x, t)$, allows us to obtain the reduced density matrix at $t = 0$,

$$\rho(k, k') = \frac{\hbar}{m} \int \tilde{n}_0(k' - k, t) |k' - k| e^{i \frac{\hbar(k'^2 - k^2)t}{2m}} dt, \quad (72)$$

where the Fourier transform of the density profile reads

$$\tilde{n}_0(k, t) = \frac{1}{2\pi} \int n_0(x, t) e^{-ikx} dx. \quad (73)$$

Alternatively, the RSPDM can be diagonalized [167] as $\rho(x, x'; t = 0) = \sum_j \lambda_j \varphi_j^*(x) \varphi_j(x')$ in terms of the orthonormal natural orbitals $\varphi_j(x)$ with occupation numbers $\lambda_j > 0$ satisfying $\int \rho(x, x') \varphi_j(x) dx = \lambda_j \varphi_j(x')$ and $\sum_{j=1}^N \lambda_j = N$. Under free evolution, having set up $c(t > 0) = 0$, the density profile reads

$$n_0(x, t) = \rho(x, x; t) = \sum_j \lambda_j |\varphi_j(x, t)|^2, \quad (74)$$

with $\varphi_j(x, t) = (2\pi)^{-1/2} \int dk \tilde{\varphi}_j(k) e^{ikx - i\hbar k^2 t/2m}$, which, using Eq. (72), leads to the density matrix $\rho(k, k') = \sum_j \lambda_j \tilde{\varphi}_j^*(k) \tilde{\varphi}_j(k')$. Experimental measurements are restricted to $t > 0$, limiting the possibility of state reconstruction by means of Eq. (72), but assuming time-reversal invariance or using spatial symmetries of the system, the integral in time can be extended over the whole real line [92]. More generally, once the interactions in the system are negligible, the reconstruction of the RSPDM of the initial quantum state from the cloud dynamics in a potential $V(x)$ has been successfully addressed by Leonhardt and coworkers within the optical tomography [168,169]. Remarkably, the Wigner function of non-interacting Helium atoms has been experimentally measured by looking at the time-evolution of the density profile [92], from which higher order correlations of the trapped gas can also be inferred [170].

6. Transient effects with external potentials

Transient effects have been considered so far mostly for motion in free space but new and interesting features arise in the presence of external potentials. Most work has been carried out within the sudden approximation for the shutter, namely, its instantaneous release. The quantum transients with short-range external potentials often admit an exact solution, as is the case for a δ -barrier [171,110,172,173,174,30,67,108], the time-dependent δ -barrier [6,40], and the Kroning-Penney lattice used to mimic the behavior of electrons in crystals [175]. Similarly, it is possible to tackle multichannel problems such as the excitation dynamics of atomic wavepackets interacting with narrow laser beams [17]. Much work on these potential-dependent transients has been carried out to understand time dependent aspects of tunneling and will be reviewed in Section 7.

6.1. Extended quasi-monochromatic initial states

Here we review an approach, first considered by García-Calderón and Rubio [61], that leads to an exact analytical solution to the time-dependent Schrödinger equation with cutoff wave initial conditions for arbitrary potentials of finite range. The approach involves the complex poles and residues (resonant states) of the outgoing Green's function of the problem and renders the time-dependent solution both along the internal and the transmitted regions of the potential. These authors solve the time-dependent Schrödinger equation

$$\left(i\hbar\frac{\partial}{\partial t} - H\right)\psi(x, t) = 0, \quad (75)$$

where $H = -(\hbar^2/2m)d^2/dx^2 + V(x)$, and $V(x)$ describes a potential of arbitrary shape extending from $x = 0$ to $x = L$, with the plane wave initial condition

$$\psi(x, t = 0) = e^{ikx}\Theta(-x), \quad (76)$$

which is the same initial condition considered by Moshinsky for the free case, see Eq. (1). García-Calderón and Rubio [61] used Laplace transform techniques to obtain along the internal region of the potential the expression [61]

$$\begin{aligned} \psi(x, k, t) = & \phi(x, k)M(0, k, t) - \\ & \sum_{n=-\infty}^{\infty} \phi_n(x)M(0, k_n, t); \quad (0 \leq x \leq L), \end{aligned} \quad (77)$$

where $\phi(x, k)$ refers to the stationary solution, and $\phi_n(x) = iu_n(0)u_n(x)/(k - k_n)$ is given in terms of the poles $\{k_n\}$ and resonant states $\{u_n(x)\}$ of the problem, discussed in Appendix E. Notice that along the internal region of the potential, the Moshinsky function does not depend on x and hence it does not correspond to a propagating solution. Similarly, along the transmitted region, the above authors provided the solution

$$\psi(x, k, t) = T(k)M(x, k, t) - \sum_{n=-\infty}^{\infty} T_n M(x, k_n, t); \quad (x \geq L), \quad (78)$$

where $T(k)$ is the transmission amplitude and $T_n = iu_n(0)u_n(L)e^{-ik_n L}/(k - k_n)$. Further notice that in the above two equations the function $M(x, k_n, t)$ corresponds to the Moshinsky function for the complex value $k = k_n$.

In the absence of a potential, the solution given by Eq. (77) vanishes exactly and in Eq. (78), $T(k) = 1$ and the resonant sum vanishes as well, so that the solution becomes the free solution. In [61], it is shown that the exact solutions given by Eqs. (77) and (78) satisfy the corresponding initial conditions, i.e., they vanish exactly for $t = 0$. Similarly, it is also shown that at asymptotically long times the terms $M(x, k_n, t)$ that appear in the above equations, tend to a vanishing value, while $M(x, k, t)$ tends to the stationary solution, as first shown by Moshinsky [5]. Along the internal region

$$\psi(x, t) \sim \phi(x, k)\exp(-iEt/\hbar), \quad (79)$$

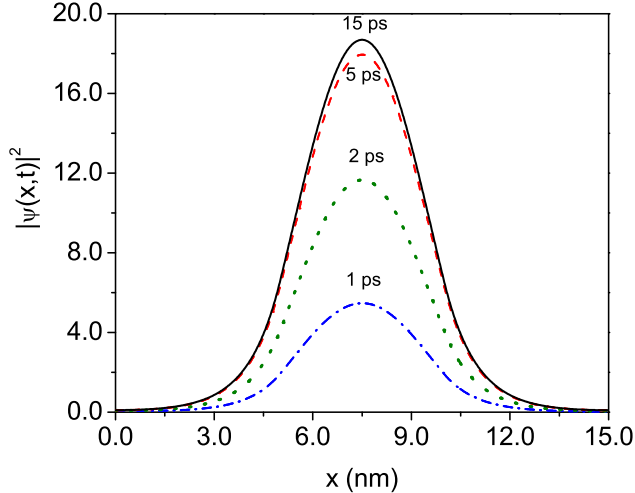


Fig. 16. Plot of the building up of $|\psi(x,t)|^2$ along the internal region of a double-barrier potential for several times with the parameters given in the text. At $t = 15$ ps, $|\psi(x,t)|^2$ becomes indistinguishable from the stationary solution.

and along the external (transmitted) region,

$$\psi(x,t) \sim T(k)\exp(ikx)\exp(-iEt/\hbar). \quad (80)$$

The above solutions allow us to study the dynamics along the full time span from zero to infinity. In [61] these solutions were used to examine the transient behavior of a double barrier resonant structure possessing an isolated resonance level and an initial plane wave with energy equal to the resonance energy of the level. The calculations showed that for times roughly of a fraction of a lifetime onwards the single-resonance approximation to the time-dependent solutions given above was in good quantitative agreement. Figure 16 exhibits the building up of the probability density $|\psi(x,t)|^2$ along the internal region of the double-barrier system (DB) for several times until it reaches the stationary solution. The parameters of the DB system, are typical of semiconductor resonant structures [207]: barrier heights $V = 0.23$ eV, barrier widths $b = 5.0$ nm, well width $w = 5.0$ nm and effective electron mass $m = 0.067m_e$, with m_e the electron mass. The isolated resonance level is characterized by the resonance parameters $\mathcal{E}_1 = 0.08$ eV and $\Gamma_1 = 1.0278$ meV. Figure 17 provides a comparison of the corresponding transmitted probability density with the free evolving solution at long times, which exhibits a delay time of the order of the theoretical estimate $\tau = 2\hbar/\Gamma_1$.

The fact that the plane wave initial state jumps from unity to zero at $x = 0$ implies that the resonant sums in Eqs. (77) and (78) have a slow convergence. For this reason, most subsequent work has considered the initial state [176,62,177,178,179,180,39,181,182]

$$\psi(x,t=0) = (e^{ikx} - e^{-ikx})\Theta(-x), \quad (81)$$

which continuously vanishes at $x = 0$. It follows then, that the time-dependent solutions along the internal and transmitted regions of the potential become, respectively,

$$\psi(x,t) = \phi(x,k)M(0,k,t) - \phi(x,-k)M(0,-k,t)$$

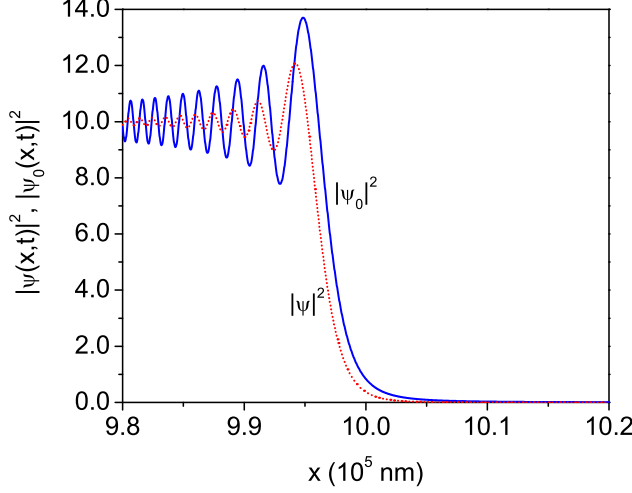


Fig. 17. Comparison of the wavefronts of the free-wave evolving solution $|\psi_0(x,t)|^2$ and the transmitted solution at resonance energy $|\psi(x,t)|^2$ through a double-barrier system at a long time $t=1540$ ps, to show that the delay time is of the order of $2\hbar/\Gamma_1$, with Γ_1 , the corresponding resonance width.

$$- \sum_{n=-\infty}^{\infty} \phi_n(x) M(0, k_n, t); \quad (0 \leq x \leq L), \quad (82)$$

and

$$\begin{aligned} \psi(x, t) &= T(k)M(x, k, t) - T(-k)M(x, -k, t) \\ &- \sum_{n=-\infty}^{\infty} T_n M(x, k_n, t); \quad (x \geq L), \end{aligned} \quad (83)$$

where the terms $\phi_n(x)$ and T_n are now given by $\phi_n(x) = 2ik_n u_n(0)u_n(x)/(k^2 - k_n^2)$ and $T_n = 2ik_n u_n(0)u_n(L)e^{-ik_n L}/(k^2 - k_n^2)$. It may be shown that at very long times $M(x, -k, t)$ goes to zero [61] and hence the above solutions tend also to the stationary values given by Eqs. (79) and (80).

In [39] an alternative procedure was derived to obtain the time-dependent transmitted solution. This procedure starts from the expression for the time-evolved wave function along the transmitted region

$$\psi(x, t) = \int_{-\infty}^{\infty} \frac{dk'}{\sqrt{2\pi}} \phi(k') T(k') e^{ik'x - i\hbar k'^2 t/2m}, \quad (84)$$

where $\phi(k')$ is the k' -space wave function (i.e., the Fourier transform of the initial wave function) defined by

$$\phi(k') = \int_{-\infty}^{\infty} \frac{dx}{\sqrt{2\pi}} e^{-ik'x} \psi(x, 0). \quad (85)$$

$T(k)$ for $k < 0$ is the analytical continuation in that domain of the transmission amplitude for left incidence, $T(k > 0)$, not to be confused with the transmission amplitude for right incidence [60].

For the initial state given by Eq. (81), it follows from Eq. (85) that

$$\begin{aligned}\phi(k') &= \int_{-\infty}^{\infty} \frac{dx}{\sqrt{2\pi}} e^{-ik'x} \psi(x, 0) \\ &= \frac{i}{\sqrt{2\pi}} \left(\frac{1}{k' - k + i\epsilon} - \frac{1}{k' + k + i\epsilon} \right),\end{aligned}\tag{86}$$

where ϵ is an infinitesimal positive number. The other ingredient to evaluate Eq. (84) is to make use of the Cauchy expansion for the transmission amplitude derived in Appendix E, *i.e.*, Eq. (E.26), written as

$$T(k') = \sum_{n=-\infty}^{\infty} \left(\frac{r_n}{k' - k_n} + \frac{r_n}{k_n} \right),\tag{87}$$

where $r_n = iu_n(0)u_n(L) \exp(-ik_nL)$. Substitution of Eqs. (86) and (87) into Eq. (84) leads, after some algebraic manipulation, to exactly the same expression given by Eq. (83). This procedure allows one to obtain more easily the time-dependent solution than the Laplace transform approach since it facilitates the consideration of other initial states. We shall refer to this approach as the Fourier transform approach. Its extension to deal with the internal region is straightforward [184].

There have been two main lines of research where the above exact time-dependent solutions for the wave function have been used in the investigation of transient phenomena. One line has addressed detailed studies on the dynamics of resonant tunneling on and off resonance energy in double [61,176,186,187], triple [179] and multiple [177,188] resonant tunneling structures, whereas the other line of research, considered in the next section, has addressed the issue of transient effects in relation to the tunneling time problem [62,178,63,180,39,174,181,182].

6.1.1. *Buildup dynamics of the transmission resonance spectra*

Most studies involving the quantum shutter setup consider a given value for the energy of the initial state, and evaluate the time-dependent solution for the probability density $|\psi(x, t)|^2$ either as a function of time for a fixed value of the distance or as a function of the distance for a fixed value of the time. In Ref. [177], however, Romo addresses the issue of the building up of the transmission resonances in a superlattice of finite range by considering the time-dependent solution for fixed values of both the distance and the time and varying instead the energy of the initial state in a relevant energy range. He considered the initial state given by Eq. (81) which leads to the time-dependent solution given by Eq. (82) to study this transient behavior for different superlattice potential profiles. In a finite superlattice involving $N + 1$ barriers the resonances group themselves in minibands involving N resonance levels isolated from each other. Romo studied the building up dynamics for a given miniband and found that the solution for $|\psi(x, t)|^2$ using Eq. (82) may be written as a simple analytic expression which involves only the N resonance levels of the miniband. Figure 18 exemplifies his findings. It consists of a

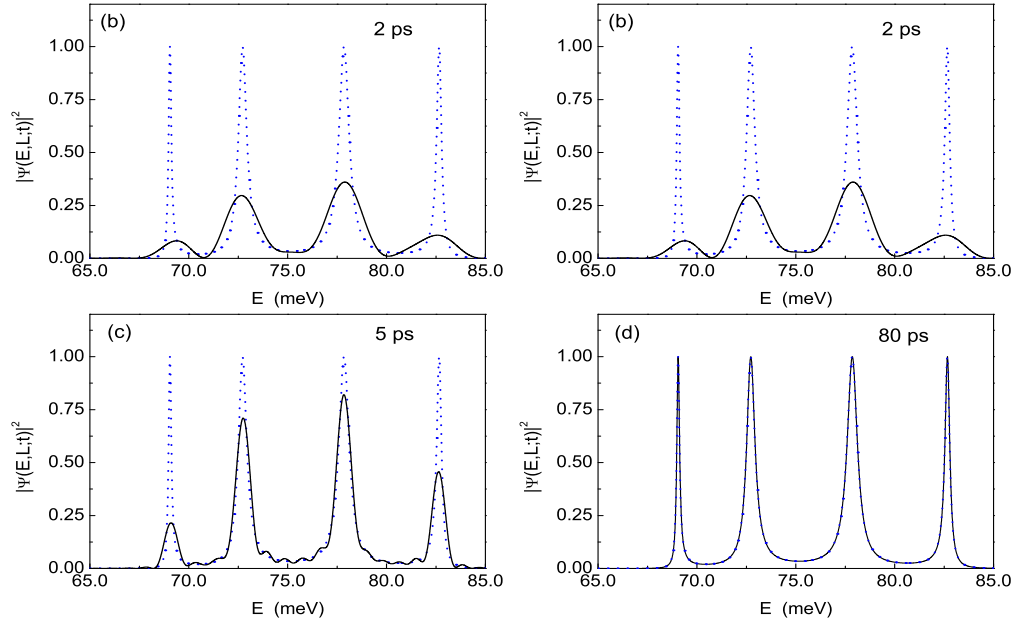


Fig. 18. Snapshots of the time-dependent probability density for a periodic superlattice of five barriers, with parameters given in the text, reproducing Fig. 4 of Ref. [177]. The values of $|\Psi(E, L; t)|^2$ vs E are calculated Eq. (7) of that paper at different fixed times (solid lines): (a) $t=0.6$ ps; (b) $t=2.0$ ps; (c) $t=5.0$ ps; (d) $t=80.0$ ps. The transmission coefficient is also included for comparison (dotted lines).

superlattice formed by five rectangular barriers with heights $V_0 = 0.2$ eV and widths $b_0 = 5.0$ nm and well widths $w_0 = 5.0$ nm, and it shows a series of plots of $|\Psi^N(E, L; t)|^2$ as a function of the energy E at different fixed times. In the snapshots depicted in Figures 18(a) to 18(d) one appreciates the “birth” of the transmission resonances and their subsequent evolution towards the stationary regime. At the very beginning of the tunneling process, one appreciates a smooth curve with no peaks, see Fig. 18(a); that is, no evidence of the resonances have appeared at this early stage. However, as time elapses some peaks in the curve gradually begin to appear as can be appreciated in Figs. 18(b) to 18(d). The height of the resonance peaks increases at different rates towards their corresponding asymptotic values. Notice that the buildup of the peaks is faster for the wider resonances ($n = 2$ and 3), and slower for the thinner ones ($n = 1$ and 4). It is also obtained that the buildup of the transmission peaks is governed by the analytic expression $T_n^{peak}[1 - \exp(-t/t_b)]$, where T_n^{peak} is the height of the corresponding transmission peak and $t_b = 2\hbar/\Gamma_n$, namely twice the lifetime \hbar/Γ_n of the resonance level.

6.2. Wavepacket initial states

The transmission of wavepackets through one-dimensional potentials is a model that has been of great relevance both from a pedagogical point of view, as discussed in many quantum mechanics textbooks, and in research, particularly since the advent of artificial semiconductor quantum structures [207,208]. In [182], Yamada, García-Calderón and Villavicencio extended the quantum shutter initial condition to certain type of wave

packets. They considered the following initial condition,

$$\psi(x, 0) = A \int_{-\infty}^{\infty} dk \left(\frac{e^{ikx}}{k - k_0 + i\Delta} + \text{c.c.} \right), \quad (88)$$

where $A = \sqrt{\Delta \{1 + (\Delta/k_0)^2\}}/2\pi$ with $\Delta > 0$, and *c.c.* stands for complex conjugate. An important feature of this initial state is that it automatically vanishes for $x > 0$. This is immediately seen from the fact that the integrand $e^{ikx}/(k - k_0 + i\Delta)$, which corresponds to a Lorentzian momentum distribution centered at $\hbar k_0$ with width $\hbar\Delta$, has a simple pole only in the lower-half of the complex k -plane. An explicit expression for $\psi(x, 0)$ can be easily obtained by the method of residues. It is found that

$$\psi(x; t = 0) = \begin{cases} 4\pi A e^{\Delta x} \sin k_0 x, & x < 0 \\ 0, & x \geq 0, \end{cases}. \quad (89)$$

A measure of the packet width is $1/\Delta$. It can be easily proved that the wave packet is normalized, i.e., $\int dx |\psi(x, 0)|^2 = 1$. The Fourier transform of the above expression is

$$\phi(k) = \sqrt{2\pi} A \left(\frac{1}{k - k_0 + i\Delta} - \frac{1}{k + k_0 + i\Delta} \right), \quad (90)$$

and then, following the same procedure of the previous example, these authors arrive at the solution

$$\begin{aligned} \psi(x, t) = & -i\sqrt{\Delta \{1 + (\Delta/k_0)^2\}} \left[T(k_0 - i\Delta) M(x, k_0 - i\Delta; t) \right. \\ & - T(-k_0 - i\Delta) M(x, -k_0 - i\Delta; t) \\ & \left. - 2k_0 \sum_{n=-\infty}^{\infty} \frac{r_n}{k_0^2 - (k_n + i\Delta)^2} M(x, k_n; t) \right], \end{aligned} \quad (91)$$

where, we recall that $r_n = iu_n(0)u_n(L) \exp(-ik_n L)$.

Most time-dependent numerical studies consider Gaussian wavepackets as initial states [208,209,210,211], though in some recent work, the formation of a quasistationary state in the scattering of wavepackets on finite one-dimensional periodic structures also involves also some analytical considerations [212]. As discussed above, analytical approaches have been mainly concerned with quasi-monochromatic initial states in a quantum shutter setup. In some recent work, however, analytical solutions to the time-dependent wave function have been discussed using initial Gaussian wavepackets for square barriers [200], delta potentials [213] and resonant tunneling systems near a single resonance [214].

In Ref. [185], Villavicencio, Romo and Cruz derive an analytical solution to the time-dependent wavefunction for an initial cutoff Gaussian wavepacket, for the free evolving case and two barrier potentials: the δ -potential and a very thin and very high rectangular barrier. They consider the Fourier transform approach and the analytical solution follows provided the center of the Gaussian wavepacket is far from the interaction region, as is usually assumed on physical grounds. In such a case, the tail of the Gaussian is small near the interaction region, a regime they refer to as the *small truncation regime*.

The cutoff Gaussian wave packet is given by the expression

$$\psi_0(x) = \begin{cases} A_0 e^{-(x-x_0)^2/4\sigma^2} e^{ik_0 x}, & x < 0 \\ 0, & x > 0 \end{cases}, \quad (92)$$

where A_0 is the normalization constant, and x_0 and σ stand, respectively, for the center and effective width of the wavepacket. The interesting point of this approach is that substitution of Eq. (92) into Eq. (85) gives an exact expression for the corresponding Fourier transform,

$$\phi_0(k) = A_0 w(iz), \quad (93)$$

where $A_0 = (1/\sqrt{2\pi})[(2\pi\sigma^2)^{1/4}/\sqrt{\omega(iz_0)}]$, $z = x_0/(2\sigma) - i(k - k_0)\sigma$, $z_0 = x_0/(\sqrt{2}\sigma)$, and $w(y)$ is the w -function [78] (see Appendix C). Along $x_0 < 0$ and $z \gg 1$ using the relationship $w(iz) = 2e^{z^2} - 1/(\pi^{1/2}z) - 1/(2\pi^{1/2}z^3) + \dots$, allows to write $w(iz) \simeq 2 \exp(z^2)$. Substituting this last expression into Eq. (93) and the resulting expression into Eq. (84) yields

$$\psi(x, t) = 2A_0 \int_{-\infty}^{\infty} \frac{dk'}{\sqrt{2\pi}} e^{z^2} T(k') e^{ik'x - i\hbar k'^2 t/2m}. \quad (94)$$

For $T = 1$, the above expression leads to an analytical expression for the free evolving Gaussian wavepacket [185],

$$\begin{aligned} \psi_a^f(x, t) &= \frac{1}{(2\pi)^{1/4}} \frac{1}{\sigma^{1/2}} \frac{e^{i(k_0 x - \hbar k^2 t/2m)}}{\sqrt{1 + it/\tau}} \times \\ &\exp \left\{ -\frac{[x - x_0 - (\hbar k_0/m)t]^2}{4\sigma^2 [1 + it/\tau]} \right\}, \end{aligned} \quad (95)$$

where $\tau = 2m\sigma^2/\hbar$, that is identical to the analytical solution for the extended free Gaussian wavepacket, *i.e.*, no cutoff Gaussian wavepacket. The above authors considered the quantum shutter setup with a cutoff Gaussian wavepacket initial state for a delta-barrier potential of intensity λ , *i.e.*, $V(x) = \lambda\delta(x)$. The corresponding transmission amplitude reads

$$T(k) = \frac{k}{k + i(m\lambda/\hbar^2)}. \quad (96)$$

Notice that the transmission amplitude given above has just one pole, an antibound pole at $k_a = -i(m\lambda/\hbar^2)$. Substitution of Eq. (85) into Eq. (84) leads to an expression that acquires a simple analytical form in the *small truncation regime*, namely,

$$\psi(x, t) = \psi_a^f(x, t) - C e^{ik_0 x - i\hbar k_0^2 t/2m} M(x', q', t), \quad (97)$$

where $\psi_a^f(x, t)$ stands for the free solution, $C = (\pi/2)^{1/4}(2m\sigma^{1/2}\lambda)/\hbar^2$ and $M(x', q', t)$ stands for a Moshinsky function where $x' = x - x_0 - v_0 t$, $q' = -(k_0 + im\lambda/\hbar^2)$, and $t' = t - i\tau$. The solution given by Eq. (97) holds also for a rectangular barrier of height

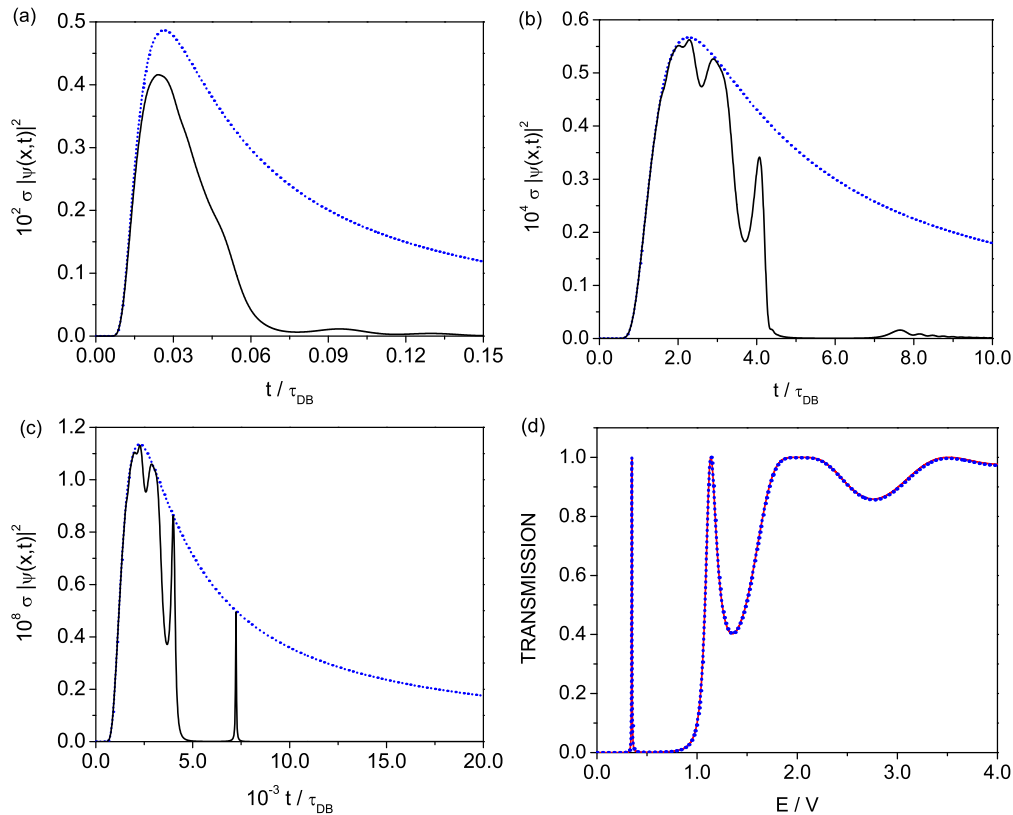


Fig. 19. Figures (a), (b) and (c) display $\sigma|\psi(x,t)|^2$ as function of time in units of the lifetime $\tau_{DB} = \hbar/\Gamma_1$ (full lines) at different distances x_d from the DB system, calculated using Eq. (99): (a) $2L$, (b) $200L$ and (c) $2 \times 10^5 L$, where L is the length of the system. Also shown in these figures is the free evolving cutoff Gaussian wavepacket (dotted line). Figure (d) exhibits the transmission spectra of the DB system as a function of energy, in units of the barrier height, using the exact numerical calculation (full line) and that obtained using the resonance expansion given by Eq. (E.26) (dot line). See text.

v_0 and width L in the limit of small opacity $[2mV_0]^{1/2}/\hbar \ll 1$, by letting $\lambda = V_0 L$ and performing the translation $x \rightarrow (x - L)$.

Recently, Cordero and García-Calderón [215] have obtained a formal solution of the transmitted time-dependent function for an arbitrary potential profile as an expansion in terms of resonance states and poles of the problem that follows by substitution of Eq. (E.26) into Eq. (84), namely,

$$\psi(x,t) = \frac{1}{\sqrt{2\pi}} \sum_{n=-\infty}^{\infty} \varrho_n e^{-ik_n L} \int_{-\infty}^{\infty} dk \frac{k}{k - k_n} \phi_0(k) e^{ikx - i\hbar k^2 t/2m}, \quad (98)$$

where $\varrho_n = u_n(0)u_n(L)/k_n$. For a cutoff Gaussian initial wavepacket, substitution of Eq. (93) into Eq. (98), leads, in the *small truncation regime*, to the expression

$$\psi(x,t) = T(k_0)\psi_a^f(x,t)$$

$$\begin{aligned}
& + i \sum_{n=-\infty}^{\infty} \varrho_n k_n e^{-ik_n L} \left[\frac{1}{k_n - k_0} \psi_a^f(x, t) \right. \\
& \left. + D(z_0) e^{ik_0 x - i\hbar k_0^2 t / 2m} M(x', t'; k'_n) \right], \tag{99}
\end{aligned}$$

where $D(z_0) = -2i(2\pi)^{1/4} \sqrt{\sigma/\text{erfc}(z_0)}$ and the Moshinsky function $M(x', t'; k'_n)$, depends now on $k'_n = k_n - k_0$, with k_n the complex resonance pole. The other parameters remain as defined above. Figures 19 (a)-(c) exhibit $\sigma|\psi(x, t)|^2$ in units of the lifetime, for a cutoff Gaussian initial wavepacket with parameters $x_0 = -5.0$ nm, $\sigma = 0.5$ nm and an incident energy E_0 of half the potential barrier height V , tunneling through a double-barrier resonant system (DB) with the same parameters as given in the discussion in 6.1. The profile of the transmitted wavepacket exhibits a transient behavior that after a very large distance, acquires a fixed shape that resembles, in time domain, the resonance spectra of the system. As a comparison, Fig. 19 (d) yields the transmission coefficient of the DB system *vs* energy in units of the potential height, using an exact numerical calculation (full line) and the resonance expansion given by Eq. (E.26).

6.3. Relativistic effects in quantum transients

An interesting feature of the solutions for cutoff initial waves, occurring both in the free case [183] and in the presence of a potential interaction [61], is that, if initially there is a zero probability for the particle to be at $x > 0$, as soon as $t \neq 0$, there is instantaneously, a finite, though very small, probability to find the particle at any point $x > 0$. In Ref. [31], García-Calderón, Rubio and Villavicencio, studied the short time behavior of the solution of the quantum shutter in the presence of a finite range potential extending through the region $0 \leq x \leq L$ with the initial conditions given, respectively, by Eqs. (76) and (81), which lead along the external region, $x \geq L$ to the solutions given by Eqs. (78) and (83). They found that at short times the above solutions behave as

$$\psi(x, t) \sim \frac{A}{x} t^{1/2}; \quad x \geq L, \tag{100}$$

where A is a constant. The above expression tells that the probability density at any distance x from the potential will rise instantaneously with time. Although this should not pose any conceptual difficulties because the treatment is not relativistic, the above authors ask themselves whether the above nonlocal behavior arises because the initial condition is a cutoff wave. In order to solve this question the authors considered the solution of the Klein-Gordon equation for a delta potential $V(x) = b_s \delta(x)$ by using Laplace transforming techniques and found an analytical solution of the problem that at short times becomes different from zero after a time $t_0 = L/c$, with c the velocity of light, thus restoring Einstein causality. Hence the non-local behavior of the Schrödinger solution is due to its nonrelativistic nature and not a result of the quantum shutter setup.

7. Time scale of forerunners in quantum tunneling

Quantum tunneling, the possibility that a particle traverses a classically forbidden region, constitutes one of the paradigms of quantum mechanics. Most textbooks usually address its stationary aspects only, and solve the stationary Schrödinger equation at a fixed energy E . In the time domain the analysis of the transient behavior of the time evolution of the wave function along the internal and transmitted regions of a potential has been considered in the framework of the quantum shutter setup as a natural extension of the free case considered by Moshinsky. Since the seminal work of Büttiker and Landauer [189], the time-dependent aspects of tunneling have attracted a great deal of attention. Much of this work has led to controversy, as several authors have proposed and defended different “tunneling times”. In fact each has its own virtues, weaknesses, physical content, and range of applicability. For reviews see [190,191,192,193,194].

An analysis of the involved non-commuting observables (the projectors that determine the final transmission and the probability to find the particle in the barrier region) shows that, from a fundamental perspective, there is no unique tunneling time, because several quantizations are possible due to different operator orderings and defining criteria [195]. It is thus necessary to specify precisely how to time the quantum particle in the tunneling regime, since different procedures lead to different relevant time scales. For example, the traversal time of Büttiker and Landauer (BL time) [189], $\tau_{BL} = L/v_{sc}$, given by the barrier length L divided by the “semiclassical” velocity $v_{sc} = [2(V - E)/m]^{1/2}$, marks the transition from sudden to adiabatic regimes for an oscillating barrier [189], and determines the rotation of the spin in a weak magnetic field in opaque conditions [196]; whereas the average over wavepacket components of the (monochromatic) “phase times” provides the mean arrival time of the transmitted wave packet [195,197]. These two time scales may be very different. The Büttiker-Landauer time increases with decreasing energies up to a finite value, whereas $\tau^{Ph}(0, L)$ (the so called extrapolated phase time) diverges as $E \rightarrow 0$, and tends for increasing L to a constant value, $2\hbar/[v_{sc}(2mE)^{1/2}]$. This latter property implies that the arrival of the transmitted wave becomes independent of L (Hartman effect [198]), although the independence only holds until a certain critical length L_c [195] where above-the-barrier components start to dominate. For $L > L_c$ the mean arrival time depends on L linearly. While τ_{BL} and τ^{Ph} are surely the most frequently found tunneling times, they do not exhaust all timing questions as we shall see.

7.1. Transients for a square barrier

A simple and physically interesting complication of the elementary shutter is the addition of a square barrier after the shutter edge. Brouard and Muga studied this problem paying attention to the “tunneling” configuration in which the carrier energy is below the barrier top, $E_0 < V_0$ [60]. They used a complex momentum plane approach associated with asymptotic expansions which has been applied later to different transient phenomena [199,63,64,32,200,36,65,201,202]. The aim of the approach is to describe the wave propagation with a minimum of elements and maximal efficiency. It provides the wave function, as well as characteristic velocities and times, and localizes the origin of the main contributions at critical points in the complex energy or momentum planes

such as poles, saddle points, and branch points, following the analysis by Sommerfeld and Brillouin for the propagation of light in dispersive media [203]. This is useful conceptually, and improves the efficiency of the numerical calculations. Pioneering work in this direction was done by Stevens [58], who proposed a sequence of “tunneling problems” for the step potential barrier. Using approximate arguments, his main conclusion was that for energies below the barrier height $E_0 < V_0$, a wave front traveling with the semiclassical velocity $v_{sc} = [2(V_0 - E_0)/m]^{1/2}$ could be identified. He related this wave front to the crossing of a pole by the steepest-descent path. This conclusion has been later shown to be generally unjustified, due to the simultaneous effect of other critical points [171,59,115,116]. More on this in 7.2 below. The study of finite width barriers is a natural extension of Stevens’s tunneling problems for the step potential. Along this line, Jauho and Jonson [59] examined numerically the propagation of an initially sharp packet (a cutoff plane wave) through a square barrier, and Moretti carried out an approximate asymptotic analysis for this system [117] as well.

Brouard and Muga [60] provided an exact solution of the dynamics that retains the basic philosophy of working out the time-dependent wave function by contour deformation in the complex momentum plane and extracting contributions from critical points, which in most cases reduce to a w -function.

It is instructive to note the main features of the analysis in [60] by first studying Moshinsky’s simplest shutter problem. The general solution for free motion takes the form

$$\psi_0(x, t) = \int_{-\infty}^{\infty} \langle x|k\rangle e^{-iE_k t/\hbar} \langle k|\psi(t=0)\rangle dk, \quad (101)$$

where $E_k = k^2 \hbar^2 / 2m$ and $\langle k|k'\rangle = \delta(k - k')$. For an initial state corresponding to a cut-off plane wave $e^{ik_0 x} \Theta(-x)$,

$$\psi_0(x, t) = \frac{i}{2\pi} \int_{-\infty}^{\infty} \frac{e^{i(kx - k^2 \hbar t / 2m)}}{k - k_0 + i0} dk. \quad (102)$$

The steepest descent path (SDP) is a -45° straight line cutting the real k axis at the saddle point ($k = mx/t\hbar$) of the exponent. For a fixed position $x > 0$, the saddle point moves from ∞ to 0 as t grows from 0 to ∞ . Deforming the contour along that path, completing the square, and using the same u -variable of Eq. (5),

$$u = \frac{1+i}{2} \left(\frac{\hbar t}{m} \right)^{1/2} \left(k - \frac{mx}{\hbar t} \right), \quad (103)$$

which is zero at the saddle, and real along the SDP, we get

$$\psi_0(x, t) = i \frac{e^{imx^2/2t\hbar}}{2\pi} \int_{\Gamma_u} \frac{e^{-u^2}}{u - u_0} du \quad (x, t > 0), \quad (104)$$

where $u_0 = u(k = k_0)$ is the pole position in the u -plane. Note that it “moves” with t and/or x ; by contrast, the pole in the k -plane is fixed at k_0 . The contour Γ_u goes along

the real u axis from $-\infty$ to ∞ plus a circle around u_0 whenever its imaginary part is positive. Finally,

$$\psi_0(x, t) = \frac{e^{imx^2/2t\hbar}}{2} w(-u_0) \quad (x, t > 0), \quad (105)$$

which is Moshinsky's solution $M(x, k, t)$, Eq. (4). At fixed x , $u_0^2 \sim ik_0^2 \hbar t / 2m$ as $t \rightarrow \infty$ and a stationary regime with constant density is reached. At small times the saddle at $u = 0$ is far from the pole and it is the only important critical point. Setting $u = 0$ in the integrand,

$$|\psi(x, t)|^2 \sim \frac{t\hbar}{4m\pi^2 x^2} \quad (x/t \rightarrow \infty). \quad (106)$$

The treatment for the square barrier starts from an integral like (101), substituting the plane waves by scattering states. Thus, for the transmitted part, $x > a$,

$$\psi_T(x, t) = \frac{1}{(2\pi)^{1/2}} \int_{-\infty}^{\infty} T(k) e^{ikx} e^{-iE_k t/\hbar} \langle k | \psi(0) \rangle dk, \quad (107)$$

which is in fact a generic result for cut-off potentials and initial states. The difference with the elementary treatment of the free motion case is the need to consider the complex poles of $T(k)$ in the lower half- k -plane, k_j , which leads to a series in terms of w -functions for each of them. The short time asymptotic behavior does not change with respect to the free case, Eq. (106), because the poles are yet very far from the saddle and integration contour. As time progresses the saddle gets near the poles, and a velocity of propagation can be assigned to each resonant pole contribution from the condition of the crossing of each pole by the contour. These contributions are transient, fade away with time, their residue terms being proportional to $e^{-ik_j^2 \hbar t / 2m}$, and only the contribution of the structural pole k_0 remains eventually,⁴ which sets in around the phase time.

The internal part, $0 < x < L$, becomes more complicated in this treatment because of the interference between different terms, but the results show clearly that a front moving with a semiclassical velocity is not seen in the exact solution.

Alternatively, using the exact analytical approach discussed in the previous section, García-Calderón [206] examined the time evolution of the initially cutoff wave given by Eq. (81) with energy $E = 0.01$ eV on a rectangular barrier. The parameters of the barrier are typical of semiconductor quantum structures [207]: Barrier height $V_0 = 0.23$ eV, barrier width $L = 5.0$ nm and effective electronic mass $m = 0.67m_e$, with m_e the bare electron mass. The results of the calculation exhibit an absence of a propagating wave along the internal region of the potential. The absence of a propagating wave along the tunneling region may also be inferred from the corresponding analytical solution (see Eq. (82) since the Moshinsky functions there are independent of x . The inset to Fig. 20 exhibits the probability density as a function of time at a fixed internal distance $x_0 = 2.0$ nm. A peaked structure at $t \approx 5.6$ fs is clearly appreciated. This is a replica of a similar structure that appears at $x = L$, named *time domain resonance* [62,178,180] which is further discussed in 7.3 and 7.4. Similar non-propagating structures with different peaked

⁴ The "structural poles" are associated with the structure of the wave-function and are to be distinguished from poles of the resolvent, in particular from resonance poles [204,205].

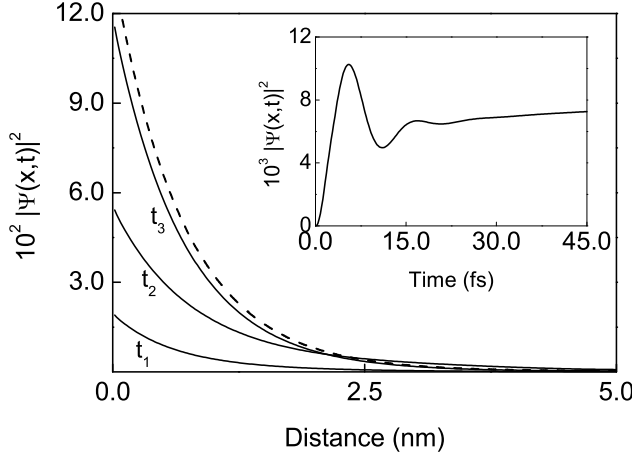


Fig. 20. Plot of the probability density normalized to the incident flux along the internal region of a rectangular potential, denoted by $|\psi(x,t)|^2$, for various times which exhibits that there is no a propagating wave along the internal region: $t_1 = 1.0$ fs, $t_2 = 3.0$ fs, and $t_3 = 30.0$ fs. For comparison the stationary solution has been also included (dashed line). The inset shows a replica *time domain resonance* at the internal distance $x_0 = 2.0$ nm. See text.

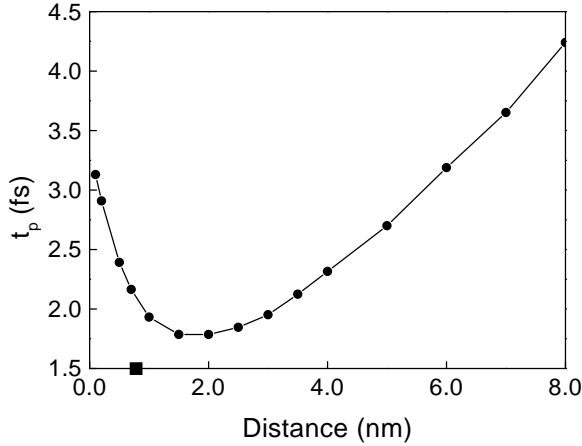


Fig. 21. Exact calculation of t_p (solid dots) as a function of the position x . The full square indicates the value of the penetration length κ_0^{-1} . See text.

values t_p appear at every internal point. In Ref. [63] this was further investigated. Figure 21 exhibits a plot of t_p (solid dots) as a function of position along internal values of the distance x_0 of a rectangular barrier with parameters: $V_0 = 1.0$ eV and $L = 40.0$ nm. Figure 21 explores distances of the order of, or smaller than, the penetration length defined as κ_0^{-1} , where $\kappa_0 = [2m(V_0 - E_0)]^{1/2}/\hbar$, and $E_0 = \hbar^2 k_0^2/2m$ stands for the incident energy.

One might clearly identify two regimes. The first of them corresponds to a basin, where for small values of the position, t_p decreases reaching a minimum value as x

increases. However, if x is further increased, t_p begins to grow as a function of the position. Apparently this second regime corresponds to a situation where t_p increases linearly with x . The result depicted in Fig. 21 appears also to be a replica of a similar behavior of the probability density at the barrier edge $x = L$, reported in Ref. [62]. Before we further clarify and interpret these effects in 7.3, it will be useful to step back from the relative complexity of the square barrier and analyze an even simpler case.

7.2. Muga-Büttiker analysis of evanescent waves

Here we shall follow [34] to study the role of the Büttiker-Landauer time in quantum transients due to the injection of particles with energy below the potential level, so that an evanescent wave is finally formed. For the Schrödinger equation

$$i\hbar \frac{\partial \psi}{\partial t} = -\frac{\hbar^2}{2m} \frac{\partial^2 \psi}{\partial x^2} + V\psi, \quad (108)$$

with $V = \text{constant}$, we define wavenumber k and frequency ω as

$$\omega = E/\hbar = V/\hbar + k^2\hbar/2m, \quad (109)$$

$$k = [2m(\omega - V/\hbar)/\hbar]^{1/2}. \quad (110)$$

Particle injection is modeled by fixing the wavefunction at the origin for all times,

$$\psi(x=0, t) = \Theta(t) e^{-i\omega_0 t}, \quad (111)$$

for a frequency $\omega_0 = \hbar k_0^2/2m$, and assuming $\psi(x, t < 0) = 0$.

The inverse Fourier transform of the source $\psi_0(x=0, k_0, t) = e^{-i\omega_0 t}\Theta(t)$ is given by

$$\widehat{\psi}(x=0, k_0, \omega) = \frac{1}{\sqrt{2\pi}} \int_{-\infty}^{\infty} \psi_0(x=0, k_0, t) e^{i\omega t} dt = \frac{i}{\sqrt{2\pi}} \frac{1}{\omega - \omega_0 + i0}. \quad (112)$$

For $x, t > 0$, the wave function evolves according to

$$\psi_0(x, k_0, t) = \frac{i}{2\pi} \int_{-\infty}^{\infty} d\omega \frac{e^{ikx - i\omega t}}{\omega - \omega_0 + i0},$$

where $\text{Im}k \geq 0$. If we are interested in carrier frequencies below threshold, $\omega_0 < V/\hbar$, it is also useful to define $\kappa_0 = [2m(V/\hbar - \omega_0)/\hbar]^{1/2}$. The integral can be written in the complex k -plane by deforming the contour of integration to Γ_+ , which goes from $-\infty$ to ∞ passing above the poles,

$$\begin{aligned} \psi_0(x, k_0, t) &= \frac{i}{2\pi} \int_{\Gamma_+} dk 2k \frac{e^{ikx - i(k^2\hbar/2m + V/\hbar)t}}{k^2 + \kappa_0^2} \\ &= \frac{i}{2\pi} \int_{\Gamma_+} dk \left(\frac{1}{k + i\kappa_0} + \frac{1}{k - i\kappa_0} \right) e^{ikx - ik^2\hbar t/2m - iVt/\hbar}. \end{aligned}$$

The contour can be deformed further along the steepest descent path from the saddle at $k_s = xm/t\hbar$, the straight line

$$k_I = -k_R + xm/t\hbar \quad (113)$$

($k = k_R + ik_I$), plus a small circle around the pole at $k_0 = i\kappa_0$ after it has been crossed by the steepest descent path, for fixed x , at the critical time

$$\tau_c \equiv xm/\hbar[\text{Re}(k_0) + \text{Im}(k_0)]. \quad (114)$$

For tunneling $\text{Re}(k_0) = 0$ so that $\tau_c = \tau_{BL}$, where now

$$\tau_{BL} = \frac{xm}{\kappa_0\hbar} \quad (115)$$

is a slight generalization of the Büttiker-Landauer time, with x playing the role of L . The solution, using the u -variable (103), real along the steepest descent path, is

$$\psi(x, t) = \frac{e^{-iVt/\hbar} e^{ix^2m/2t\hbar}}{2} [w(-u_0) + w(-u'_0)], \quad (116)$$

where $u_0 = u(k = k_0)$, and $u'_0 = u(k = -k_0)$.⁵ Eq. (116) can be written for $x\kappa_0 \gg 1$ (opaque conditions) as the sum of contributions from the saddle point and the pole,

$$\psi(x, t) = \psi_p(x, t) + \psi_s(x, t), \quad (117)$$

$$\psi_p(x, t) = e^{-i\omega_0 t + ik_0 x} \Theta(t - \tau_c), \quad (118)$$

$$\psi_s(x, t) = \frac{e^{-iVt/\hbar} e^{ik_s^2 \hbar t/2m}}{2i\pi^{1/2}} \left(\frac{1}{u_0} + \frac{1}{u'_0} \right). \quad (119)$$

Asymptotically, only the “monochromatic” pole contribution remains and a stationary evanescent wave is formed, but, before that regime, a forerunner (bump in the density with a well defined maximum) is observed at fixed x . For carrier frequencies below the cut-off τ_{BL} plays clearly a role in the exact solution since

$$u_0 = \frac{1+i}{2} \sqrt{\frac{\hbar t}{m}} \kappa_0 (i - \tau_{BL}/t), \quad (120)$$

$$u'_0 = \frac{1+i}{2} \sqrt{\frac{\hbar t}{m}} \kappa_0 (-i - \tau_{BL}/t). \quad (121)$$

However, it cannot be identified with the transition to the asymptotic regime since the saddle contribution dominates up to an exponentially large time $t_{tr} = t_{tr}(x) > \tau_{BL}$ that can be identified from the condition $|\psi_p| = |\psi_s|$ [34]. (By contrast above threshold, τ_c in Eq. (114) is a good scale for the arrival of the main peak.) A different instant is the time of arrival, $t_p = t_p(x)$, of the temporal peak of the forerunner at a point x . It can

⁵ This formal result holds for all carrier frequencies ω_0 , above or below threshold. Putting $V = 0$ it reads simply $\psi(x, t) = M(x, k_0, t) + M(x, -k_0, t)$ in terms of Moshinsky functions, i.e., the source boundary condition imposed at $x = 0$ gives the same wavefunction as the shutter with reflection amplitude $R = 1$ opened at $t = 0$. The case $R = -1$ and its relation to inhomogeneous sources was examined by Moshinsky [216] and is reviewed in Appendix D.

be obtained from $\partial|\psi_s|^2/\partial t = 0$ and, for opaque conditions, t_p turned out to be (surprisingly) proportional to the BL time τ_{BL} ,

$$t_p = \tau_{BL}/3^{1/2}, \quad (122)$$

even though the time-frequency analysis of the forerunner [217,34] confirmed that it was composed by frequencies above threshold so it was not tunneling.⁶ The frequency of the saddle is $\omega_s = E_s/\hbar$, where $E_s = V + x^2m/(2t^2) = V + k_s^2\hbar^2/(2m)$, coincides with the energy of a classical particle traveling from the source to x in a time t . It is very remarkable that in spite of its frequency content, the forerunner's peak "travels" with a velocity proportional to v_{sc} , $v_p = 3^{1/2}v_{sc}$, which increases with decreasing energies, and its intensity diminishes exponentially as it progresses along the coordinate x . Other works had already pointed out the dominance of non-tunneling components in the forerunner [218,219,171,59,60] but had not characterized its time dependence.

7.3. Forerunners which do tunnel

Büttiker and Thomas [33] proposed to enhance the importance of the monochromatic front associated with ω_0 compared to the forerunners by limiting the frequency band of the source or of the detector; it was shown later in [34] that the monochromatic front could not be seen in opaque conditions even with the frequency band limitation. However, a clear separation of the amplitude into two terms, one associated with saddle and forerunner and the other with the pole and the "monochromatic front", is only possible for opaque conditions. Non-semiclassical conditions have been much less investigated [220], even though these are actually easier to observe because a stronger signal may be obtained. Ref. [63] and this subsection are mainly concerned with them.

García-Calderón and Villavicencio [62] examined the time evolution of an initial cutoff wave truncated at the left edge of a rectangular barrier potential (quantum shutter setup). There it was found that the probability density at the barrier edge $x = L$, exhibits at short times a transient structure named *time domain resonance*, see Fig. 22. The behavior of the maximum, t_p , of the *time domain resonance* showed a plateau region for small L , or more accurately a shallow basin, followed by a linear dependence for larger L ; this behavior is reminiscent of the Hartman effect, but the time of the plateau did not coincide with the phase-time estimate. It was found that for a broad range of parameters, t_p in the basin may be written approximately as

$$t_p^B = \frac{\hbar\pi}{\epsilon_1 - E_0}, \quad (123)$$

where ϵ_1 and E_0 , correspond to the energy of the first top-barrier resonance and the incidence energy, respectively. On the other hand, along the linear regime, at larger values of L , t_p is described by

$$t_p^L = \frac{L}{v_1}, \quad (124)$$

⁶ The simplest time-frequency information is contained in the local instantaneous frequency. Writing $\psi(x, t) = |\psi(x, t)|e^{i\phi(x, t)}$ it is defined as $\bar{\omega}(x, t) = -\partial\phi(x, t)/\partial t$. More sophisticated treatments such as spectrograms, Wigner functions or other time-frequency distributions provide further moments and information [217,34].

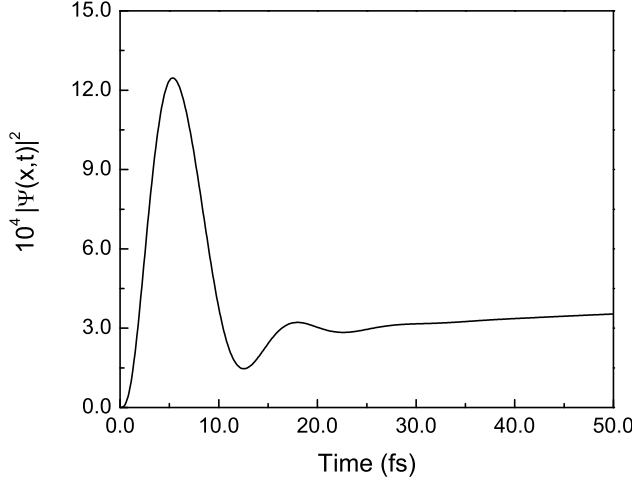


Fig. 22. Time evolution of $|\psi(x,t)|^2$ for a rectangular barrier of height $V = 0.3$ eV and width $L = 5.0$ nm, evaluated at $x = L$, exhibiting a *time domain resonance* peaked at $t_p = 5.3$ fs. The incident energy is $E = 0.01$ eV and the effective electron mass is $m = 0.067m_e$, where m_e stands for the electron mass.

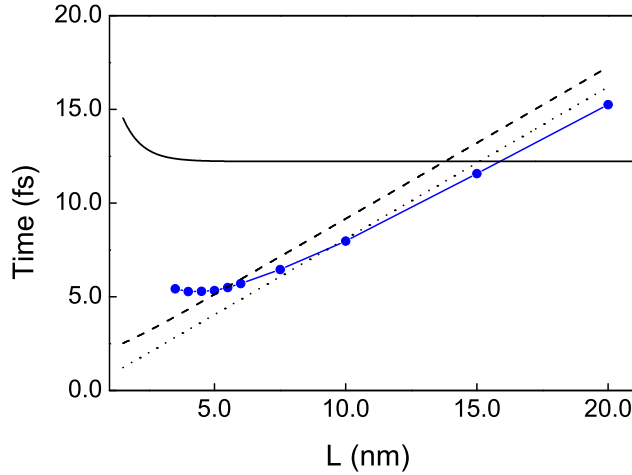


Fig. 23. Maximum of the *time-domain resonance* t_p (solid dots) as a function of the barrier width L with fixed barrier height $V = 0.3$ eV and incidence energy $E = 0.001$ eV. For comparison, are also plotted the Büttiker traversal time t_B , the Büttiker-Landauer time t_{BL} and the phase-delay time t_D .

where $v_1 = \hbar a_1/m$, with a_1 the real part of the first top-barrier pole $k_1 = a_1 - ib_1$. The above considerations are illustrated in Fig. 23. This figure also shows a comparison with exact calculations for the Büttiker traversal time t_B , the semiclassical Büttiker-Landauer time t_{BL} and the phase-delay time t_D , see Eqs. (3.12), (1.7) and (3.2) of [196]. Notice that t_B and t_{BL} do not describe the basin regime and that they are close to the values of t_p along the regime that increases linearly with L .

It was shown in [63] that this basin dependence, and the corresponding time scale, is not only present at the transmission edge of the square barrier studied in [62]. It may also

be found, *mutatis mutandis*, in the sharp onset source model with constant V examined in [34] for small $x\kappa_0$. As discussed above, the basin is also found for the time of the forerunner versus position in the internal region of the rectangular barrier, and for a step potential barrier. There are no resonances in the sharp onset source model, or for the step potential, so the time scale of the forerunner at the basin minimum is in these cases inversely proportional to κ_0^2 , namely to the difference between the “potential level” V and the source main energy E_0 . This is to be contrasted with the dependence on κ_0^{-1} of the traversal time τ_{BL} . Apart from certain peculiarities, all models show a small length region of the order of the penetration length κ_0^{-1} where the forerunner is dominated by tunneling components and arrives at a time proportional to κ_0^{-2} .

The time-frequency analysis showed that the peak of the *forerunner* at small lengths, in the evanescent region, is composed predominantly by under-the-barrier components, so that indeed there is a genuine tunneling time scale different from the phase or BL times [63].

In Ref. [178] the analytic solution to the Schrödinger equation for cutoff wave initial conditions given by Eq. (83) was used to investigate the time evolution of the transmitted probability density for a rectangular potential. For a broad range of values of the *opacity* defined as

$$\alpha = [2mV]^{1/2}L/\hbar, \quad (125)$$

it was found that the transmitted probability exhibits two evolving structures. One refers to a *forerunner* which follows from the propagation of the *time-domain resonance* whereas the other structure consists of a semiclassical propagating wavefront, that resembles the time evolution of the free term modulated by the value of the transmission coefficient. A regime is also found for values of the opacity α below a critical value α_c where there are no *time domain resonances* and hence no *forerunners*. Moreover, it is also found that this situation is related to a *time advance*, i.e. a positive *delay time*. This occurs for very thin or very shallow potential barriers. For the effective electron mass $m = 0.067m_e$, typical of *GaAs* semiconductor materials, $\alpha_c = 2.0653$.

7.4. Barrier opacity and time scale for tunneling as a transient effect

The short-length tunneling time scale discussed before is further investigated in Ref. [180]: García-Calderón and Villavicencio look at the peak value of the probability density at the barrier edge $x = L$ in the shutter problem and characterize the regime that corresponds to under-the-barrier tunneling by the *opacity* of the system, *i.e.*, Eq. (125). A time-frequency analysis establishes the existence of a range of values of the *opacity*, independent of the incidence energy, where the peak value of the *time domain resonance* is governed by a single frequency, which suggests that the system acts as a frequency filter. Figure 24 exhibits the relative frequency ω_{av}/ω_V as a function of the *opacity* for three different values of the parameter $u = V/E$. Here $\omega_{av} = \text{Im}[(d\psi/dt)/\psi]$, and the cutoff frequency $\omega_V = V/\hbar$. The time-dependent solution is given by Eq. (82). Notice the existence of an *opacity* “window”, in the range of values $2.065 \leq \alpha \leq 3.3$, where the average frequencies are always below the cutoff frequency, *i.e.*. In this example the value of $V = 0.3$ eV and the mass $m = 0.067m_e$, with m_e the bare electron mass.

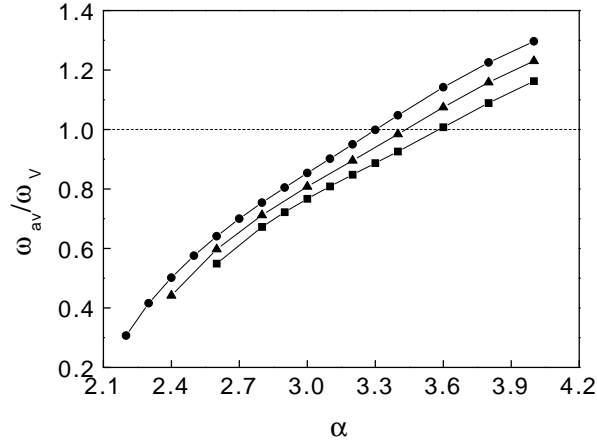


Fig. 24. Relative frequency ω_{av}/ω_V measured at the barrier edge $x = L$, as a function of the opacity α . The parameters: $u = 300$ (solid dot), $u = 10$ (solid triangle), and $u = 5$ (solid square). Note that for values of the opacity smaller than $\alpha \simeq 3.3$, the relative frequencies for all values of u are below the cutoff-frequency $\omega_{av}/\omega_V = 1$ (dashed line). See text.

7.5. Time scales for relativistic equations

In [32] the authors investigated the role played by τ_{BL} , and the characteristics of the forerunners at large and small distance from the source for under-cut-off, unit-step modulated excitations with the (dimensionless) relativistic wave equation

$$\left[\frac{\partial^2}{\partial T^2} - \frac{\partial^2}{\partial Y^2} + 1 \right] \Psi = 0, \quad (126)$$

which turns out to be more accessible experimentally (with waveguides in evanescent conditions [220,221]) than the corresponding Schrödinger equation

$$i\partial\Psi/\partial t = -\partial^2\Psi/\partial Y^2 + \Psi. \quad (127)$$

The stationary equations corresponding to Eqs. (126) and (127) are equal and have equal solutions, but the two cases are not equivalent in the time domain, because of the dispersion relations between frequency and wavenumber. In fact a wealth of qualitative changes with respect to the Schrödinger scenario were found [32].

Eq. (126) leads to the Klein-Gordon equation for spin-0 particles by means of the substitutions

$$Y = x(m_0c)/\hbar, \quad (128)$$

$$T = tm_0c^2/\hbar, \quad (129)$$

where x and t denote dimensional position and time, and m_0 and c are the particle's rest mass and the velocity of light in vacuum. Another interesting connection, much more promising to implement the analysis experimentally [221], and free from the conceptual puzzles of the former, may be established with the equation that governs the electro-

magnetic field components in waveguides of general constant cross section with perfectly conducting walls. This requires the substitutions

$$Y = x\lambda, \tag{130}$$

$$T = t\lambda c, \tag{131}$$

where $\lambda > 0$ is one of the eigenvalues of the waveguide. The main differences between the relativistic and non-relativistic cases are: (a) the relativistic solutions are not simply related to each other by time and position scaling as in the non-relativistic case, so that qualitatively different “shallow” and “deep” tunneling regimes may be distinguished; (b) tunneling is more robust relativistically, both in the precursors (more tunneling frequencies) and asymptotically (more “density”); (c) the “first” relativistic precursor, right after the limit imposed by causality does not have a non-relativistic counterpart, and does tunnel; (d) the “second” precursor, which tends to the non-relativistic one for excitation frequencies near cut-off, has an oscillating structure that may be characterized by its envelopes. The traversal time τ_{BL} is not an exact measure of their arrival except in the non-relativistic limit.

8. Transient phenomena caused by a sudden perturbation

We now turn our attention to the dynamics following a general sudden perturbation in which the potential of the system changes from $V_-(x)$ to $V_+(x)$ abruptly.

8.1. Potential steps, resonant tunneling

One of the most important tunneling processes is resonant tunneling, which has been employed in several semiconductor devices since the original double-barrier diode of Tsu and Esaki [222], and more recently to control the energy levels, transport through, and state occupancy of semiconductor quantum dots and wells [223] and nanowire resonant tunneling diodes [224]. Quantum dots are candidates as elements in quantum circuits, and basic quantum manipulation is possible by applying sharp voltage pulses or microwave signals to the contact leads surrounding the dot region [225,226,227]. The response of quantum dots to these stimuli in the sub-nano-second to almost milli-second time domain is of much current interest. Two basic manipulations that can significantly affect charge transport across the quantum well (dot) are the change (*i*) in the source-drain voltage applied across the quantum well (dot), which tilts the whole potential structure, and (*ii*) in the gate electrode voltage, which may modify essentially (and electrostatically) the quantum well (dot) depth [228,229]. At resonance, full transmission occurs, whereas off-resonance, there is essentially full reflection. Understanding the transitions that fill or deplete a resonance or a bound state following a change in potential and determining the speed of the change is clearly of fundamental interest.

For scattering systems, an elementary transient process is the transition between eigenstates of the original and final Hamiltonian in the continuum. A stationary scattering wave function responds to an abrupt change in the potential shape by forming a new stationary state at any finite position x . A physical realization would be an abrupt change in the bias voltage of an electronic device. The characteristic times of the transient are of

practical interest to determine the transport properties of small mesoscopic structures, but modelling the process by means of a grid discretization of space in a “finite box” is far from simple [230], since the boundary conditions at the box edges are not known a priori and involve simultaneous injection to and absorption from the simulation (box) region. Some approximate ways to deal with the transients have been proposed [231,230,232,233]. An exact numerical solution generally requires non-local in time “transparent” boundary conditions [234]. Some cases are solvable analytically in terms of known functions: Delgado *et al.* [64] worked out an explicit and exact solution of the transition between stationary monochromatic waves due to an abrupt potential switch for a step potential $-V_0\Theta(x)$ that changes the step height suddenly to $-V'_0\Theta(x)$, $V'_0 > V_0 > 0$, and other potential profiles, e.g., containing square single or double barriers can be treated similarly. The basic trick to find the exact solution is to implement the action of the evolution operator of the new Hamiltonian on the initial state using an integral expression in the complex momentum plane obtained by Hammer, Weber and Zidell [235]. For the step barrier that changes its height abruptly one starts with a stationary wave function of the original Hamiltonian with incident (momentum q_0), reflected and transmitted waves, $\psi(t=0) = \psi_1 + \psi_2 + \psi_3$. Each part is treated separately as a modified Moshinsky shutter problem and combined later. Let us analyze, for example, the incident case: The eigenstates of the final Hamiltonian can be written as the incident plane wave (for all x) plus a rest. The time evolution for ψ_1 is then given by

$$\psi_1(x,t) = \int_{C_1} dq \psi_q(x) \phi_1(q, t=0) e^{-iE_q t/\hbar}, \quad (132)$$

where q is the momentum from the left potential, C_1 goes from $-\infty$ to ∞ above all singularities and $\phi_1(q, t=0)$ is the momentum representation of $\psi_1(x, t=0)$. From here the integral is solved by deforming the contour along the steepest descent path. This provides w -function terms and branch-cut contributions, but the latter can be neglected in many cases. The characteristic time scales for the transitions in the step potential admit simple classical analogs. Essentially the same method can be applied to the outer parts of the wave for more complex cut-off potentials such as a double barrier with a well that can be adjusted to make the wave on or off-resonance [65,201]. The contour deformation speeds up convergence and provides physical insight as discussed in 7.1. However the method is difficult to apply for the evolution of the wave component initially inside the quantum well region which was calculated with the systematic pole expansion of García-Calderón and coworkers [65], see Section 6. In summary, the build-up process is dominated by the interference between the incident and resonance poles, leading to a non-exponential growth in which the resonance lifetime is a relevant characteristic time; the decay process is dominated by the displaced resonance; and the trapping process involves very long time transients due to interferences between a non-exponential resonance contribution and a bound-virtual state pair. Although a real quantum dot structure is much more complicated, a simple model potential, with realistic parameters, shows the importance of transient behavior over a wide (on the pico-second to nano-second and even longer) time scale. This work was extended to the case of interacting electrons at the mean field level by coupling Poisson and Schrödinger equations [66]. A critical coupling was found (determined by the electron sheet density in the well) above which permanent trapping does not occur.

Julve and Urriés have similarly described the transient from a pure plane wave on all space and the corresponding state for a square barrier using Laplace transform techniques [236], and Moshinsky and Sadurní have studied the dynamics of a deuteron suddenly subjected to an electrostatic field [237]. Finally, Abdallah and Pinaud [238] have determined non-local in time “transparent boundary conditions” necessary to solve the coupled Schrödinger-Poisson equation for the transient evolution of a resonant tunneling diode when the incoming amplitude representing the electron injection is prescribed, and Antoine *et al.* have recently reviewed different techniques to solve numerically the time-dependent linear and non-linear Schrödinger equation on unbounded domains [234].

9. Other transient phenomena

9.1. Ultrafast propagation and simultaneous arrival of information in absorbing media

Delgado, Ruschhaupt and Muga have shown that the temporal peak of a quantum wave may arrive at different locations simultaneously in an absorbing medium [36,221]. The arrival occurs at the lifetime of the particle in the medium from the instant when a point source with a sharp onset is turned on, or when a Moshinsky shutter is opened. (The effect remains for smoothed pulses [221].) Other characteristic times may be identified. In particular, the “traversal” or “Büttiker-Landauer” time (which grows linearly with the distance to the source) for the Hermitian, non-absorbing case is substituted by several characteristic quantities in the absorbing case. The simultaneous arrival due to absorption, unlike the Hartman effect, occurs for carrier frequencies under or above the cut-off, and for arbitrarily large distances. It holds also in a relativistic generalization but limited by causality, i.e., limited to distances where the time of arrival of the peak is larger than the time of the very first front. The ubiquitous peak is dominated by the saddle-point contributions above the cutoff frequency. A proposal for an experimental verification is described in [36] making use of a quantum optical measurement of atomic densities in a metastable state by fluorescence. Another interesting possibility is the use of absorbing wave guides and electromagnetic waves. One advantage of the waveguide realization with respect to quantum particles is that the effect could be measured in a non-invasive way. It also makes it possible to trigger several devices at the same time or transmit information so that it arrives simultaneously at unknown locations. This cannot be achieved by standard transmission methods because a receiver could not resend an information bit to the closest one faster than the velocity of light in vacuum c ; nor can we design the timing of a series of signals from the source so that they arrive simultaneously at different receivers if their locations are unknown.

The simplest case is that of a source with a sharp onset, and the treatment is very similar to the one used in 7.2, substituting the real potential by a complex one,

$$i\hbar \frac{\partial \psi}{\partial t} = -\frac{\hbar^2}{2m} \frac{\partial^2 \psi}{\partial x^2} + (V_R - iV_I)\psi. \quad (133)$$

k_0 becomes also a complex number so that the role of τ_{BL} in the formal solutions (see Eq. (120)) is now played by the complex number

$$\tau_{cBL} = mx/(-ik_0\hbar), \quad (134)$$

and the steepest descent path in the k -plane crosses the pole in k_0 at a time τ_c , Eq. (114). For carrier frequencies below the cut-off the saddle contribution dominates up to exponentially large times as in the Hermitian case [34], so that τ_c is not of much significance whereas, above threshold, τ_c gives approximately the arrival of the main peak. From $\partial|\psi(x,t)|^2/\partial x = 0$ we may obtain the position $x(t)$ of the “spatial” maximum at time t . This also defines (by inverting $x(t)$) a function $\tau_S(x)$, namely, the time when this spatial maximum arrives at x . One finds that the spatial maximum in the large- x region is given by $\tau_S = |\tau_{cBL}|$, a role played by the real τ_{BL} in the absence of absorption [239].

Thus a single real quantity τ_{BL} in the Hermitian case has been substituted, for a non-zero V_I , by three different quantities: the time for pole-cutting τ_c , a complex τ_{cBL} , and its modulus $|\tau_{cBL}|$, all of which tend to the “Büttiker-Landauer” traversal time $\tau_{BL} \equiv \tau_{cBL}(V_I = 0)$ without absorption [189].

Similarly, we may fix x and solve $\partial|\psi(x,t)|^2/\partial t = 0$ to get $\tau_t(x)$, namely, the time of the first “temporal” maximum. At variance with the Hermitian case, the time of arrival of the maximum is *not* proportional to τ_{BL} ($\tau_t = \tau_{BL}/\sqrt{3}$ when $V_I = 0$). The equation $\partial|\psi_s|^2/\partial t = 0$ cannot be solved analytically for $V_I \neq 0$ in a generic case, so there is no explicit formula for $\tau_t(x)$. Nevertheless, if $x \gg 2^{-1/2}|k_0|\hbar^2/mV_I$, one finds

$$\tau_t \approx \frac{\hbar}{2V_1}, \quad (135)$$

i.e., the temporal maximum coincides with the mean “life time” $\hbar/2V_1$ of a particle immersed in the absorbing potential, and it is independent of x and ω_0 , which is the most important result of [36]. A time-frequency analysis [217,34] shows that the maximum is not tunneling but it is dominated by frequencies above the cut-off, in particular by the saddle frequency corresponding to the “classical” velocity required to arrive at x at time $\tau_t(x)$.

9.2. Breakdown of classical conservation of energy in quantum collisions

In most quantum interferometers the phase differential between paths that meet in a coordinate-space point or region at a given time lead to constructive or destructive wave combinations and thus to fringes, but the paths can also interfere in momentum space and produce momentum-space fringes. An example of interference in momentum representation is the collisional, transitory enhancement of the high momentum components of a wave packet [240,241,199,202]. This enhancement leads to a violation of the classical conservation of energy since the probability of finding the particle with a momentum larger than a given value may exceed the classical bound during the collision. The effect was shown to be quantitatively significant for incident energies well above the barrier top when a transient suppression of the main incident momentum components “pushes” the momentum distribution towards lower and higher values [199,202]. This was explained as an interference in momentum representation between components associated with incidence and transmission. A simple picture emerges by assuming that in the midst of the collision the wavepacket density is unaltered with respect to free motion, but the transmitted part acquires the phase of the transmission amplitude $e^{i\phi_T}$. Adjusting this phase with the incident or barrier energies constructive or destructive interferences ap-

pear in momentum space. For Gaussian states impinging on square barriers, an analytical approximate expression for the wave function is [199]

$$\psi(k, t) \propto w[u_I(k, t)] + T(k)w[-u_T(k, t)], \quad (136)$$

where $u_I(k, t)$ and $u_T(k, t)$ are known functions of momentum and time [199], and $T(k)$ is the transmission amplitude. If, for the central momentum components, the modulus $|T|$ is close to unity and its phase is an odd multiple of π , the two contributions in Eq. (136) interfere destructively to cause the transitory suppression of the main momentum components of the incident wave packet. This is rather surprising from a classical perspective since only a negligible part of the wave packet is located at the potential barrier or, equivalently, most of the wave packet is on regions with zero potential energy. Both transmitted and incident components are dominated by the central momentum of the distribution, but instead of adding up classically, they interfere destructively.

By sending the wave packet towards the appropriate barrier potential and then switching the potential off at the time when the maximum interference occurs, this effect may be used to convert a Gaussian-shaped wave packet into a bimodal one in momentum representation, since the free evolution afterwards will not modify the momentum distribution. However, the transitory character of the effect could hinder its observation or its use as a preparation tool for controlling the atomic state of motion in atom optics or quantum information applications. To remedy this problem an extra potential barrier was added in [202]. The interference effect becomes more complex but it is possible to increase its duration significantly making it more robust and easier to observe.

For an alternative to the scattering configuration using trapped atoms and “phase imprinting” by detuned lasers which illuminate only half the atomic cloud see [242]. If a π phase is imprinted, the interference dip formed in momentum space is centered at $k = 0$, but the minimum is displaced linearly if the phase deviates slightly from π . Turning off the external trap thus creates a dark notch in coordinate space moving with controllable velocity, similar to the “dark solitons” observed experimentally [243]. In [242] the perturbation of imprinting imperfections and many body effects are investigated as a necessary step to determine the potential applicability of momentum space interferometry. The imprinted phase carries information about the laser interaction (time, laser intensity, frequency) that can be obtained from the observable notch.

9.3. Effect of classically forbidden momenta

Suppose that a classical ensemble of independent particles in one dimension is initially confined (at $t = 0$) in the spatial interval $a < x < b \leq 0$, and allowed to move freely after $t = 0$. Only particles with positive momenta may arrive at positive positions for $t > 0$. In contrast, the quantum wave function involves negative-momentum contributions as well,

$$\psi(x, t) = (2\pi)^{-1/2} \int_{-\infty}^{\infty} dk e^{ikx} \tilde{\psi}(k) e^{-iE_k t/\hbar}, \quad (137)$$

where $E_k = k^2 \hbar^2 / 2m$, and

$$\tilde{\psi}(k) = (2\pi)^{-1/2} \int_{-\infty}^{\infty} dx e^{-ikx} \psi(x, 0) \quad (138)$$

is the wavenumber representation of the initial state. The effect of negative momenta for $x, t > 0$ is however a transient one; the total final probability to find the particle at $x > 0$ is given only by positive momentum components,

$$P_T(\infty) \equiv \lim_{t \rightarrow \infty} \int_0^{\infty} dx |\psi(x, t)|^2 = \int_0^{\infty} dk |\tilde{\psi}(k)|^2, \quad (139)$$

see e.g. [244] or [245], since there are no bound states. This negative-momentum effect is also present in collisions, where it may be combined with other classically forbidden effects [246]. Consider the family of cut-off potentials of the form

$$V(x) = \begin{cases} 0 & \text{if } x < c, \\ U(x), & \text{if } c \leq x \leq d, \\ V_0, & \text{if } x > d, \end{cases} \quad (140)$$

where $V_0 \geq 0$ and $V(x)$ are real. Let us suppose that the maximum value of the potential is V_M . For a classical ensemble confined between a and b (such that $a < b \leq c \leq d \leq 0$) only particles with *initial* momentum above the barrier, $k > k_M$, $k_M \equiv (2mV_M)^{1/2}/\hbar$, may pass to the right of the potential region. In the quantum case however, there are contributions from all the components of the initial wave packet: (a) $k > k_M \equiv (2mV_M)^{1/2}/\hbar$ (above-the-barrier transmission); (b) $k_0 < k < k_M$ (“asymptotic” tunneling, these momenta contribute to the transmission probability $P_T(\infty)$); (c) $0 < k < k_0$ (“transient tunneling”, these momenta do not contribute to $P_T(\infty)$); (d) $-\infty < k < 0$ (transient negative-momentum effect); (e) $k_j = i\gamma_j$, $\gamma_j > 0$ (tunnel effect associated with bound states, which do contribute to $P_T(\infty)$).

The negative momentum effect is the only one that survives for free motion, and it has been frequently overlooked, exceptions being [235,247,248,246,119].

9.4. Time of arrival and Zeno effect

An elementary model for the time of arrival measurement at a point in space, $x = 0$, consists in performing instantaneous and frequent projections [245] $\psi(x, t_{j+}) = \psi(x, t_{j-})\Theta(-x)$, with the rate of norm lost playing the role of an operational time-of-arrival distribution. After each chopping, the time evolution can be expressed as a combination of Moshinsky functions [197], and from their short-time asymptotics it follows that when the projections are performed very frequently the wave packet is totally reflected, according to the quantum Zeno effect. The first discussions of the Zeno effect, understood as the hindered passage of the system between orthogonal subspaces because of frequent instantaneous measurements, emphasized its problematic status and regarded it as a failure to simulate or define quantum passage-time distributions [245,249]. Muga *et al.* however [250], have recently showed that in fact there is a “bright side” of the effect: by normalizing the little bits of norm N removed at each projection step,

$$\Pi_{Zeno} = \lim_{\delta t \rightarrow 0} \frac{-\delta N / \delta t}{1 - N(\infty)}, \quad (141)$$

a physical time distribution defined for the freely moving system emerges, which turns out to be in correspondence with a kinetic energy density [251], rather than with a time-of-arrival distribution.

10. Experiments

Compared to the abundant theoretical work on elementary quantum transients, the pace of experimental observations has been relatively slow, but fortunately the trend is changing very rapidly. One reason for the difficulties is the feebleness of diffraction in time in some systems. Dissipation [38], environmental noise [15], and repulsive interatomic interactions [48] tend to suppress DIT-like phenomena. Moreover, the smoothing of the aperture function of the shutter [12] leads to apodization in time, which delays the manifestation of quantum transients until the revival time [15] discussed in Section 4. Similarly, DIT may be suppressed by superposition of carrier frequencies. A finite width Δv of the velocity distribution induces a spreading Δvt in coordinate space which should be negligible compared to the width of the main fringes in (8). Hence, DIT weakens with the width-broadening of the velocity distribution [48,34], which often arises as a direct consequence of the uncertainty principle. In particular, it comes into play in the dynamics of beams of finite-size and velocity selection processes [7,8] as well as localized states under confinement [9,10,48].

The analysis of Goldemberg and Nussenzveig [7] rightly pointed out that the experimental observation of quantum transients would be simpler for the time-energy uncertainty principle than for interference effects on the density profile, though the latter can be enhanced in matter-waves with attractive interactions [152] and using constructive interference with reflected components from moving mirrors [42].

Despite the hindrance, a number of remarkable experiments have focused on quantum transients and time-dependent optics of different matter waves. A series of experiments [26,27,28] culminated in the confirmation of the time-energy uncertainty relation derived by Moshinsky for pulse formation [24]. The matter wave source consisted of caesium atoms in a magneto-optical trap (MOT) which are released and fall under gravity to bounce off of a mirror, made of an evanescent laser wave. A selection of atoms with a given total energy was achieved in a first bounce, while the double-slit in time was implemented during the second bounce, after which the resulting pulse was probed. In such a way the energy distribution of the beam when chopped in pulses was measured in agreement with the time-energy uncertainty relation [23,24]. Moreover, it was possible to register the interference pattern in the arrival-time distribution of the cold atoms after reflection at the double temporal slit. A similar setup was used by Colombe *et al.* [75] in which a Bose-Einstein condensate, with negligible non-linear interactions, was dropped over a harmonically vibrating mirror which can act as a phase modulator [26]. After the bounce the atomic carrier and sidebands were directly measured by absorption imaging of the density profile [75].

Cold atoms imply long wavelengths and time scales favorable to the observation of transients. The recent development of guided atom lasers [253,254], may pave the way for the direct observation of the DIT fringes of a suddenly turned on matter wave beam [15,121], allowing for a close implementation of the initial setup discussed by Moshinsky [5].

Historically, ultracold neutrons were initially the favorite matter waves to study such phenomena. In this case, the interaction with a potential periodically modulated in time, was shown to induce frequency side-bands. The resulting energy spread of the matter wave could be detected using a high-resolution time-of flight instrument [71,21,72] and was shown to be in agreement with previous theoretical insight [68,69,70,13,14]. The interaction with a grating moving across a beam of ultracold neutrons similarly induces an energy spreading measured in [252].

Further studies on the time-energy uncertainly relation have been performed at the attosecond scale during the photoionization of Argon atoms. A double slit in time was implemented using few-cycle ionizing fields, where the momentum distribution of the resulting photoelectron carries the information of the time at which the ionization occurs. The interference in the energy distribution was then measured as a function of the time interval between the generation of different isoenergetic photoelectrons [73].

A boost in the experimental progress on quantum transients has recently taken place [76] exploiting the analogy between paraxial optics and the time-dependent Schrödinger equation [255]. By means of this analogy, the bifurcation in the density profile of freely expanding excited states of a hard-wall trap predicted in [48] (see section 3) has been reported. The free propagation of eigenstates and coherent states of square quantum billiards (essentially a 2D hard-wall potential), was *simulated* using the transverse modes of oxide-confined vertical-cavity surface-emitting lasers and recorded with a CCD camera. The analogy with matter-wave dynamics holds under the replacements $t \rightarrow z$, where the z -axis is the direction of vertical emission, and $m/\hbar \rightarrow 2\pi/\lambda$, λ being the lasing wavelength. Moreover, for a laser cavity chaotically shaped a random branching interference of the coherent lasing modes was observed.

One more recent new route for experimental access to quantum transients and DIT phenomena is based on the time evolution of the population of an atomic level, i.e., transients do not only occur for translational degrees of freedom but also for internal degrees of freedom after or during laser excitations. Specifically, linearly chirped pulses where the instantaneous frequency changes in time passing through the resonance condition for a particular transition of rubidium atoms have been shown to produce DIT oscillations (“coherent transients”) of the excited state in the low field regime [77,256]. They are probed with pulses by a second laser on the subpicosecond time scale and can be attributed to the interference between resonant and off-resonant excitations.

These later developments and, in addition, the fact that techniques of ultra-short laser pulses in the attosecond time scale (without the need for high-intensity X-rays) are a gateway to a plethora of time-dependent electronic processes that were too fast to be observed, [257] make the prospects for quantum transient experiments rather brilliant.

11. Final comments

More than fifty years after Moshinsky’s pioneering investigation on the quantum shutter, quantum transients keep posing theoretical and experimental challenges and fascinating open questions. The initial interest in nuclear physics has shifted to applications in cold atoms, quantum optics, and semiconductor structures. Recent experimental capabilities to prepare and control light pulses, atoms, electrons and their interactions make possible a whole new world of quantum transients that has been barely explored and

will provide insight into many aspects of fundamental physics that had been until now difficult to probe or change. Few and many-body physics will offer, for example, ample opportunities for discovering and exploiting interesting phenomena without single-particle counterparts. At the single particle level, new techniques, ideas, and physical realizations of quantum transients set a sound ground for realizing many effects described in the theoretical studies, and will itself motivate further theoretical work. A challenge is the direct observation of matter-wave diffraction-in-time oscillations, but promising and versatile substitutes are the electromagnetic analogy that has been experimentally realized near the completion of this work, and “coherent transients” of atomic populations under controlled field excitation. Applications such as the control and understanding of quantum dot dynamics, quantum gates operation, tunneling, atom lasers, momentum interferometry, coherent control, or simultaneous transmission of information hold promise of a vigorous development of research on quantum transients, technological advances and exploration of new physics.

AcknowledgementsThe authors pay homage to Marcos Moshinsky, who unfortunately has passed away recently, and acknowledge discussions over the years with him; also with D. G. Austing, S. Brouard, H. Buljan, M. Büttiker, S. Cordero, F. Delgado, I. L. Egusquiza, M. D. Girardeau, S. Godoy, D. Guéry-Odelin, C. Grosche, M. Kleber, V. V. Konotop, V. I. Man’ko, J. P. Palao, M. G. Raizen, R. Romo, A. Ruschhaupt, E. Sadurní, R. F. Snider, E. Torrónategui and J. Villavicencio and S. Weber. Support by the Ministerio de Educación y Ciencia (FIS2006-10268-C03-01), the Basque Country University (UPV-EHU, GIU07/40), the EU Integrated Project QAP, and the EPSRC Project QIP-IRC (GR/S82176/0) is acknowledged.

Appendix A. Propagators in quantum transients

Many relevant quantum transients can be formulated as an initial value problem. A rather general setting considers a given eigenstate $|\psi(t = 0)\rangle$ of a Hamiltonian H_0 which is suddenly perturbed to a new Hamiltonian H . The initial state undergoes a non-trivial evolution $|\psi(t)\rangle$, which for non-relativistic particles is governed by the time-dependent Schrödinger equation. Formally, the time-dependent state vector becomes $|\psi(t)\rangle = U(t, 0)|\psi(0)\rangle$ where the evolution operator for Hermitian Hamiltonians satisfies unitarity, $U^\dagger U = U U^\dagger = 1$, and the composition property $U(t, t')U(t', 0) = U(t, 0)$.

The most general form of the time-evolution operator is given by the Dyson series,

$$U(t, t') = 1 + \sum_{n=0}^{\infty} \left(\frac{1}{i\hbar}\right)^n \int_{t'}^t dt_1 \int_{t'}^{t_1} dt_2 \cdots \int_{t'}^{t_{n-1}} dt_n H(t_1)H(t_2) \dots H(t_n), \quad (\text{A.1})$$

though as it is generally the case specific problems admit simpler forms. Indeed, for a time-independent Hamiltonian, $U = \exp(-iHt/\hbar)$; while, if $\partial_t H \neq 0$ but the Hamiltonian

at different times commute ($[H(t), H(t')] = 0$ for any t and t'), $U(t, 0) = \exp(-i \int_0^t dt' H(t')/\hbar)$. In coordinate representation, and using the resolution of the identity,

$$\langle x|\psi(t)\rangle = \int dx' \langle x|U(t, t')|x'\rangle \langle x'|\psi(t')\rangle, \quad (\text{A.2})$$

one naturally arrives at the concept of the propagator, which is the kernel $K(x, t|x', t') = \langle x|U(t, t')|x'\rangle$, this is, the coordinate representation of U . In the general case in which the Hamiltonian has both a discrete set of eigenstates $\{\phi_n\}$ labelled by the quantum number n , and scattering states $\{\varphi_E\}$ of energy E , the *spectral decomposition* of the propagator reads

$$K(x, t|x', t') = \sum_n \phi_n(x)\phi_n(x')^* e^{-iE_n(t-t')/\hbar} + \int_0^\infty dE \varphi_E(x)\varphi_E(x')^* e^{-iE(t-t')/\hbar}, \quad (\text{A.3})$$

where $*$ denotes complex conjugation. A path integral representation of the propagator is possible,

$$K(x, t|x', t') = \int \mathcal{D}x[t] \exp\left(\frac{i}{\hbar} S[x]\right), \quad (\text{A.4})$$

in terms of the classical action $S[x] = \int_{t'}^t d\tau (m\dot{x}^2/2 - V(x))$. The propagator is thus an integral over all paths $x[\tau]$ satisfying the boundary conditions $x[t'] = x'$ and $x[t] = x$. Without intention of being exhaustive, we next point out some specific features relevant to the study of quantum transients:

- The propagator for quadratic Hamiltonians acquires the simple form [258]

$$K(x, t|x', t') = \mathcal{A}(t) \exp\left(\frac{i}{\hbar} S_{cl}[x]\right), \quad (\text{A.5})$$

where $S_{cl}[x]$ is the action corresponding to the classical path, as it follows from the stationary phase approximation. Here $\mathcal{A}(t)$ is just a time-dependent function independent of the position variables. For bounded regions, other propagators are known to collapse into a countable sum of classical paths [259].

- Hamiltonians with an arbitrary time-dependent linear potential can be mapped to the free particle problem [260].
- Perturbations of the delta function type can be taken into account via path integral summation of perturbation series [261] and the Laplace method [110,17].
- There are important classes of time-dependent problems which can be mapped to time-independent ones making use of integrals of motion [43] or the so-called Duru's method [262].
- The propagator for a problem with Dirichlet, von Neumann and mixed boundary conditions can be obtained from the unconstrained one using the method of images [258,263,264,261,265]. Simple examples involve a hard-wall at the origin, $K_{wall}(x, t|x', t') = K(x, t|x', t') - K(-x, t|x', t')$, where K is for instance the propagator for the free Hamiltonian or harmonic oscillator. Similarly, the dynamics of a particle in a box can be

described by taking into account infinite images, even in the presence of moving boundaries [266,261].

The general theory for the path integral approach to quantum mechanics can be found in [258,263,264]. In particular, explicit expressions for propagators are collected in [261], an excellent account of exactly solvable path integral problems. A recent extension of some of these results exploits methods of supersymmetric quantum mechanics [267,268,269]. Finally, one should mention representations of the retarded time-dependent Green function as expansions involving resonant states [280,287], which are summarized in Appendix E.

Appendix B. The Moshinsky function

The Moshinsky function arises in most of the problems where 1D quantum dynamics involves sharp boundaries well in time or space domains [4,5,24,16]. Indeed, it can be considered “the basic propagator of the Schrödinger transient mode” [274]. Similarly, it is found when considering free propagators perturbed with point-interactions. Its standard definition reads

$$M(x, k, t) := \frac{e^{i\frac{mx^2}{2\hbar t}}}{2} w(-z), \quad (\text{B.1})$$

where

$$z = \frac{1+i}{2} \sqrt{\frac{\hbar t}{m}} \left(k - \frac{mx}{\hbar t} \right). \quad (\text{B.2})$$

An equivalent expression is

$$M(x, k, t) := \frac{e^{-i\frac{\hbar k^2 t}{2m} + ikx}}{2} \operatorname{erfc} \left[\frac{x - \hbar kt/m}{\sqrt{2i\hbar t/m}} \right]. \quad (\text{B.3})$$

Its absolute square value, $|M(x, k, t)|^2$, admits a simple geometric interpretation in terms of the Cornu spiral or clothoid, which is the curve that results from a parametric representation of the Fresnel integrals. Indeed, another frequent representation of the Moshinsky makes use of the complex Fresnel function \mathcal{F} ,

$$M(x, k, t) = \frac{1}{\sqrt{2i}} e^{-i\frac{\hbar k^2 t}{2m} + ikx} \left[\sqrt{\frac{i}{2}} - \mathcal{F}(\theta) \right], \quad (\text{B.4})$$

where $\mathcal{F}(\theta) = \int_0^\theta \exp(i\pi u^2/2) du = C(\theta) + iS(\theta)$ is an odd function of its argument

$$\theta = \sqrt{\frac{\hbar t}{m\pi}} \left(k - \frac{mx}{\hbar t} \right). \quad (\text{B.5})$$

Directly from Eq.(B.4), or using Eqs. (C.6), (C.7), and (B.1), it follows that

$$|M(x, k, t)|^2 = \frac{1}{2} \left\{ \left[\frac{1}{2} + C(\theta) \right]^2 + \left[\frac{1}{2} + S(\theta) \right]^2 \right\}, \quad (\text{B.6})$$

which, up to the definition of θ , is identical to the result from Fresnel diffraction from a straight edge [19,20]. It is possible to understand physically the Moshinsky function as a freely evolved cut-off plane wave. Using the free propagator (3),

$$M(x, k, t) = \int_{-\infty}^{\infty} dx' K_0(x, t|x', 0) e^{ikx'} \Theta(-x') = \int_{-\infty}^0 dx' \sqrt{\frac{m}{2\pi i \hbar t}} e^{i \frac{m(x-x')^2}{2\hbar t} + ikx'}. \quad (\text{B.7})$$

An integral representation in the k -variable, follows from the same physical problem,

$$M(x, k, t) = \frac{i}{2\pi} \int_{-\infty}^{\infty} dk' \frac{e^{-i\hbar k'^2 t/2m + ik'x}}{k' - k + i0} = \frac{i}{2\pi} \int_{\Gamma_+} dk' \frac{e^{-i\frac{\hbar k'^2 t}{2m} + ik'x}}{k' - k}, \quad (\text{B.8})$$

where Γ_+ is a contour in the complex z -plane which goes from $-\infty$ to ∞ passing above the pole.

Many properties of the Moshinsky function directly follow from its relation to the Faddeyeva $w(z)$ function. In particular, under inversion of both x and k , it satisfies

$$M(x, k, t) + M(-x, -k, t) = e^{ikx - i\frac{\hbar k^2}{2m}t}. \quad (\text{B.9})$$

Similarly, the asymptotic behavior of the Moshinsky functions for $|x - \hbar kt/m| \rightarrow \infty$ can be found from those of $w(z)$ when $z \rightarrow \infty$ [34]. For $x \leq \hbar kt/m$, and z as in Eq. (B.2), one finds in terms of the Gamma function $\Gamma(y)$ that

$$\begin{aligned} M(x, k, t) &\sim e^{ikx - i\frac{\hbar k^2 t}{2m}} + \frac{e^{i\frac{mx^2}{2\hbar t}}}{2i\sqrt{\pi z}} \left[1 + \sum_{n=1}^{\infty} \frac{(2n-1)!!}{(2z^2)^n} \right] \\ &= e^{ikx - i\frac{\hbar k^2 t}{2m}} + \frac{e^{i\frac{mx^2}{2\hbar t}}}{2\pi i} \sum_{n=0}^{\infty} \frac{\Gamma(n + \frac{1}{2})}{z^{2n+1}}, \end{aligned} \quad (\text{B.10})$$

whereas in the complementary region $x > \hbar kt/m$ only the series survives.

B.1. Integral and differential equations

The following relations are known [110]

$$\partial_x M(x, k, t) = ikM(x, k, t) - K_0(x, t|0, 0), \quad (\text{B.11})$$

$$\partial_k M(x, k, t) = ikM(x, k, t) - \frac{\hbar t}{m} \partial_x M(x, k, t), \quad (\text{B.12})$$

$$\partial_t M(x, k, t) = \frac{i\hbar}{2m} \partial_x^2 M(x, k, t), \quad (\text{B.13})$$

$$= \frac{x}{2t} K_0(x, t|0, 0) - \frac{\hbar k}{2m} \partial_x M(x, k, t), \quad (\text{B.14})$$

where $K_0(x, t|0, 0) = \sqrt{\frac{m}{2\pi i \hbar t}} e^{i\frac{mx^2}{2\hbar t}}$, this is, the free propagator from the origin. In addition, the indefinite integral (which arises in tunneling problem through short-range potentials [110,17]) holds

$$\int^x M(ax' + b, c, t) e^{iqx'} dx = \frac{e^{iqx}}{i(q + ca)} [M(ax + b, c, t) - M(ax + b, -q, t)], \quad (\text{B.15})$$

but for $q = -ac$, when l'Hopital's rule is to be applied.

Appendix C. The w -function

The Faddeyeva function is also known as the complex error or plasma function [78]. It is an entire function related to the complementary error function [79],

$$w(z) := e^{-z^2} \operatorname{erfc}(-iz). \quad (\text{C.1})$$

Moreover, it admits the integral representation

$$w(z) = \frac{1}{i\pi} \int_{\Gamma_-} du \frac{e^{-u^2}}{u - z}, \quad (\text{C.2})$$

where Γ_- is a contour in the complex z -plane which goes from $-\infty$ to ∞ passing below the pole. Actually, it satisfies the following equation,

$$\int_{-\infty}^{\infty} du \frac{e^{-u^2}}{u - z} = i\pi \operatorname{sign}(\Im z) w[\operatorname{sign}(\Im z)z], \quad (\text{C.3})$$

and it obeys the so-called Faddeyeva identity, which follows from Cauchy's theorem

$$w(z) + w(-z) = 2e^{-z^2}. \quad (\text{C.4})$$

Moreover,

$$w(z^*) = w(-z)^*. \quad (\text{C.5})$$

We further notice that the Fresnel integrals

$$\begin{aligned} S(\theta) &= \int_0^\theta \cos \frac{\pi t^2}{2} dt, \\ C(\theta) &= \int_0^\theta \sin \frac{\pi t^2}{2} dt, \end{aligned} \quad (\text{C.6})$$

are related to the w -function by [79],

$$C(\theta) + iS(\theta) = \frac{1+i}{2} \left[1 - e^{i\pi\theta^2/2} w\left(\frac{1+i}{2}\pi^{1/2}\theta\right) \right]. \quad (\text{C.7})$$

It has a series expansion

$$w(z) = \sum_{n=0}^{\infty} \frac{(iz)^n}{\Gamma\left(\frac{n}{2} + 1\right)}, \quad (\text{C.8})$$

whereas, its asymptotic expansion reads (expanding $(u - z)^{-1}$ around the origin in Eq. (C.2) and integrating term by term)

$$w(z) \sim \frac{i}{\sqrt{\pi}z} \left[1 + \sum_{m=1}^{\infty} \frac{(2m-1)!!}{(2z^2)^m} \right] + 2e^{-z^2} \Theta(-\Im z), \quad (\text{C.9})$$

for $z \rightarrow \infty$. We also note that its derivatives can be evaluated in a recursive way, using the relation

$$w'(z) = -2zw(z) + \frac{2i}{\sqrt{\pi}}. \quad (\text{C.10})$$

In the upper half-plane, $0 \leq |w(z)| < 1$, and its efficient computation is described in [270,271]. The real part of the w -function is proportional to the Voigt spectral-line profile, a convolution of a Lorentz and a Gaussian profile.

Apart from its close connection with the Moshinsky function, w -functions arise also naturally in the dynamics of some initial states which are not truncated in position space: for Gaussian-like examples in free motion see [272], and for Lorentzian states in momentum representation [110] impinging on a separable interaction see [273].

Appendix D. Inhomogeneous quantum sources

The time-dependent Schrödinger equation for a freely moving particle with an inhomogeneous source term switched on at $t = 0$ reads

$$L\psi(x, t) = \Theta(t)\sigma(x, t),$$

$$L = i\hbar \frac{\partial}{\partial t} + \frac{\hbar^2}{2m} \frac{\partial^2}{\partial x^2}. \quad (\text{D.1})$$

Using the free Green's function,

$$G_0(x, t|x', t') = \Theta(t - t')K_0(x, t|x', t'), \quad (\text{D.2})$$

which obeys

$$LG_0(x, t|x', t') = i\hbar\delta(x - x')\delta(t - t'), \quad (\text{D.3})$$

the solution for $\psi(x, t \geq 0)$, assuming $\psi(x, t < 0) = 0$, is given by

$$\psi(x, t) = \frac{1}{i\hbar} \int_0^{t^+} dt' \int dx' G_0(x, t|x', t')\sigma(x', t'), \quad (\text{D.4})$$

as can be verified by substitution, note the upper limit t^+ in the time integral.

In what follows we shall be interested in the dynamics of an inhomogeneous source of the form $\sigma(x, t) = e^{-i\omega t}\varrho(x)$, where $\hbar\omega = (\hbar k)^2/2m$. This can be related to the Moshinsky shutter problem with the initial condition $\psi(x, 0) = \sin(kx)\Theta(-x)$, which evolves into $\psi(x, t) = [M(x, k, t) - M(x, -k, t)]/(2i)$. We note that

$$\psi(x, t) = \frac{1}{\sqrt{2\pi}} \int g(q)e^{iqx - i\frac{\hbar q^2 t}{2m}} dq, \quad (\text{D.5})$$

where

$$g(q) = \frac{1}{\sqrt{2\pi}} \int \psi(x, 0) e^{-iqx} dx = \frac{k}{\sqrt{2\pi}[(q + i\epsilon)^2 - k^2]}, \quad (\text{D.6})$$

has two poles in the lower half-plane, close to the real axis. The integral can be deformed along the contour Γ_+ which goes from $-\infty$ to ∞ passing above the poles at $q = \pm k$,

$$\psi(x, t) = \frac{k}{2\pi} \int_{\Gamma_+} \frac{e^{-i\frac{\hbar q^2 t}{2m}}}{q^2 - k^2} e^{iqx} dq. \quad (\text{D.7})$$

Rewriting

$$\frac{e^{-i\frac{\hbar q^2 t}{2m}}}{q^2 - k^2} = \frac{\hbar e^{-i\frac{\hbar k^2 t}{2m}}}{2im} \int_0^{t^+} e^{-i\frac{\hbar(\kappa^2 - k^2)t'}{2m}} dt' + \frac{e^{-i\frac{\hbar k^2 t}{2m}}}{\kappa^2 - k^2}, \quad (\text{D.8})$$

only the first term contributes along the contour Γ_+ , and therefore

$$\psi(x, t) = \frac{\hbar k}{2im} \int_0^{t^+} e^{-i\frac{\hbar k^2 t'}{2m}} \left[\frac{1}{2\pi} \int_{\Gamma_+} e^{iqx - i\frac{\hbar q^2 (t-t')}{2m}} dq \right] dt'. \quad (\text{D.9})$$

Identifying the term in brackets with the free Green's function and comparing (D.9) with (D.4), it follows that

$$\rho(x) = \frac{\hbar^2 k}{2m} \delta(x). \quad (\text{D.10})$$

In other words, the DIT setup with a totally reflecting shutter (reflection amplitude $R = -1$) is equivalent to an inhomogeneous point-like source suddenly turned on. This result was first obtained by Moshinsky [216].

Appendix E. Resonant states

The first ideas for a theory of resonant states originated at the end of the twenties of the last century with the work of Gamow on nuclear radioactive decay [275]. He considered a situation where a particle, initially confined inside a three dimensional region by a potential barrier, goes out of it by tunneling. In order to describe the above process, Gamow restricted the discussion to spherically symmetric systems and looked for solutions to the Schrödinger equation which at large distances consist of purely outgoing waves. He realized that the absence of incoming waves in the solution is fulfilled if the energy eigenvalues are complex. In 1939, Siegert used these purely outgoing boundary conditions to derive a dispersion formula for elastic scattering by a potential of finite range [276]. The same definition of resonant states was also used by Humblet and Rosenfeld to formulate a theory of nuclear reactions [277]. One sees that resonant states provide a unified description of decay and scattering problems. Following an idea by Peierls [278], subsequent developments involved a consideration of the analytical properties of the

outgoing Green function to the problem [279,280]. These led to expansions of this function and to a consistent normalization condition for resonant states [280]. The extension of resonant states to one dimension (i.e. to the full line) was made in Ref. [281]. Along the full line, the fact that there are two edges to the potential leads to a modification of expression for the normalization condition [282,61]. For the half-line the resonance formalism is similar to the case of zero angular momentum in three dimensions.

Here we present some properties of resonant states relevant for the discussion of sections 6 and 7.

Most of the work on resonant states in one dimension refers to interactions of finite range, *i.e.*, extending along a finite region of space. A given resonant state satisfies the Schrödinger equation of the problem with complex energy eigenvalues [61],

$$\frac{d^2}{dx^2}u_n(x) + [k_n^2 - U(x)]u_n(x) = 0 \quad (\text{E.1})$$

where $k_n^2 = 2mE_n/\hbar^2$, with the complex energy $E_n = \mathcal{E}_n - i\Gamma_n/2$, $U(x) = [2mV(x)]^{1/2}/\hbar$ where $V(x)$ vanishes beyond the interval $0 \leq x \leq L$. The solutions to the above equation satisfy outgoing boundary conditions at $x = 0$ and $x = L$, given respectively by

$$\left[\frac{d}{dx}u_n \right]_{x=0} = -ik_n u_n(0), \quad (\text{E.2})$$

and

$$\left[\frac{d}{dx}u_n \right]_{x=L} = ik_n u_n(L). \quad (\text{E.3})$$

The amplitude of a resonant state increases exponentially with distance beyond the interaction region, *i.e.*, since $k_n = \alpha_n - i\beta_n$, say for $x > L$, $u_n(x) \sim \exp(i\alpha x) \exp(\beta x)$, and therefore the usual rules concerning normalization, orthogonality and completeness do not apply for resonant states. For that reason it was generally believed that these functions were not very useful for calculations. As mentioned above, developments involving the analytical properties of the outgoing Green function to the problem have led to a consistent normalization condition and completeness condition for resonant states. Notice also that at distances beyond the interaction region, say $x > L$, the resonant state may be written as

$$u_n(x, t) \sim e^{i(\alpha_n x - \mathcal{E}_n t/\hbar)} e^{\beta_n x} e^{-\Gamma_n t/\hbar}, \quad (\text{E.4})$$

which represents an outgoing wave of wave number α_n associated with a state of positive energy \mathcal{E}_n . The second factor shows that this state decays at the rate Γ_n/\hbar , in agreement with the usual interpretation of the width of a resonance level. Since the velocity of the outgoing particle is $v_n = \hbar\alpha_n/m$, one sees that the exponential increase with x of the last factor in Eq. (E.4), may be interpreted as due to the fact that at a distance x one finds those particles which left the interaction region at a time $t - x/v_n$ when the amplitude there was larger by the factor $\exp[\Gamma_n x/(2\hbar v_n)] = \exp(\beta_n x)$.

It is well known that for finite range interactions the outgoing Green function $G^+(r, r'; k)$, as a function of k , can be extended analytically to the whole complex k -plane where it possesses an infinite number of poles distributed in a well known manner [283,284]. Purely imaginary poles, situated on the upper half k -plane, correspond to bound states of the

problem whereas purely imaginary poles seated on the lower half k -plane are related to antibound states, also called virtual states by some authors. On the other hand, complex poles are only found on the lower half k -plane and are associated with resonant states. To each complex pole at $k_n = \alpha_n - i\beta_n$ with $\alpha_n, \beta_n > 0$ there corresponds, from time reversal invariance, a complex pole k_{-n} situated symmetrically with respect to the imaginary axis, i.e., $k_{-n} = -k_n^*$. Also $u_{-n}(x) = u_n^*(x)$.

E.1. Time-independent resonance expansions

The outgoing Green function to the problem satisfies the equation

$$\frac{\partial^2}{\partial x^2} G^+(x, x'; k) + [k^2 - U(x)] G^+(x, x'; k) = \left(\frac{2m}{\hbar^2} \right) \delta(x - x'), \quad (\text{E.5})$$

where $k^2 = 2mE/\hbar^2$, with E the energy. The solution to Eq. (E.5) satisfies outgoing boundary conditions at $x = 0$ and $x = L$ given respectively by

$$\left[\frac{\partial}{\partial x} G^+(x, x'; k) \right]_{x=0_-} = -ikG^+(0, x'; k) \quad (\text{E.6})$$

and

$$\left[\frac{\partial}{\partial x} G^+(x, x'; k) \right]_{x=L_-} = ikG^+(L, x'; k). \quad (\text{E.7})$$

It may be shown that the residue $C_n(x, x')$ of $G^+(x, x'; k)$ at a pole k_n seated on the complex k -plane is given by [61]

$$C_n(x, x') = \left(\frac{2m}{\hbar^2} \right) \frac{u_n(x)u_n(x')}{2k_n}, \quad (\text{E.8})$$

provided the resonant states are normalized according to the condition

$$\int_0^L u_n^2(x) dx + i \frac{u_n^2(0) + u_n^2(L)}{2k_n} = 1. \quad (\text{E.9})$$

Notice that for a bound state (i.e., $k_n = i\gamma_n$) the contribution of the two terms on right-hand side of Eq. (E.8) corresponds exactly to two integral terms that allow to express the normalization condition for the bound state in the usual form $\int_{-\infty}^{\infty} u_n^2(x) dx = 1$.

An interesting expression follows by considering the Green theorem between Eq. (E.1) for $u_n(x)$ and a similar equation for $u_m(x)$ and then using the corresponding boundary conditions for $u_n(x)$, i.e., Eqs. (E.2) and (E.3), and similarly for $u_m(x)$, to obtain

$$\int_0^L u_n(x)u_m(x) dx + i \frac{u_n(0)u_m(0) + u_n(L)u_m(L)}{k_n + k_m} = 0. \quad (\text{E.10})$$

The above results suggest to look for an expansion of the outgoing Green function of the problem in terms of the set of resonant states. This may be achieved by considering the following integral,

$$I = \frac{1}{2\pi i} \int_C \frac{G^+(x, x'; k)}{k' - k} dk', \quad (\text{E.11})$$

where C represents a large closed contour of radius L in the k -plane about the origin in the *clockwise* direction which excludes all the poles, k_n and the value at $k' = k$. Using Cauchy theorem it follows that $I = 0$ and hence one may write

$$I = \frac{1}{2\pi i} \left[- \int_{C_R} \frac{G^+(k')}{k' - k} dk' + \sum_n \int_{C_n} \frac{G^+(k')}{k' - k} dk' + \int_{C_k} \frac{G^+(k')}{k' - k} dk' \right] = 0, \quad (\text{E.12})$$

where for simplicity of notation $G^+(x, x'; k)$ is denoted by $G^+(k')$ and C_R represents a large circle centered at the origin; the contours C_n encircle each of the poles k_n that are enclosed by C_R , and the contour C_k encloses the value $k' = k$. All these contours are in the *counterclockwise* direction.

Using the theorem of residues and Eq. (E.8) one may write Eq. (E.12) as

$$G^+(x, x'; k) = \left(\frac{2m}{\hbar^2} \right) \sum_{n=-N}^N \frac{u_n(x)u_n(x')}{2k_n(k - k_n)} + \frac{1}{2\pi i} \int_{C_R} \frac{G^+(x, x'; k)}{k' - k} dk'. \quad (\text{E.13})$$

The above equation is defined for all $x, x' \geq 0$. However, for many applications we need to know $G^+(x, x'; k)$ only along the internal region of the interaction. In this case it has been proved rigorously along the half-line that the outgoing Green function goes exponentially to zero along all directions in the complex k -plane for all values of x and x' along the internal interaction region, except at the points $x = x' = 0 = L$ [285,286]. This is denoted as $0 \preceq (x, x') \preceq L$ *i.e.*,

$$G^+(x, x'; k) \rightarrow 0 \text{ as } |k| \rightarrow \infty, \quad 0 \preceq (x, x') \preceq L. \quad (\text{E.14})$$

Therefore by extending the radius R of the contour C_R up to infinity one then obtains that the integral term along C_R in Eq. (E.12) vanishes exactly. Hence, one is left with an infinite sum over the full set of resonant terms,

$$G^+(x, x'; k) = \left(\frac{2m}{\hbar^2} \right) \sum_{n=-\infty}^{\infty} \frac{u_n(x)u_n(x')}{2k_n(k - k_n)}, \quad 0 \preceq (x, x') \preceq L. \quad (\text{E.15})$$

Substitution of Eq. (E.15) into Eq. (E.5) implies the fulfillment of the relations

$$\sum_{n=-\infty}^{\infty} \frac{u_n(x)u_n(x')}{k_n} = 0, \quad 0 \preceq (x, x') \preceq L, \quad (\text{E.16})$$

and

$$\frac{1}{2} \sum_{n=-\infty}^{\infty} u_n(x)u_n(x') = \delta(x - x'), \quad 0 \preceq (x, x') \preceq L. \quad (\text{E.17})$$

The first of the above two expressions indicates that resonance states are not independent of each other and the second one may be seen as a modified closure relationship.

Let us now consider a relationship between the outgoing Green function and the continuum wave function of the problem. The continuum wave function satisfies the equation

$$\frac{d^2}{dx^2}\psi(k, x) + [k^2 - U(x)]\psi(k, x) = 0. \quad (\text{E.18})$$

For a particle approaching the potential from the left ($x < 0$), the solutions to the above equation read, respectively for $x < 0$ and $x > L$,

$$\psi(k, x) = e^{ikx} + R(k)e^{-ikx}, \quad (\text{E.19})$$

and

$$\psi(k, x) = T(k)e^{ikx}, \quad (\text{E.20})$$

where $R(k)$ and $T(k)$ are, respectively, the reflection and transmission coefficients to the problem. It then follows by applying Green theorem between Eqs. (E.18) and (E.5), and using the boundary relations given by Eqs. (E.2) and (E.3), that

$$\psi(k, x) = \left(\frac{\hbar^2}{2m}\right) 2ikG^+(0, x; k), \quad 0 < x \leq L. \quad (\text{E.21})$$

By considering the solution of the wave function at $x = L$, given by Eq. (E.20), into the above expression yields for the transmission amplitude

$$T(k) = \left(\frac{\hbar^2}{2m}\right) 2ikG^+(0, L; k)e^{-ikL}, \quad (\text{E.22})$$

and similarly, using Eq. (E.19), yields for the reflection amplitude

$$R(k) = \left(\frac{\hbar^2}{2m}\right) 2ikG^+(0, 0; k) - 1. \quad (\text{E.23})$$

Using Eq. (E.15) into Eqs. (E.21) and (E.22) then leads, respectively, to resonance expansions for the wave solution and the transmission amplitude, namely,

$$\psi(k, x) = ik \sum_{n=-\infty}^{\infty} C_n u_n(x) \quad 0 < x \leq L, \quad (\text{E.24})$$

where $C_n = u_n(0)/[k_n(k - k_n)]$, and

$$T(k) = ik \sum_{n=-\infty}^{\infty} \frac{u_n(0)u_n(L)}{k_n(k - k_n)} e^{-ikL}. \quad (\text{E.25})$$

The expansion for the reflection amplitude requires of subtraction terms. For the transmission amplitude one may alternatively expand $G^+(x, x'; k) \exp(-ikL)$, to obtain

$$T(k) = ik \sum_{n=-\infty}^{\infty} \frac{u_n(0)u_n(L)}{k_n(k - k_n)} e^{-ik_n L}. \quad (\text{E.26})$$

E.2. Resonance expansion of the retarded time-dependent Green function

The solution $|\psi(t)\rangle$ to the time-dependent Schrödinger equation may be written in terms of the retarded time evolution operator of the problem $\exp(-iHt)$, where $t \geq 0$, and the known arbitrary initial state $|\psi(0)\rangle$ as

$$|\psi(t)\rangle = e^{-iHt}|\psi(0)\rangle. \quad (\text{E.27})$$

In coordinate representation $g(x, x'; t) = \langle x | \exp(-iHt) | x' \rangle$ is referred to as the retarded Green function. It may be written, using Laplace transform techniques, in terms of the outgoing Green function to the problem,

$$g(x, x'; t) = \left(\frac{\hbar^2}{2m} \right) \frac{i}{2\pi} \int_{C_o} G^+(x, x'; k) e^{-i\hbar k^2 t / 2m} 2k dk, \quad (\text{E.28})$$

where C_o stands for the Bromwich contour and corresponds to an hyperbolic contour along the first quadrant on the complex k plane.

One may write a representation of the time-dependent Green function involving resonant states plus an integral contribution in a similar fashion as discussed for the half-line in [280]. This may be done by deforming appropriately the integration contour C_o on the complex k -plane. Since the variation of $G^+(x, x'; k)$ with k is at most exponential, the behavior of the integrand with k in Eq. (E.28) is dominated by $\exp(-i\hbar k^2 t / 2m)$. A convenient choice is to deform it to a contour involving two semi-circles C_s along the second and fourth quadrants of the k -plane plus a straight line C_L that passes through the origin at 45° off the real k -axis. In doing that one passes over some poles of the outgoing Green function. In general these include bound states and the subset of complex poles associated with the so called proper resonant states, *i.e.*, $\text{Re } k_p > \text{Im } k_p$. By extending the integration contour up to infinity one obtains that the semi-circles C_s yield a vanishing contribution so that one is left with a infinite sum of terms plus an integral contribution [280], namely,

$$g(x, x'; t) = \sum_{n=1}^{\infty} u_n(x) u_n(x') e^{-iE_n t / \hbar} + \left(\frac{\hbar^2}{2m} \right) \frac{i}{2\pi} \int_{C_L} G^+(x, x'; k) e^{-i\hbar k^2 t / 2m} 2k dk. \quad (\text{E.29})$$

Here the summation includes all bound states u_b , and all proper resonant states, u_p . In this last case, the energies are complex, *i.e.*, $E_p = \mathcal{E}_p - i\Gamma_p/2$. In order to derive the above expression, one makes use of Eq. (E.8) for the residue of a complex pole, with the resonant functions normalized according to the condition given by Eq. (E.9). One may manipulate the integrand in the integral term of Eq. (E.29), as in Ref. [280] for the half-line, to write the retarded Green function as a sum over bound and resonance terms plus a continuum integral term along the negative imaginary energy axis, a form that resembles the usual expansion as a sum of bound states and a continuum contribution along the real energy axis.

The time-dependent expansion given by Eq. (E.29) holds for arbitrary values of x and x' . However, by restricting these values according to the condition $0 \preceq (x, x') \preceq L$, discussed above, one may obtain a time-dependent expansion that includes the full set of bound, antibound and resonant states (associated with both the third and fourth quadrant poles of the complex k -plane). Noticing that

$$\frac{1}{2k_n(k-k_n)} \equiv \frac{1}{2k} \left[\frac{1}{k-k_n} + \frac{1}{k_n} \right], \quad (\text{E.30})$$

allows to write Eq. (E.15), using Eq. (E.16), as

$$G^+(x, x'; k) = \left(\frac{2m}{\hbar^2} \right) \frac{1}{2k} \sum_n^{\infty} \frac{u_n(x)u_n(x')}{(k-k_n)}; \quad 0 \preceq (x, x') \preceq L. \quad (\text{E.31})$$

The above representation is very convenient because substituting it into the integral term in Eq. (E.29) leads to an expansion over the full set of bound, antibound and resonance states of the system, similar to that obtained for the half-line [287,288],

$$g(x, x'; t) = \sum_{n=-\infty}^{\infty} u_n(x)u_n(x')M(k_n, t), \quad (\text{E.32})$$

where $M(k_n, t) \equiv M(0, k_n, t)$ stands for the Moshinsky function.

References

- [1] H. Haug and A.P. Jauho, *Quantum Kinetics in Transport and Optics of Semiconductors*, Springer, Berlin, 1997.
- [2] M. Bonitz, *Quantum Kinetic Theory*, Teubner, Stuttgart, 1998.
- [3] L. Fonda, G. C. Ghirardi and A. Rimini, *Rep. Prog. Phys.* 41 (1978) 587.
- [4] M. Moshinsky, *Phys. Rev.* 84 (1951) 525.
- [5] M. Moshinsky *Phys. Rev.* 88 (1952) 625.
- [6] G. Scheitler, M. Kleber, *Z. Phys. D* 9 (1988) 267.
- [7] J. Goldemberg and H. M. Nussensveig, *Rev. Mex. Fis.* 3 (1957) 117.
- [8] A. S. Gerasimov, M. V. Kazarnovskii, *Sov. Phys. JETP* 44 (1976) 892.
- [9] S. Godoy, *Phys. Rev. A* 65 (2002) 042111.
- [10] S. Godoy, *Phys. Rev. A* 67 (2003) 012102.
- [11] C. Brukner, A. Zeilinger, *Phys. Rev. A* 56 (1997) 3804.
- [12] A. del Campo, J. G. Muga, *J. Phys. A*, 38 (2005) 9802.
- [13] A. I. Frank and V. G. Nosov, *J. Moscow Phys. Soc.* 1 (1991) 1.
- [14] A. I. Frank and V. G. Nosov, *Phys. Lett.* 188 (1994) 120.
- [15] A. del Campo, J. G. Muga, and M. Moshinsky, *J. Phys. B* 40 (2007) 975.
- [16] M. Kleber *Phys. Rep.* 236 (1994) 331.
- [17] A. del Campo, J. G. Muga, *J. Phys. A*, 39 (2006) 14079.
- [18] D. Schneble, M. Hasuo, T. Anker, T. Pfau, J. Mlynek, *J. Opt. Soc. Am. B* 20 (2003) 648.
- [19] G. R. Fowles, *Introduction to modern optics*, Dover, New York, 1968.
- [20] M. Born and E. Wolf, *Principles of Optics: Electromagnetic Theory of Propagation, Interference and Diffraction of Light*, Cambridge, London, 1999.
- [21] S. Bernet, R. Abfalterer, C. Keller, J. Schmiedmayer, A. Zeilinger, *J. Opt. Soc. Am. B* 15 (1998) 2817.
- [22] H. J. Metcalf and P. van der Straten, *Laser Cooling and Trapping*, Springer, London, 1999.

- [23] M. Moshinsky, Rev. Mex. Fis. 1 (1952) 28.
- [24] M. Moshinsky, Am. Jour. Phys. 44 (1976) 1037.
- [25] P. Busch in Time in Quantum Mechanics, edited by J. G. Muga, R. Sala, I. Egusquiza, Springer, Berlin, 2002, Chap. 3.
- [26] A. Steane, P. Szriftgiser, P. Desbiolles, J. Dalibard Phys. Rev. Lett. 74 (1995) 4972.
- [27] M. Arndt, P. Szriftgiser, J. Dalibard, A.M. Steane, Phys. Rev. A 53 (1996) 3369.
- [28] P. Szriftgiser, D. Guéry-Odelin, M. Arndt, J. Dalibar, Phys. Rev. Lett.77 (1996) 4.
- [29] V. Mánko, M. Moshinsky, A. Sharma, Phys. Rev. 59 (1999) 1809.
- [30] M. Moshinsky, Centre de Recherches Mathématiques, CRM Proceedings and Lecture Notes 24 (2004) 153.
- [31] G. García-Calderón, A. Rubio, J. Villavicencio, Phys. Rev. A 59 (1999) 1758.
- [32] F. Delgado, J. G. Muga, A. Ruschhaupt, G. García-Calderón, J. Villavicencio, Phys. Rev. A 68 (2003) 032101.
- [33] M. Büttiker, H. Thomas, Superlatt. Microstruct. 23 (1998) 781.
- [34] J. G. Muga, M. Büttiker, Phys. Rev. A 62 (2000) 023808.
- [35] J. Villavicencio, J. Phys. A 33 (2000) 6061.
- [36] F. Delgado, J. G. Muga, A. Ruschhaupt, Phys. Rev. A 69 (2004) 022106.
- [37] G. Kälbermann, J. Phys. A 34 (2001) 6465.
- [38] M. Moshinsky, D. Schuch, J. Phys. A 34 (2001) 4217.
- [39] G. García-Calderón, J. Villavicencio, N. Yamada, Phys. Rev. A 67 (2003) 052106.
- [40] T. Kramer, M. Moshinsky, J. Phys. A 38 (2005) 5993.
- [41] T. Kramer, M. Moshinsky, Rev. Mex. Fís. 51 (2005) 407.
- [42] A. del Campo, J. G. Muga, and M. Kleber, Phys. Rev. A 77 (2008) 013608.
- [43] V. V. Dodonov, V. I. Man'ko, and D. E. Nikonov, Phys. Lett. A 162 (1992) 359.
- [44] M. Gaudin, Phys. Rev. A 4 (1971) 386.
- [45] M. A. Cazalilla, Europhys. Lett. 59 (2002) 793.
- [46] M. A. Cazalilla, J. Phys. B 37 (2004) S1.
- [47] M. T. Batchelor, X. W. Guan, N. Oelkers, C. Lee, J. Phys. A 38 (2005) 7787.
- [48] A. del Campo, J. G. Muga, Europhys. Lett. 74 (2006) 965.
- [49] T. P. Meyrath, F. Schreck, J. L. Hanssen, C-S. Chuu, M. G. Raizen, Phys. Rev. A R71 (2005) 041604.
- [50] W. Hänsel, P. Hommelhoff, T.W. Hänsch, J. Reichel, Nature 413 (2001) 498.
- [51] I. Bloch, J. Dalibard, and W. Zwerger, Rev. Mod. Phys. 80 (2008) 885.
- [52] W. Ketterle, D. S. Durfee, D. M. Stamper-Kurn, cond-mat/9904034 (1999).
- [53] C. J. Pethick, H. Smith, Bose-Einstein condensation in dilute gases, Cambridge University Press, Cambridge, 2002.
- [54] P. Öhberg, L. Santos, Phys. Rev. Lett. 89 (2002) 240402.
- [55] A. del Campo, V. I. Man'ko, and G. Marmo, Phys. Rev. A 78 (2008) 025602.
- [56] G. M. Moy, J. J. Hope, C. M. Savage, Phys. Rev. A 55 (1997) 3631.
- [57] E. W. Hagley, L. Deng, M. Kozuma, J. Wen, K. Helmerson K, S.L. Rolston, W. D. Phillips, Science 283 (1999) 1706.
- [58] K.W.H. Stevens, Eur. J. Phys. 1 (1980) 98; J. Phys. C 16 (1983) 3649.
- [59] A. P. Jauho, M. Jonson, Superlatt. Microstruct. 6 (1989) 303.
- [60] M. Brouard, J.G. Muga, Phys. Rev. A 54 (1996) 3055.
- [61] G. García-Calderón, A. Rubio, Phys. Rev. A 55 (1997) 3361.
- [62] G. García-Calderón, J. Villavicencio, Phys. Rev. A 64 (2001) 012107.
- [63] G. García-Calderón, J. Villavicencio, F. Delgado, J.G. Muga, Phys. Rev. A 66 (2002) 042119.
- [64] F. Delgado, H. Cruz, J. G. Muga, J. Phys. A 35 (2002) 10377.
- [65] F. Delgado, J. G. Muga, D. G. Austing, G. García-Calderón, J. Appl. Phys. 97 (2005) 013705.
- [66] F. Delgado, J. G. Muga, H. Cruz, D. Luis, D. G. Austing, Phys. Rev. B (2005) 195318.
- [67] E. Granot, A. Marchewka, Phys. Rev. A 73 (2006) 032111.
- [68] R. Gähler, A.G. Klein, A. Zeilinger, Phys. Rev. A 63 (1981) 1611.
- [69] R. Gähler, A. Zeilinger, Am. J. Phys. 59 (1991) 316.
- [70] H. Rauch, H. Wölwitsch, R. Clothier, H. Kaiser, S.A. Werner, Phys. Rev. A46 (1992) 49.
- [71] T. Hils, J. Felber, R. Gähler, W. Gläser, R. Golub, K. Habicht, P. Wille Phys. Rev. A 58 (1998) 4784.

- [72] S. Bernmet, R. Abfalterer, C. Keller, M.K. Oberthaler, J. Schmiedmayer, A. Zeilinger, Phys. Rev. A, 62, (2000) 023606.
- [73] F. Lindner *et al.*, Phys. Rev. Lett. 95 (2005) 040401.
- [74] C. Henkel, A. M. Steane, R. Kaiser, J. Dalibard, J. Phys. II 4 (1994) 1877.
- [75] Y. Colombe, B. Mercier, H. Perrin, V. Lorent, Phys. Rev. A 72 (2005) 061601(R).
- [76] C. C. Chen *et al.*, Phys. Rev. Lett. 102 (2009) 044101.
- [77] S. Zamith *et al.*, Phys. Rev. Lett. 87 (2001) 033001.
- [78] V. N. Faddeyeva, N. M. Terentev, Mathematical Tables: Tables of the values of the function $w(z)$ for complex argument, Pergamon, New York, 1961.
- [79] A. Abramowitz, I. A. Stegun, Handbook of Mathematical Functions, Dover, New York, 1965.
- [80] P. Caldirola, Nuovo Cimento 18 (1941) 393.
- [81] E. Kanai, Prog. Theor. Phys. 3 (1948) 440.
- [82] C. Sun and L. Yu, Phys. Rev. A 51 (1995) 1845.
- [83] M. Moshinsky, Rev. Mex. Fis. 1 (1952) 151.
- [84] A. M. Perelomov, Y. B. Zel'dovich, Quantum mechanics, World Scientific, Singapore, 1998.
- [85] V. V. Dodonov, A. B. Klimov, and D. E. Nikonov, J. Math. Phys. 34 (1993) 3391.
- [86] S. Godoy and Y Okamura, Statistical physics and beyond: 2nd Mexican Meeting on Mathematical and Experimental Physics. AIP Conference Proceedings, 757 (2005) 56.
- [87] S. Godoy, Physica B 390 (2007) 112.
- [88] E. P. Wigner, Phys. Rev. 40 (1932) 749.
- [89] D. T. Smithey *et al.*, Phys. Rev. Lett. 70 (1993) 1244.
- [90] D. Leibfried *et al.*, Phys. Rev. Lett. 77 (1996) 4281.
- [91] G. Breitenbach, S. Schiller, and J. Mlynek, Nature 387 (1997) 471.
- [92] Ch. Kurtsiefer, T. Pfau, and J. Mlynek, Nature 386 (1997) 150.
- [93] A. I. Lvovsky *et al.*, Phys. Rev. Lett. 87 (2001) 050402.
- [94] P. Lougovski *et al.*, Phys. Rev. Lett. 91 (2003) 010401.
- [95] A. del Campo, J. G. Muga, J. Phys. A, 39 (2006) 5897.
- [96] M. Moshinsky and A. Sharma, Ann. Phys. 282 (2000) 138.
- [97] S. Schuch and M. Moshinsky, Rev. Mex. Fis. 51 (2005) 516.
- [98] A. M. de Almeida, Phys. Rep. 295 (1998) 265.
- [99] R. E. Wyatt, Quantum dynamics with trajectories, Springer, New York, 2005.
- [100] Y. E. Lozovik, V. A. Sharapov, and A. S. Arkhipov, Phys. Rev. A 69 (2004) 022116.
- [101] W. R. Frensley, Phys. Rev. B 36 (1987) 1570.
- [102] R. Brunetti, S. Monastra, and C. Jacoboni, Semicond. Sci. Technol. 19 (2004) S250.
- [103] J. G. Muga and R. F. Snider, Phys. Rev. A 45 (1992) 2940.
- [104] J. G. Muga and R. F. Snider, Physica Scripta 47 (1993) 732.
- [105] S. Mancini, V. I. Man'ko, and P. Tombesi, Phys. Lett. A 213 (1996) 1.
- [106] P. Facchi, S. Pascazio, A. Scardicchio, and L. S. Schulman, Phys. Rev. A 65 (2002) 012108.
- [107] E. Granot, A. Marchewka, Europhys. Lett. 72 (2005) 341.
- [108] E. Granot, A. Marchewka, Phys. Rev. A 76 (2006) 012708.
- [109] A. Marchewka, Z. Schuss, quant-ph/0504105.
- [110] W. Elberfeld, M. Kleber, Am. J. Phys. 56 (1988) 154.
- [111] R. Gähler, R. Golub, Z. Phys. B 56 (1984) 5.
- [112] J. Felber, R. Gähler, R. Golub, Physica B 151 (1988) 135.
- [113] J. Felber, G. Müller, R. Gähler, R. Golub, Physica B 162 (1990) 191.
- [114] H. R. Brown, J. Summhammer, R. E. Callaghan, P. Kaloyerou, Phys. Lett. A, 163 (1992) 21.
- [115] A. Ranfangi, D. Mugnai, P. Fabeni, P. Pazzi, Phys. Scr. 42 (1990) 508.
- [116] A. Ranfangi, D. Mugnai, A. Agresti, Phys. Lett. A 158 (1991) 161.
- [117] P. Moretti, Phys. Scripta 45 (1992) 18.
- [118] W. Guerin, J.-F. Riou, J. P. Gaebler, V. Josse, P. Bouyer, A. Aspect, Phys. Rev. Lett. 97 (2006) 200402.
- [119] A. D. Baute, I. L. Egusquiza, J. G. Muga, J. Phys. A 34 (2001) 4289.
- [120] S. Godoy, N. Olvera, A. del Campo, Physica B 396 (2007) 108.
- [121] A. del Campo, I. Lizuain, M. Pons, J. G. Muga, M. Moshinsky, J. Phys.: Conf. Ser. 99 (2008) 012003.
- [122] R. B. Blackman and J. W. Tukey, The measurement of power spectra from the point of view of communications engineering, Dover, New York, 1959.

- [123] G. Brooker, *Modern classical optics*, Oxford, New York, 2003.
- [124] E. W. Hagley *et al.*, *Science* 283 (1999) 1706.
- [125] M. Trippenbach *et al.*, *J. Phys. B* 33 (2000) 47.
- [126] O. Vainio *et al.*, *Phys. Rev. A* 73 (2006) 063613.
- [127] E. W. Hagley *et al.*, *Phys. Rev. Lett.* 83 (1999) 3112.
- [128] M. Shapiro, P. Brumer, *Principles of the Quantum Control of Molecular Processes* (Hoboken, N.J.: Wiley-Interscience, 2003).
- [129] H. A. Rabitz, M. M. Hsieh, C. M. Rosenthal, *Science* 303 (2004) 1998.
- [130] K. Ohmori, *Ann. Rev. Phys. Chem.* 60 (2009), 487.
- [131] M. Olshanii, N. Dekker, C. Herzog, M. Prentiss, *Phys. Rev. A* 64 (2000) 033612.
- [132] M. Uiberacker *et al.*, *Nature* 446 (2007), 627.
- [133] P. Eckle *et al.*, *Science* 322 (2008) 1525.
- [134] G. G. Paulus, D. Bauer, in *Time in Quantum Mechanics*, Vol. 2, edited by J. G. Muga, A. Ruschhaupt and A. del Campo (Springer, Berlin, 2009).
- [135] K. W. H. Stevens, *J. Phys. C* 17 (1984) 5735.
- [136] M. Olshanii, *Phys. Rev. Lett.* 81 (1998) 938.
- [137] V. Dunjko, V. Lorent, M. Olshanii, *Phys. Rev. Lett.* 86 (2001) 5413.
- [138] E. H. Lieb and W. Liniger, *Phys. Rev.* 130 (1963) 1605.
- [139] K. Huang, *Statistical mechanics*, 2nd ed., Wiley, New York, 1987.
- [140] D. S. Petrov, G. V. Shlyapnikov, and J. T. M. Walraven, *Phys. Rev. Lett.* 85 (2000) 3745.
- [141] M. Girardeau, *J. Math. Phys.* 1 (1960) 516.
- [142] V. I. Yukalov and M. D. Girardeau, *Laser Phys. Lett* 2 (2005) 375.
- [143] T. Cheon and T. Shigehara, *Phys. Rev. Lett.* 82 (1999) 2536.
- [144] M. D. Girardeau and E. M. Wright, *Phys. Rev. Lett.* 84 (2000) 5239.
- [145] P. Pedri, L. Santos, P. Öberg, and S. Stringari, *Phys. Rev. A* 68 (2003) 043601.
- [146] M. Rigol and A. Muramatsu, *Phys. Rev. Lett.* 94 (2005) 240403.
- [147] A. Minguzzi and D. M. Gangardt, *Phys. Rev. Lett.* 94 (2005) 240404.
- [148] E. B. Kolomeisky, T. J. Newman, J. P. Straley, and X. Qi, *Phys. Rev. Lett.* 85 (2000) 1146.
- [149] R. Pezer and H. Buljan, *Phys. Rev. Lett.* 98 (2007) 240403.
- [150] H. Buljan, K. Lelas, R. Pezer, and M. Jablan, *Phys. Rev. A* 76 (2007) 043609.
- [151] A. del Campo, *Phys. Rev. A* 78 (2008) 045602.
- [152] A. M. Kamchatnov, A. Gammal, F. Kh. Abdullaev, R. A. Kraenkel, *Phys. Lett. A* 319 (2003) 406.
- [153] M. D. Girardeau, *Phys. Rev. Lett.* 91 (2003) 040401.
- [154] H. Buljan, R. Pezer, and T. Gasenzer, *Phys. Rev. Lett.* 100 (2008) 080406.
- [155] D. Jukić, R. Pezer, T. Gasenzer, H. Buljan, *Phys. Rev. A* 78 (2008) 053602.
- [156] M. Gaudin, *La fonction d'Onde de Bethe*, Masson, Paris, 1983.
- [157] D. M. Gangardt and G. V. Shlyapnikov, *Phys. Rev. Lett.* 90 (2003) 010401.
- [158] Y. Castin and R. Dum, *Phys. Rev. Lett.* 77 (1996) 5315.
- [159] Yu. Kagan, E. L. Surkov, G.V. Shlyapnikov, *Phys. Rev. A* 54 (1996) R1753; 55 (1997) R18.
- [160] A. Ruschhaupt, A. del Campo, and J. G. Muga, *Eur. Phys. J. D* 40 (2006) 399.
- [161] L. Salasnich, N. Manini, F. Bonelli, M. Korbman, and A. Parola, *Phys. Rev. A* 75 (2007) 043616.
- [162] B. Damski, *J.Phys. B*37 (2004) L85; *Phys. Rev. A* 69 (2004) 043610; *Phys. Rev. A* 73 (2006) 043601.
- [163] Y. S. Kivshar and B. A. Malomed, *Rev. Mod. Phys.* 61 (1989) 763.
- [164] Y. B. Zel'dovich and Yu. P. Raizer, *Physics of Shock Waves and High-Temperature Hydrodynamic Phenomena*, Dover, New York, 2002.
- [165] F. K. Abdullaev, V. V. Konotop, *Nonlinear Waves: Classical and Quantum Aspects*, Springer, London, 2004.
- [166] A. Iucci, M. A. Casalilla, arXiv:0903.1205.
- [167] See for instance, J. L. DuBois and H. R. Glyde, *Phys. Rev. A* 68 (2003) 033602.
- [168] U. Leonhardt and M. G. Raymer, *Phys. Rev. Lett.* 76 (1996) 1985.
- [169] U. Leonhardt and S. Schneider, *Phys. Rev. A* 56 (1997) 2549.
- [170] E. Altman, E. Demler, and M. D. Lukin, *Phys. Rev. A* 70 (2004) 013603; L. M. Duan, *Phys. Rev. Lett.* 96 (2006) 103201; V. Gritsev, E. Altman, E. Demler, and A. Polkovnikov, *Nature Phys.* 2 (2006) 705; Q. Niu, I. Carusotto, and A. B. Kuklov, *Phys. Rev. A* 73 (2006) 053604.
- [171] N. Teranishi, A. M. Kriman, D. K. Ferry, *Superlatt. Microstruct.* 3 (1987) 509.
- [172] M. A. Andreata, V. Dodonov, *J. Phys. A*, 35 (2002) 8373.

- [173] V. Dodonov, M.A. Andreata, *Laser. Phys.* 12 (2002) 57.
- [174] A. Hernández, G. García-Calderón, *Phys. Rev. A* 68 (2003) 014104.
- [175] G. Monsivais, M. Moshinsky, G. Loyola, *Physica Scripta* 54 (1996) 216.
- [176] R. Romo and J. Villavicencio, *Phys. Rev. B* 60 (1999) R2142.
- [177] R. Romo, *Phys. Rev. B* 66 (2002) 245311.
- [178] G. García-Calderón, J. Villavicencio, *Phys. Rev. A* 66 (2002) 032104.
- [179] R. Romo, J. Villavicencio, G. García-Calderón, *Phys. Rev. B* 66 (2002) 033108.
- [180] G. García-Calderón, J. Villavicencio, *Phys. Rev. A* 68 (2003) 052107.
- [181] J. Villavicencio, G. García-Calderón, *Phys. Rev. A* 70 (2004) 032107.
- [182] N. Yamada, G. García-Calderón, J. Villavicencio, *Phys. Rev. A* 72 (2005) 012106.
- [183] P. R. Holland, *The Quantum Theory of Motion*, Cambridge University Press, Cambridge, 1995 p. 490.
- [184] S. Cordero and G. García-Calderón, unpublished.
- [185] J. Villavicencio, R. Romo, and E. Cruz, *Phys. Rev. A* 75 (2007) 012111.
- [186] J. Villavicencio and R. Romo, *Appl. Phys. Lett.* 77 (2000) 379.
- [187] R. Romo and J. Villavicencio, *Appl. Phys. Lett.* 78 (2001) 1769.
- [188] J. Villavicencio and R. Romo, *Phys. Rev. B* 68 (2003) 153311.
- [189] M. Büttiker and R. Landauer, *Phys. Rev. Lett.* 49 (1982) 1739.
- [190] E. H. Hauge, J. A. Stovngeng, *Rev. Mod. Phys.* 61 (1989) 917.
- [191] C. R. Leavens, G. C. Aers: in *Scanning Tunneling Microscopy and Related Techniques*, ed. by R. J. Behm, N. García, H. Rohrer (Kluwer, Dordrecht, 1990).
- [192] R. Landauer and Th. Martin, *Rev. Mod. Phys.* (1994) 217.
- [193] P. Ghose, *Testing Quantum Mechanics on New Ground*, Cambridge University Press, Cambridge, 1999, Chapter 10.
- [194] J. G. Muga, R. Sala, I. L. Egusquiza (eds.) *Time in Quantum mechanics*, Lect. Notes Phys. 734, Springer-Verlag, Berlin, 2008.
- [195] S. Brouard, R. Sala and J. G. Muga, *Phys. Rev. A* 49 (1994) 4312.
- [196] M. Büttiker, *Phys. Rev. B* 27 (1983) 6178.
- [197] J. G. Muga and C. R. Leavens, *Phys. Rep.* 338 (2000) 353.
- [198] T. E. Hartman, *J. Appl. Phys.* 33 (1962) 3427.
- [199] A. L. Pérez, S. Brouard, J. G. Muga, *Phys. Rev. A* 64 (2001) 012710.
- [200] A. Pérez, S. Brouard, J. G. Muga, *J. Phys. A* 36 (2003) 2371.
- [201] F. Delgado, J. G. Muga, D. G. Austing, G. García-Calderón, *J. Appl. Phys.* 99 (2006) 089901.
- [202] A. L. Pérez, S. Brouard, J. G. Muga, *Phys. Rev. A* 71 (2005) 012703.
- [203] L. Brillouin, in *Wave Propagation and Group Velocity*, Academic Press, New York, 1960.
- [204] J. G. Muga, G. W. Wei, R. F. Snider, *Annals of Physics (NY)* 252 (1996) 336.
- [205] J. G. Muga, G. W. Wei, R. F. Snider, *Europhysics Letters* 35 (1996) 247.
- [206] G. García-Calderón, *Phys. Sta. Sol. (b)* 230 (2002) 401.
- [207] D. K. Ferry and M. S. Goodnick, *Transport in Nanostructures*, Cambridge University Press, United Kingdom, 1997.
- [208] H. Mizuta and T. Tanoue, *The Physics and Applications of Resonant Tunneling Diodes*, Cambridge University Press, Cambridge, 1995.
- [209] S. L. Konsek and T. P. Pearsall, *Phys. Rev. B* 67 (2003) 045306.
- [210] N. Harada and S. Kuroda, *Jpn. J. Appl. Phys., Part 2*, 25 (1986) L871.
- [211] J. A. Støvneng and E. H. Hauge, *Phys. Rev. B* 44 (1991) 13582.
- [212] Yu. G. Peisakhovich and A. A. Shtygashev, *Phys. Rev. B* 77 (2008) 075326; Yu. G. Peisakhovich and A. A. Shtygashev, *Phys. Rev. B* 77 (2008) 075327.
- [213] M.A. Andreata, V. Dodonov, *J. Phys. A*, 37 (2004) 2423.
- [214] U. Wulf and V. V. Skalozub, *Phys. Rev. B* 72 (2005) 165331.
- [215] S. Cordero and G. García-Calderón, unpublished.
- [216] M. Moshinsky, *Rev. Mex. Fis.* 3 (1954) 236.
- [217] L. Cohen, *Time-Frequency analysis*, Prentice Hall, New Jersey, 1995.
- [218] A. Ranfagni, D. Mugnai, P. Fabeni and P. Pazzi, *Physica Scripta* 42 (1990) 508.
- [219] A. Ranfagni, D. Mugnai and A. Agresti, *Phys. Lett. A* 158 (1991) 161.
- [220] G. Nimtz, A. Haibel, and R. M. Vetter, in *Time's arrows, quantum measurement and superluminal behaviour*, (C.N.R., Roma, 2001) p. 125.

- [221] A. Ruschhaupt and J. G. Muga, Phys. Rev. Lett. 93 (2004) 020403.
- [222] R. Tsu and L. Esaki, Appl. Phys. Lett. 22 (1973) 562.
- [223] S. Tarucha, D. G. Austing, T. Honda, R. J. van der Hage, and L. P. Kouwenhoven, Phys. Rev. Lett. 77 (1996) 3613.
- [224] M. T. Bjork, B. J. Ohlsson, C. Thelander, A. I. Persson, K. Deppert, L. R. Wallenburg, and L. Samuelson, Appl. Phys. Lett. 81 (2002) 4458.
- [225] T. H. Oosterkamp, T. Fujisawa, W. G. van der Wiel, K. Ishibashi, R. V. Hijman, S. Tarucha, and L. P. Kouwenhoven, Nature 395 (1998) 873.
- [226] T. Fujisawa, D. G. Austing, Y. Tokura, Y. Hirayama, and S. Tarucha, Nature 419 (2002) 278.
- [227] T. Fujisawa, D. G. Austing, Y. Tokura, Y. Hirayama, and S. Tarucha, Phys. Rev. Lett. 88 (2002) 236802.
- [228] T. Fujisawa, D. G. Austing, Y. Tokura, Y. Hirayama, and S. Tarucha, Nature 419 (2002) 278.
- [229] T. Fujisawa, D. G. Austing, Y. Tokura, Y. Hirayama, and S. Tarucha, Phys. Rev. Lett. 88 (2002) 236802.
- [230] W. R. Frensley, Rev. Mod. Phys. 62 (1990) 745.
- [231] R. K. Mains and G. I. Haddad, J. Appl. Phys. 64 (1988) 3564.
- [232] K. Register, U. Ravaioli, K. Hess, J. Appl. Phys. 69 (1991) 7153; 71 (1992) 1555 (E).
- [233] M. C. Yalabik and M. I. Ecemis, Phys. Rev. B 51 (1995) 2082.
- [234] X. Antoine, A. Arnold, C. Besse, M. Ehrhardt, and A. Schädle, Commun. Comput. Phys. 4 (2008) 729.
- [235] C. L. Hammer, T. A. Weber, and V. S. Zidell, Am. J. Phys. 45 (1977) 933.
- [236] J. Julve and F. J. de Urries, J. Phys. A 41 (2008) 304010.
- [237] M. Moshinsky and E. Sadurni, SIGMA 1 (2005), 003.
- [238] N. Ben Abdallah and O. Pinaud, C. R. Math. Acad. Sci. Paris 334 (2002) 283.
- [239] J. Villavicencio, R. Romo, and S. Sosa y Silva, Phys. Rev. A 66 (2002) 042110.
- [240] S. Brouard and J. G. Muga, Phys. Rev. Lett. 81 (1998) 2621.
- [241] S. Brouard, J. G. Muga, Ann. Phys. (Leipzig) 7 (1998) 679.
- [242] A. Ruschhaupt, A. del Campo, and J. G. Muga, Phys. Rev. A 79 (2009) 023616.
- [243] K. Bongs and K. Sengstock, Rep. Prog. Phys. 67 (2004) 907.
- [244] W. Jaworski and D. M. Wardlaw, Phys. Rev. A 37 (1988) 2843.
- [245] G. R. Allcock, Ann. Phys. (N.Y.) 53 (1969) 253; 53 (1969) 286; 53 (1969) 311.
- [246] A. Baute, I. L. Egusquiza and J. G. Muga, Int. J. of Theor. Phys. Group Theor. Nonlin. Opt. 8 (2002) 1.
- [247] T. A. Weber and C. L. Hammer, J. Math. Phys. 18 (1977) 1562.
- [248] J. G. Muga, S. Brouard, and R. F. Snider, Phys. Rev. A 46 (1992) 6075.
- [249] B. Misra, E. C. G. Sudarshan, J. Math. Phys. 18 (1977) 756.
- [250] J. Echanobe, A. del Campo, and J. G. Muga, Phys. Rev. A 77 (2008) 032112.
- [251] J. G. Muga, D. Seidel, G. C. Hegerfeldt, J. Chem. Phys. 122 (2005) 154106.
- [252] S. N. Balashov *et al.* Physica B 350 (2004) 246 (2004).
- [253] W. Guerin, J.-F. Riou, J. P. Gaebler, V. Josse, P. Bouyer, and A. Aspect, Phys. Rev. Lett. 97 (2006) 200402.
- [254] A. Couvert, M. Jeppesen, T. Kawalec, G. Reinaudi, R. Mathevet, and D. Guéry-Odelin, Europhys. Lett. 83 (2008) 50001.
- [255] D. Dragoman and M. Dragoman, Quantum-classical analogies, Springer, Berlin, 2004.
- [256] A. Monmayrant, B. Chatel, and B. Girard, Phys. Rev. Lett. 87 (2001) 033001; 96 (2006) 103002.
- [257] E. Goulielmakis *et al.*, Science 317 (2007) 769.
- [258] R. P. Feynman, A. R. Hibbs, Quantum Mechanics and Path Integrals, McGraw-Hill, New York, 1965.
- [259] R. E. Crandall, J. Phys. A: Math. Gen. 26 (1993) 3627.
- [260] D. Y. Song, Europhys. Lett. 65 (2003) 622.
- [261] C. Grosche and F. Steiner, Handbook of Feynman Path Integrals, Vol. 145 of Springer Tracts in Modern Physics, Springer, Berlin, 1998.
- [262] I. H. Duru, J. Phys. A: Math. Gen. 22 (1989) 4827.
- [263] L. S. Schulman, Techniques and Applications of Path Integration, Wiley, New York, 1981.
- [264] H. Kleinert, Path Integrals in Quantum Mechanics, Statistics and Polymer Physics, World Scientific, Singapore, 1990.

- [265] A. Auerbach and L. S. Schulman, *J. Phys. A: Math. Gen.* 30 (1997) 5993.
- [266] M. G .E. da Luz and B. K. Cheng, *J. Phys. A: Math. Gen.* 25 (1992) L1043.
- [267] A. M. Pupasov and B. F. Samsonov, *SIGMA* 1 (2005), 020.
- [268] B. F. Samsonov and A. M. Pupasov, *Phys. Lett. A* 356 (2006) 210.
- [269] A. M Pupasov, B. F. Samsonov, and U. Günther, *J. Phys. A: Math. Theor.* 40 (2007) 10557.
- [270] G. P. M. Poppe and C. M. J. Wijers, *ACM Trans. on Math. Software* 16 (1990) 38, and 47.
- [271] J. A. C. Weideman, *SIAM J. Numer. Anal.* 31 (1994) 1497.
- [272] J. G. Muga, J. P. Palao, and C. R. Leavens, *Phys. Lett. A* 253 (1999) 21.
- [273] J. G. Muga, J. P. Palao, *J. Phys. A* 312 (1998) 9519.
- [274] H. M. Nussenzveig, in *Symmetries in Physics*, edited by A. Frank and F. B. Wolf, Springer-Verlag, Berlin, 1992, Chap. 19.
- [275] G. Gamow, *Z. Phys.* 51 (1928) 204; G. Gamow and C. L. Critchfield, *Theory of Atomic Nucleus and Nuclear Energy-Sources*, Oxford Clarendon Press, 1949. p 156.
- [276] A. F. J. Siegert, *Phys. Rev.* 56 (1939) 750.
- [277] J. Humblet and L. Rosenfeld, *Nucl. Phys.* 26 (1961) 529.
- [278] R. E. Peierls, in *The Proceedings of the 1954 Glasgow Conference on Nuclear and Meson Physics*, edited by E. H. Bellamy and R. G. Moorhouse (Pergamon Press, London and New York, 1955) p. 296-299.
- [279] R. M. More and E. Gerjuoy, *Phys. Rev.* 7 (1973) 1288.
- [280] G. García-Calderón and R. Peierls, *Nucl.Phys. A*265 (1976) 443.
- [281] G. García-Calderón, *Solid State Commun.* 71 (1989) 237.
- [282] G. García-Calderón, R. Romo and A. Rubio, *Phys. Rev. B* 47 (1993) 9572.
- [283] J. R. Taylor, *Scattering Theory: The Quantum Theory of Nonrelativistic Collisions*, Dover Publications, New York, 2006.
- [284] R. G. Newton, *Scattering Theory of Waves and Particles*, Second edition, Springer-Verlag, New York, 1982.
- [285] G. García-Calderón and M. Berrondo, *Lett. Nuovo Cimento* 26 (1979) 562.
- [286] W. J. Romo, *J. Math. Phys.* 21 (1980) 2704.
- [287] G. García-Calderón, J. L. Mateos, M. Moshinsky, *Phy. Rev. Lett.* 74 (1995) 337.
- [288] G. García Calderón, R. Romo, J. Villavicencio, *Phys. Rev. B* 76 (2007) 035340.